

RELATIONSHIPS AMONG GEOCHEMICAL PROCESSES AND MICROBIAL
COMMUNITY STRUCTURE IN A UNIQUE HIGH-ARSENIC, SULFIDIC
GEOHERMAL SPRING IN YELLOWSTONE NATIONAL PARK

by

William "Peyton" Taylor Jr.

A thesis submitted in partial fulfillment
of the requirements for the degree

of

Master of Science

in

Land Rehabilitation

MONTANA STATE UNIVERSITY
Bozeman, Montana

May 2007

© COPYRIGHT

by

William Peyton Taylor Jr.

2007

All Rights Reserved

APPROVAL

of a thesis submitted by

William Peyton Taylor Jr.

This thesis has been read by each member of the thesis committee and has been found to be satisfactory regarding content, English usage, format, citations, bibliographic style, and consistency, and is ready for submission to the Division of Graduate Education.

Dr. William P. Inskip

Approved for the Department of Land Resources and Environmental Science

Dr. Jon M. Wraith

Approved for the Division of Graduate Education

Dr. Carl A. Fox

STATEMENT OF PERMISSION TO USE

In presenting this thesis in partial fulfillment of the requirements of a master's degree at Montana State University - Bozeman, I agree that the Library shall make it available to borrow under the rules of the Library.

If I have indicated my intention to copyright this thesis by including a copyright notice page, copying is allowable only for scholarly purposes, consistent with the "fair use" as prescribed in the U.S. Copyright Law. Requests for permission for extended quotation from or reproduction of this thesis in whole or in parts may be granted only by the copyright holder.

William Peyton Taylor Jr.
May 2007

The work herein is dedicated to
my wife, Emily, daughter, Avery, and dog, Kimbell.

ACKNOWLEDGEMENTS

I thank foremost Yellowstone National Park for allowing this research to take place, my funding source, the Thermal Biology Institute for making my work possible by paying for my research and providing for my salary. I also owe a great debt to Dr. Bill Inskeep, Dr. Rich Macur, Dr. Cathy Zabinski, and Dr. Mark Skidmore for being teachers, mentors, and most of all friends. For their friendship, advice, and assistance with my research in and out of the lab, many thanks go to: Mark Kozubal, Sarah Korf, Deanne Masur, Amanda Nagy, Zack Jay, Galena Ackerman, Seth D'Imperio, Katie Schultz, Yusuke Odake, and Erica Miller.

I am grateful to my family for their comfort, support and patience throughout my higher education, particularly my wife, Emily, who never let me give up, and has always been there through the good times and bad. Special thanks to my parents, for making me the man I am, and through their support, both financially and emotionally.

TABLE OF CONTENTS

LIST OF TABLES	viii
LIST OF FIGURES	ix
ABSTRACT	xiii
1. INTRODUCTION	1
Life at the Extremes	1
Geothermal Environments	4
Linking Geochemistry with Microbial Function	7
The Case for Cultivation	10
Geothermal Systems of Yellowstone National Park	11
Joseph's Coat Spring	17
Objectives	19
2. MATERIALS AND METHODS	21
Geothermal Site	21
Aqueous geochemistry and dissolved gases	26
Thiosulfate and polythionate analysis	39
Solid Phase Characterization	30
Chemical Speciation and Thermodynamic Calculations	30
Microbial Community 16S rDNA Gene Analysis	31
Ex-Situ Bioassay	32
Isolation of Anaerobic Crenarchaea	33
Fluorescence Microscopy	35
Growth Curves and Growth Optima	36
Isolate Metabolism	37
Archiving Isolates	38
3. RESULTS	39
Aqueous Geochemistry	39
Dominant Cations and Anions	41
Gas Exchange: Foundation for Understanding Outflow Channel Processes	42
Iron	47
Arsenic	48
Thiosulfate	50
Antimony and boron	52

TABLE OF CONTENTS - CONTINUED

Other important soluble constituents	53
Energetic Analysis of Potential Chemotrophic Metabolisms	54
Solid Phase Analysis.....	58
Solid Phase Identification	59
Microbial Community Structure	67
Isolation and Characterization of Numerically Relevant Archaea	72
Isolation.....	72
Morphology.....	76
Growth Optima	78
Metabolism	80
4. DISCUSSION	83
Geochemistry: Foundation for Understanding Chemotrophy	83
Energetics and Chemotrophy.....	85
Possible Microbial Metabolisms Inferred from 16S rDNA Gene Sequence Distribution..	87
Isolation of Relevant Microorganisms.....	92
Summary and Conclusions	95
REFERENCES	97
APPENDIX A: AQUEOUS CHEMISTRY DATA	108

LIST OF TABLES

Table	Page
3.1. Average total dissolved concentrations and standard deviations of predominant chemical constituents measured in the source water of Joseph's Coat Spring (JC3) over four annual sampling events (2003 – 2006).....	42
3.2. Oxidation-reduction reactions considered in the energetic analyses of potential chemosynthetic metabolisms occurring in the geothermal environment of Joseph's Coat Spring (JC3). Reactions are written with the electron donor as the first reactant followed by the electron acceptor. The standard state free energy value ($\Delta G^{\circ}_{\text{rxn}}$, $\text{kJ mol}^{-1} \text{e}^{-1}$) for each reaction is given at 85°C	55
3.3. Saturation indices ($[\log (\text{IAP}/\text{K}_{\text{SP}})]$) with respect to various mineral phases calculated using measured total soluble concentrations after chemical speciation using the aqueous equilibrium program, MINTeq (IAP=ion activity product; K_{sp} = solubility product constant).....	61
3.4. Small-spot energy dispersive analysis of x-ray (EDAX) compositional data of the brittle metallic phase lined the source pool of Joseph's Coat Spring (JC3). Data presented are averages over separate spots (n = 3). Pyrite and Stibnite standards (Wards) generated the same ratios respectively as environmental samples.....	62
3.5. Total chemical composition of solid phases and sediments sampled from the source pool and outflow channel (2004) of Joseph's Coat spring (JC3). Si and O were not measured in this analysis.....	62
3.6. Evaluation of potential carbon sources and possible electron acceptors supporting growth of <i>Thermofilum</i> -like strain WP28t. Experiments were conducted in 100% synthetic media contained in 10 mL serum bottles at 75 °C and pH 6.1.....	81

LIST OF FIGURES

Figure	Page
1.1. Rooted phylogenetic tree based on 16S rRNA	2
1.2. Map of YNP showing geothermal areas, geological features and caldera.	13
1.3. Histogram of pH values of 7703 geothermal sites.....	14
1.4. Piper plots of major dissolved cations and anions in geothermal source waters	15
2.1. A. Map of YNP showing major roads and the location of Joseph's Coat Springs (JC3; courtesy of http://www.yellowstonenationalpark.com). B. Photograph looking west into the Joseph's Coat Spring complex. C. Photo showing JC3 source pool from a distance. D. Close up of JC3 source pool in August of 2004.	22
2.2. A. JC3 source pool showing the location of the outflow channel. B. Close-up of the unique metallic solid phases formed in the JC3 source pool. C. Photograph showing the outflow channel exiting the east side of the source pool. D. Sampling the source pool shelf sediments E. Core sample from shelf sediments showing stratification F. Stratified layers in outflow channel sediment. Photos were taken in August of 2004.	24
2.3. Photographs showing the outflow channel exiting the east side of the source pool (A) and extending down gradient (B) (August of 2004).	25
3.1. Temperature values within the outflow channel of geothermal spring JC3 measured as a function of distance from the source pool (results shown for four annual sampling trips).	40
3.2. Aqueous pH values measured as a function of distance from the geothermal source for annual sampling events during 2003 - 2006 (only source water pH is reported for 2003).	40
3.3. Relative concentrations of dissolved gases plotted as a function of distance (cm) from the geothermal source (n=4). The relative concentrations of H ₂ , CO ₂ , H ₂ S, and CH ₄ are calculated based on C ₀ values measured within the source pool (Table 3.1). Conversely, dissolved O ₂ values are calculated as a fraction of theoretical saturation values (theoretical saturation = 143 μM).....	43

LIST OF FIGURES CONT.

Figure	Page
3.4. The oxidation of arsenite as function of distance from the geothermal source is shown as a ratio of As^{V} to total soluble As concentration (As_{TS}). Total soluble As remains essentially constant throughout the outflow channel at $\sim 130 \mu\text{M}$. Consequently, arsenate increases from as low as $10 \mu\text{M}$ at the source to as high as $100 \mu\text{M}$ at 12 m..	48
3.5. Concentrations of arsenate (As^{V}) as a function of time in an ex situ bioassay experiment conducted with JC3 outflow channel sediments. Relative to killed or filtered controls, replicated inoculated treatments show arsenite oxidation.	49
3.6. Oxidation of antimonite in Joseph's Coat spring (JC3) as a function of distance from geothermal source. The production of antimonate is shown as a ratio to Sb^{V} to total soluble Sb concentrations (TS). Data presented here are averages over annual sampling events in 2004 and 2006.	52
3.7. Reaction free energy (ΔG_{rxn} , kJ mol^{-1}) profile for the geothermal system at Joseph's Coat springs (JC3) showing Gibbs free energy values (kJ/mole e^-) for individual oxidation-reduction reactions (Reaction Numbers, Table 3.2) based on 7 differing terminal electron acceptors, indicated in legend. Arrows highlight the reactions with a fixed electron donor, in this case H_2 , and the effect changing electron acceptors has on free energy.	57
3.8. Site photographs showing (A) sample collection at the southeast rim of the main source pool of Joseph's Coat Spring (JC3), and (B) a close-up view of the pyritic, stibnite-rich 'metallic' solid phase submerged below the water surface.	59
3.9. Scanning electron micrographs (SEM) of JC3 source pool mineral deposits. Low magnification image (A) shows the edge and top surface of the 2 mm thick FeS_2 mineral deposit. Higher magnification images (B, C) reveal the presence of highly structured Sb-S crystals forming on the top of the FeS_2 surface. High magnification image of what are most likely individual cells imbedded into surrounding pyritic material (D).	64
3.10. SEM image of stibnite (Sb_2S_3) generated synthetically under laboratory conditions (An et al., 2003).	64

LIST OF FIGURES CONT.

Figure	Page
3.11. Scanning electron micrographs (SEM) of JC3 source pool mineral stibnite deposits, low magnification (A), and higher magnification (B) of stibnite crystals. Alunite is clearly seen and identified in panel (C) from JC3B position within the outflow channel. Quartz crystals, alunite, along with amorphous SiO _x is identified in (D), samples taken from JC3B.	66
3.12. Pie charts showing bacterial community composition based on 16S rDNA sequences detected at each sampling position in JC3 (2004 samples only). Names of the sequences are based on sequences of nearest cultivated relatives obtained using BLAST (Altschul et al., 1997). (Clone sequence data collected by S. Korf, Inskeep laboratory).....	68
3.13. Pie charts showing archaeal community composition based on 16S rDNA sequences detected at each sampling position in JC3 (2004 samples only). Names of the sequences are based on sequences of nearest cultivated relatives obtained using BLAST (Altschul et al., 1997). (Clone sequence data collected by S. Korf, Inskeep laboratory).....	69
3.14. Pie charts showing archaeal community composition based on 16S rDNA sequences detected at each sampling position in JC3 (2004 samples only). Names of the sequences are based on sequences of nearest cultivated relatives obtained using BLAST (Altschul et al., 1997). (Clone sequence data collected by S. Korf, Inskeep laboratory).....	73
3.15. Pie charts showing archaeal community composition based on 16S rDNA sequences detected at each sampling position in JC3 (2004 samples only). Names of the sequences are based on sequences of nearest cultivated relatives obtained using BLAST (Altschul et al., 1997). (Clone sequence data collected by S. Korf, Inskeep laboratory).....	74
3.16. Rooted phylogenetic tree based on bacterial 16S rDNA sequences detected in Joseph's Coat Spring (JC3) showing environmental clones, microorganisms isolated from JC3, important related microorganisms, and taxonomic clades. The trees were constructed using the neighbor joining method. The scale bar indicates one estimated substitution per 100 nt. The internal numbers indicate absolute bootstrap values per 100 bootstraps.	77

LIST OF FIGURES CONT.

Figure	Page
3.17. Rooted phylogenetic tree based on archaeal 16S rDNA sequences detected in Joseph's Coat Spring (JC3) showing environmental clones, microorganisms isolated from JC3, important related microorganisms, and taxonomic clades. The trees were constructed using the neighbor joining method. The scale bar indicates one estimated substitution per 100 nt. The internal numbers indicate absolute bootstrap values per 100 bootstraps.	77
3.18. Images of isolate WP28t obtained using SYBR-green II stained cells and phase contrast microscopy. Cells were mostly rod-shaped 3 - 8 μm in length (A, D), but occasionally grew to lengths of 20 μm or more (B, G). Aggregates of cells were common (E, F). Cells are shown with globular bodies (B, C). Bars are 10 μm	79
3.19. Light microscopy using SYBR-green II of a co-culture containing WP28t and WP29d. Strain WP29d appears as a regularly-shaped cocci 1 μm in diameter (A, B). Bars are 10 μm	79
3.18. Growth (cells/mL) of <i>Thermofilum</i> -like strain WP28t at optimum growth temperature and media conditions (75 $^{\circ}\text{C}$, pH 6.1) plotted along with the concentrations of dissolved sulfide as a function of time.	81
3.20. Growth (cells/mL) and dissolved sulfide production of <i>Thermofilum</i> -like strain WP28t as a function of temperature. Cell counts and sulfide production were assessed after 5 days in cultures inoculated with 10^5 cells mL^{-1} at a pH = 6.1.	80
4.1. SEM images of curved rods and rods observed in the yellow sediment layers of JC3E (A, B).....	91

ABSTRACT

The metabolisms of chemotrophic microorganisms are linked with the geochemical transformation of redox-active chemical species and mineral precipitation-dissolution reactions in geothermal environments. The objectives of the current work were to correlate the spatial distribution of microbial populations with changes in aqueous geochemistry and mineralogy in a unique Yellowstone National Park (YNP) geothermal spring, and to cultivate thermophilic microorganisms with phylogenetic and metabolic relevance to spring conditions. The geothermal spring (hereafter referenced as Joseph's Coat Spring -JC3) contains the highest reported concentrations of arsenic, antimony and thiosulfate of any geothermal feature studied in YNP. A suite of analytical and molecular approaches including aqueous geochemical and dissolved gas analysis, solid phase characterization, energetic calculations, microscopy and 16S rRNA gene sequence distribution were utilized to correlate specific microbial populations with biogeochemical processes. Predominant geochemical changes observed within the outflow channel were disappearance of methane, dissolved sulfide and ingassing of dissolved oxygen. Oxidation of arsenite was significant within the outflow channel despite the slow ingassing rates of dissolved oxygen. Microbial 16S rRNA gene sequences were determined at locations in the source pool and within the outflow channel. Shifts in microbial community structure were observed as a function of distance from the source. Source pool pyritic phases and Sb and S rich sediments were dominated by *Geothermobacterium*, *Desulfurococcus*, and *Thermofilum*-like sequences. Shifts in microbial community structure were observed within the outflow channel including appearance of Aquificales and Thermales sequences down gradient. Cultivation strategies based on spring geochemistry and energetic analysis were successful in isolating two novel thermophilic Crenarchaeota with high 16S rRNA gene sequence similarity to those determined within the spring sediments. An anaerobic, heterotrophic, S-respiring *Thermofilum*-like strain (WP28t) exhibits characteristics consistent with spring geochemistry, and confirms the importance of microbial reduction of elemental S in this spring. Detailed geochemical characterization and phylogenetic analysis of 16S rRNA gene sequences will continue to guide cultivation strategies for isolating novel microorganisms. This research indicates the importance of correlating microbial community analysis with geochemical measurements as an integrated approach for understanding the primary carbon and energy sources that link microbial populations with specific geochemical processes.

CHAPTER 1

INTRODUCTION

Life at the Extremes

Although many extreme environments were once thought to be uninhabitable, molecular approaches reveal that many of these environments host an incredible diversity of prokaryotic life. Extreme environments are defined as those environments that make it difficult for organisms to function and include deep-sea hydrothermal vents, freezing subglacial sediments and ice (Rothschild and Mancinell, 2001), high-temperature ground waters, geothermal outflows, highly saline brines, and sites containing elevated levels of toxic trace elements or radionuclides (Jannasch and Mottl, 1985; Bada, 2004; Foght et al., 2004; Ley et al., 2006). Microorganisms inhabiting extreme environments are referred to as extremophiles. Phylogenetically, these organisms often branch deeply within the universal tree of life (based on 16S rRNA gene sequences), and may represent groups of microorganisms that were important under early earth conditions (Figure 1.1; Barns and Nierzwicki-Bauer, 1997; Reysenbach and Cady, 2001).

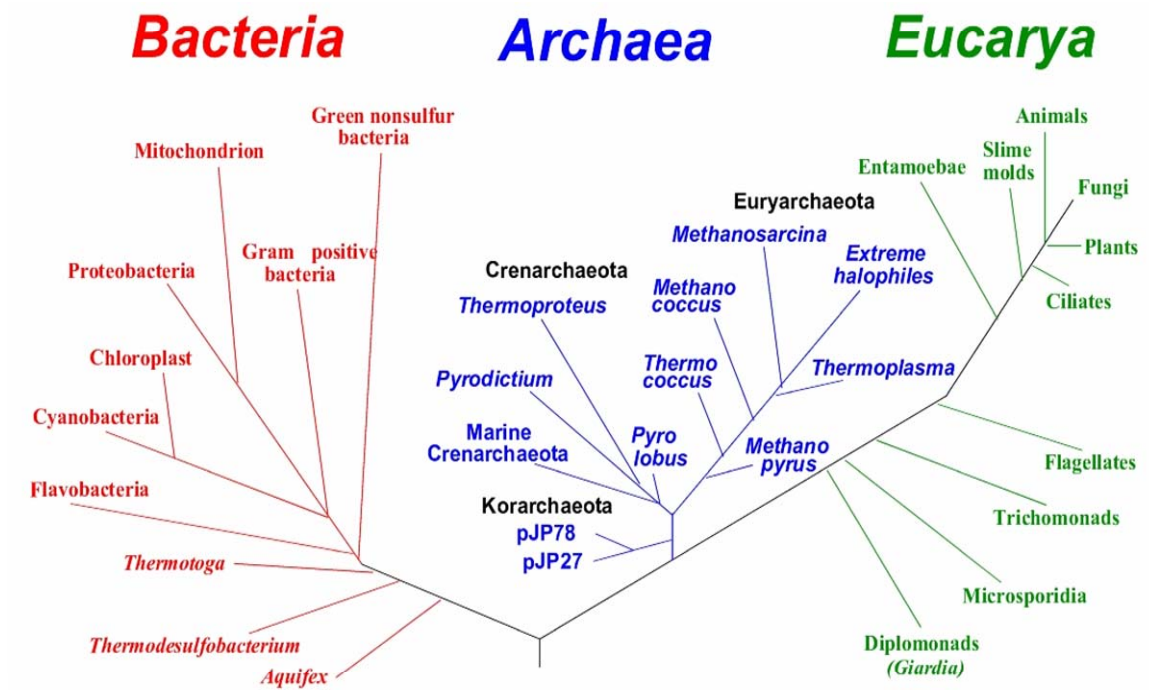


Figure 1.1. Rooted phylogenetic tree based on 16S rRNA gene sequences highlighting the importance of deeply rooted thermophilic *Bacteria* and *Archaea* (Reproduced from Brock 10ed).

Numerous thermophilic microorganisms are capable of living on inorganic constituents for their sole C and energy source, and many are obligate anaerobes. These present-day microorganisms occupy environmental niches that are thought to be representative of habitats important in early Earth, and their past relatives may have been especially important prior to oxygenation of the earth's atmosphere some 2.2 billion years ago (Nisbet and Sleep, 2001; Catling et al., 2001). Consequently, there is significant interest in understanding the novel physiologies of extremophiles, and the unique environments in which they have evolved. These habitats are potentially analogous to conditions on other planets (e.g. Mars), where temperature and chemical extremes are expected to be less hospitable for mesophilic, heterotrophic prokaryotes common under Earth surface conditions. The biological complexity within extreme

environments is often much simpler compared to microbial habitats important in soils and natural surface waters (Reysenbach et al., 2000; Nannipieri et al., 2003). Nevertheless, an understanding of the ecology of these low-diversity microbial communities has direct application to understanding more complex systems (Ward, 1998; Ward et al., 1998; Hunter-Cevera, 1998; Robertson et al., 2005). The relatively low microbial diversity, coupled with the limited number of possible carbon and energy sources makes extreme habitats ideal for understanding many of the fundamental questions in environmental microbiology including:

- What are the primary C and energy sources that link prokaryotic life and biological productivity to geochemical cycling?
- What are the relationships among available electron donors and acceptors and microbial community structure?
- What environmental or organismal processes drive temporal or successional dynamics in microbial community structure?
- What are the primary interspecies interactions that define community metabolic networks, and how have these factors influenced the co-evolution of prokaryotic organisms?
- How do rates of dispersal, genetic exchange and natural selection act to explain the distribution of genetic signatures in prokaryotes?

Extreme environments generally offer greater simplicity, hence may represent excellent model systems in which to make progress towards a more fundamental understanding of how microbial communities function. *Model systems* receive significant focus in science

because, while they retain the likeness of more complex systems, the reduced number of different biological species and or abiotic components provides definitive mechanistic information regarding linkages among biota and geochemical processes. Microbial habitats and communities in temperate soils and natural waters are invariably complex and it is often beneficial to simplify the number of confounding variables, and minimize the number of different species present to understand individual factors that may impact microbial growth and function. Extreme environments offer an advantage in that the selection pressures inherent to such habitats often result in lower microbial diversity, where it is not uncommon to observe only several predominant genera (Reysenbach et al., 2000; Edwards et al., 2000; Baker and Banfield, 2003).

Geothermal Environments

Microorganisms capable of obtaining energy by catalyzing the oxidation of reduced constituents are referred to as *chemotrophs*. Chemoautotrophic microorganisms, capable of fixing inorganic C (i.e. CO₂ or CO), often represent the primary producers in geothermal environments, thriving at temperatures exceeding the upper limit (~ 74 °C) of known photosynthetic organisms (Cox and Shock, 2003; Spear et al., 2006). Chemical constituents dissolved or precipitated in geothermal environments are often used for energy conserving reactions to drive metabolism and incorporate inorganic carbon into biomass. Geothermal source waters often contain an abundance of reduced constituents including potential electron donors such as H₂, CH₄, H₂S, S⁰, S₂O₃, Fe^{II}, As^{III}, and NH₄ (Ball et al., 2002; Nordstrom et al., 2005). The concentrations of dissolved CO₂, H₂, CH₄ and H₂S in geothermal source waters are generally oversaturated with respect to earth

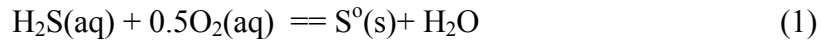
surface conditions, while the concentrations of dissolved O₂ are often below detection (Langner et al., 2001; Macur et al., 2004a; Inskeep et al., 2005; Meyer-Dombard et al., 2005; Spear et al., 2005). The substantial redox disequilibrium characteristic of geothermal discharge yields numerous possible exergonic oxidation-reduction reactions that may serve as energy sources for chemotrophic microorganisms (Amend and Shock, 2001; Amend et al., 2003; Inskeep et al., 2005). Furthermore, additional diverse niche environments are created down gradient from geothermal discharge due to a host of geochemical processes including degassing of CO₂, H₂, H₂S and CH₄, ingassing of O₂, and precipitation or biomineralization of oversaturated chemical constituents.

Geothermal waters may support a large number of exergonic reactions when various electron donors are coupled with electron acceptors present in the system (e.g., O₂, NO₃⁻, Fe^{III}, As^V, Sb^V, SO₄²⁻, S₂O₃²⁻, S⁰ and CO₂). Many of these redox reactions may be suitable for microbial energy generation. The ability to determine which constituents are important to the physiology of chemotrophic thermophiles is dependent in part on accurately measuring the concentrations of relevant aqueous and solid phase chemical constituents. Lower aqueous chemical and gas detection limits, greater portability in instrumentation and improved real-time measurements coupled with more accurate temperature-dependent standard state Gibbs free-energy values ($\Delta G^{\circ}_{\text{rxn}}$) has provided data necessary for energetic analysis of chemical reactions at spring conditions. An accurate determination of the activity of relevant chemical species along with energetic calculations can be used to evaluate the favorability and energy potentially available for numerous electron donor-acceptor combinations (Amend and Shock, 2001). Although

favorability of a redox reaction does not necessitate its utilization by microorganisms, knowledge of reaction energetics is useful for predicting reactions that may be important to microbial populations.

Geothermal source waters are also oversaturated with respect to various mineral phases such as silicates, oxides, carbonates, sulfates, arsenates and sulfides. These solid phases may be deposited through either abiotic or microbially-mediated reactions (Inskeep et al., 2005; Nordstrom et al., 2005). For example, Macur et al. (2004a) linked the biomineralization of $\text{As}^{\text{V}}\text{-Fe}^{\text{III}}$ solid phases in a Yellowstone geothermal spring to the appearance of specific microbial populations using 16S rRNA gene and geochemical analysis conducted during the succession of microbial mats lining the outflow channel of an acid-sulfate-chloride geothermal spring. This and other studies have provided evidence that chemolithotrophic microorganisms are among the main catalysts for Fe^{III} oxide mineralization in acidic geothermal systems (Langner et al., 2001; Inskeep et al., 2004; Kozubal et al., 2007).

Elemental sulfur (S^0) is known to play an important role in the metabolism of several thermophilic microorganisms and may serve either as an electron donor or electron acceptor for energy generation (Amend and Shock, 2001). The oxidation, reduction, or disproportionation of sulfur compounds can generate a host of possible metabolic strategies used to harness energy. For example, dissolved sulfide may be oxidized via O_2 to produce elemental S^0 (Rxn 1), thiosulfate may disproportionate to sulfite and elemental S^0 (Rxn. 2), and elemental S^0 may be reduced back to sulfide via the oxidation of H_2 (Reaction 3):



Consequently, elemental S^0 is an extremely important solid phase in geothermal systems, and often forms rapidly upon geothermal discharge. It has generally been accepted that the rates of abiotic sulfide oxidation to yield thiosulfate, followed by rapid disproportionation to sulfite and elemental sulfur is responsible for the deposition of copious amounts of elemental S^0 when sulfidic waters contact oxygen (Nordstrom and Southam, 1997; Xu et al., 1998; Xu et al., 2000; Druschel et al., 2003). However, it is likely that thermophilic microorganisms are also contributing to the oxidation of H_2S for metabolic energy gain (Inskeep and McDermott, 2005). In most cases, the rates and mechanisms of mineral formation and dissolution within geothermal outflow channels are not well characterized, and further study is necessary to understand relationships among microorganisms and the geochemical processes that shape these environments (Inskeep and McDermott, 2005).

Linking Geochemistry with Microbial Function

Detailed geochemical analysis of aqueous and solid phase components coupled with molecular analysis (e.g. 16S rRNA gene) of hot spring microbial communities has allowed researchers to gain insight into the likely physiologies of thermophilic microorganisms (Macur et al., 2004a; Inskeep et al., 2004; Inskeep et al., 2005; Phoenix et al., 2005). During the last decade, numerous potential members of hot spring microbial mats have been identified using culture-independent approaches based on small subunit

16S rRNA gene sequences amplified by Polymerase Chain Reaction (PCR) from community DNA (Barnes and Nierzwicki-Bauer, 1997; Ward et al., 1998; Hugenholtz et al., 1998; Jackson et al., 2001; Meyer-Dombard et al., 2005; Inskeep et al., 2005). This approach has provided an unprecedented view of microbial diversity and relative abundance of phylotypes important in these communities. The metabolisms of these uncultured populations can be estimated from nearest cultivated relatives. Inferred metabolisms coupled with detailed geochemical analyses allow researchers to test hypotheses regarding metabolisms of specific populations *in situ*.

Recent studies have emphasized the importance of linking geochemical processes with microbial physiology and function in natural systems (Amend and Shock, 2001; Newman and Banfield, 2002; Reysenbach and Shock, 2002; Amend et al., 2003; Croal et al., 2004; Macur et al., 2004a; Inskeep et al., 2005; Meyer-Dombard et al., 2005; Spear et al., 2005; Rogers and Amend, 2005; 2006). Although difficult in most natural systems, it may be possible to assemble these relationships in simpler geothermal communities. Assessment of free energy values of various oxidation-reduction reactions coupled with the known physiologies of cultivated relatives have been used to infer the function of 16S rRNA clones obtained from geothermal environments (Spear et al., 2005; Inskeep et al., 2005). For example, the highly exergonic oxidation of H₂ using O₂ as an electron acceptor (knall-gas reaction) coupled with the observation of numerous Aquificales-like 16S sequence clones has led some scientists to implicate H₂ as a predominant chemical energy source driving metabolism in geothermal systems (Spear et al., 2005). However, the fact remains that many redox couples are exergonic in all natural systems, and

progress towards understanding these linkages must move beyond the informal assumption that the magnitude of estimated free energy values will be useful for understanding microbial metabolism in situ (Inskeep et al., 2005). Other studies also document that numerous oxidation-reduction reactions may serve as the basis for chemotrophic metabolism in extreme environments (Amend and Shock, 2001; Amend et al., 2003; Rogers and Amend, 2005; 2006). Furthermore, the calculated free energy values (ΔG_{rxn} , kJ mol^{-1}) for particular reactions may be especially sensitive to pH (or other chemical species that are dependent on pH); consequently, it is useful to assess the *free energy profile* of an environment (Amend et al., 2003; Inskeep et al., 2005).

However, given the plethora of reduced constituents in geothermal source waters and the nonequilibrium nature of these systems, energetic profiles do not provide the resolution necessary for predicting the distribution of microbial populations in geothermal source pools and outflow channels (Inskeep et al., 2005; Kappler et al., 2005).

Additional measurements and complementary approaches will be necessary to build a stronger case for linking microbial growth and or activity with geochemical processes. For example, Macur et al. (2004a) described the succession of microbial communities in a newly formed geothermal outflow channel and correlated the appearance of specific populations with changes in the geochemistry of As and Fe in space and time. Visual observations of Fe^{III} oxide formation at specific locations within the outflow channel correlated with the growth of cells coated with As^{V} -rich Fe^{III} -oxyhydroxides, as determined using cryo-scanning electron microscopy and energy-dispersive analysis of x-rays (SEM/EDAX). Simultaneous 16S rRNA gene sequence

analysis of the same material revealed the emergence of possible Fe-oxidizing populations (e.g., *Metallosphaera*, *Thiomonas*, and *Acidimicrobium*) as well as several other novel 16S rRNA gene sequences only known to be associated with Fe hydrothermal deposits (Jackson et al., 2001; Inskeep et al., 2004). The study by Macur et al. (2004a) also clearly demonstrated that anaerobic hyperthermophiles such as *Caldococcus*, *Caldisphaera* and *Stygiolobus*-like populations are important near geothermal source waters containing high dissolved sulfide and copious amounts of elemental S⁰, and where dissolved oxygen levels are consistently below detection (< 2-3 μM). The known physiology of the cultured relatives of these thermophiles involves reduction of elemental S⁰ using H₂ or organic constituents as electron donors (Amend and Shock, 2001; Itoh, 2003; Nakagawa et al., 2005). Invariably, these reactions yield considerably less energy compared to the knall-gas reaction; consequently, free energy values alone would not necessarily have predicted the importance of these organisms at particular locations within the outflow channel.

The Case for Cultivation

Phylogenetic assessment (e.g., 16S rRNA gene sequence analysis) of microbial community structure coupled with detailed geochemical analysis of aqueous constituents and solid phases allow significant insight and inference regarding the properties and function of uncultured organisms. However, inferring microbial physiology from phylogenetic (16S rRNA gene) analysis or observed geochemical transformations can have serious limitations. For example, members of the order Aquificales are capable of using multiple electron donor/acceptor combinations for energy generation and can adjust

their metabolism depending on specific environmental conditions (Reysenbach et al., 2005). It is not uncommon for members of the same genera to exhibit different physiologies in culture (Macur et al., 2004b), consequently, the metabolism of uncultured populations detected *in situ* may be different than their nearest phylogenetic relatives. Moreover, many environmental 16S rRNA gene sequences amplified from high temperature environments are so distantly related to any cultured relatives, that assigning a metabolism and ecological role for these uncultured organisms is essentially a guess. Furthermore, biases in DNA extraction and or PCR amplification can limit accurate detection of microbial community members (Suzuki and Giovannoni, 1996). Consequently, while chemical and microbial community analysis are important tools for understanding the ecology of geothermal springs, the isolation of relevant microorganisms is extremely vital to understanding the potential capabilities of specific microbial populations in geothermal ecosystems, especially if it can be shown through quantitative approaches that the isolated organisms are numerically relevant members of the microbial community.

Geothermal Systems of Yellowstone National Park

With roughly 10,000 geothermal features, Yellowstone contains the greatest number and highest diversity of terrestrial thermal environments on Earth. Most of these geothermal features are located along the margins of the 0.6 Ma (million years ago) Yellowstone caldera (Figure 1.2). Data collected using a variety of geological and geophysical methods suggests that much of the 0.6 Ma caldera is underlain by magma or partially molten material, possibly as close as 3 km beneath the surface on the eastern

edge of the caldera (Fournier, 2005). As geothermally heated waters in the earth's subsurface contact rocks and mineral deposits, the dissolved concentrations of inorganic constituents are influenced by temperature-dependent weathering reactions, influx of magmatic gases and base-exchange reactions between dissolved species and minerals (Fournier, 2005). Two categories of hydrothermal activity are used to classify hot springs in YNP. *Hot water systems* emanate from heated reservoirs and tend to emerge where faults cut across the topographically low basins (Fournier, 2005). The chemical signature of these waters is controlled largely through contact with mineral phases while migrating to the surface via convection and pressure. *Vapor dominated systems* are controlled by open pore spaces filled with steam and other gases beneath an impermeable cap rock. Fractures through this cap act as a throttle releasing high pressure and temperature gases into meteoric waters perched above. These mixed waters and gasses then rise to the surface (Fournier, 2005). Vapor-phase partitioning, relative mixing ratios of meteoric and hydrothermal waters, varying temperatures, pressures and bedrock mineral phase composition all interact to create an incredible diversity in the aqueous phase geochemical composition across the YNP geothermal ecosystem.

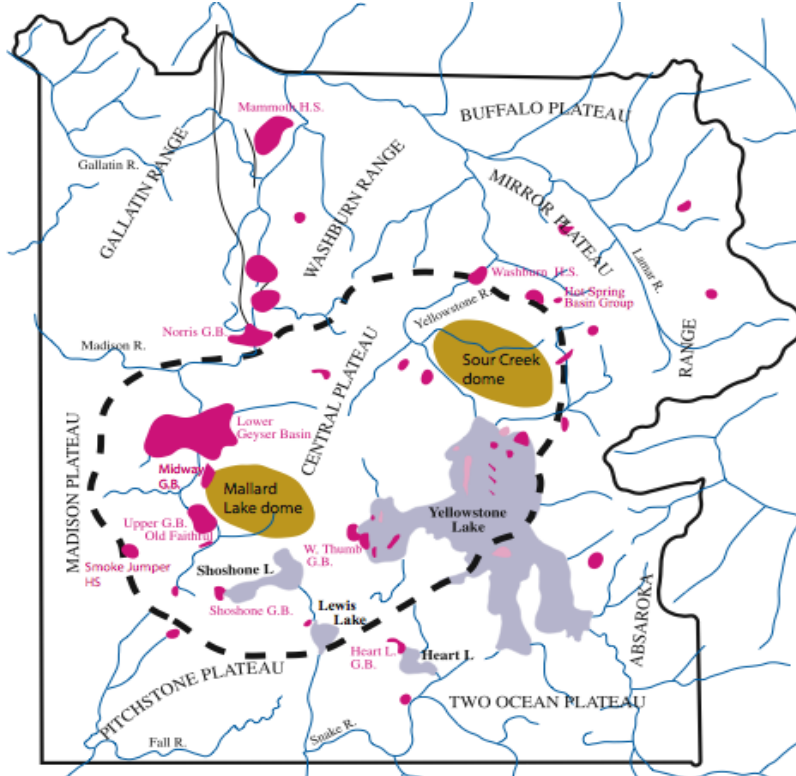


Figure 1.2. Map of Yellowstone National Park showing significant geothermal and geological features. Areas in magenta represent active locations of geothermal areas; areas in pink represent inactive geothermal areas; the dashed line represents the caldera margin. (Source: Reproduced from Morgan and Shanks, 2005)

Over the last century, many researchers have been involved in characterizing the geochemistry of Yellowstone's geothermal springs and geysers. Data from these investigations indicate that source water temperatures in YNP range from ambient to 93 °C (boiling at YNP elevation) and pH values range from 1 to 10 (Figure 1.3).

Yellowstone's geothermal waters often contain relatively high concentrations of dissolved Na^+ , NH_4^+ , K^+ , Cl^- , SO_4^{2-} , and inorganic C, and the relative concentration of these major constituents serves as a basis for differentiating among various spring types.

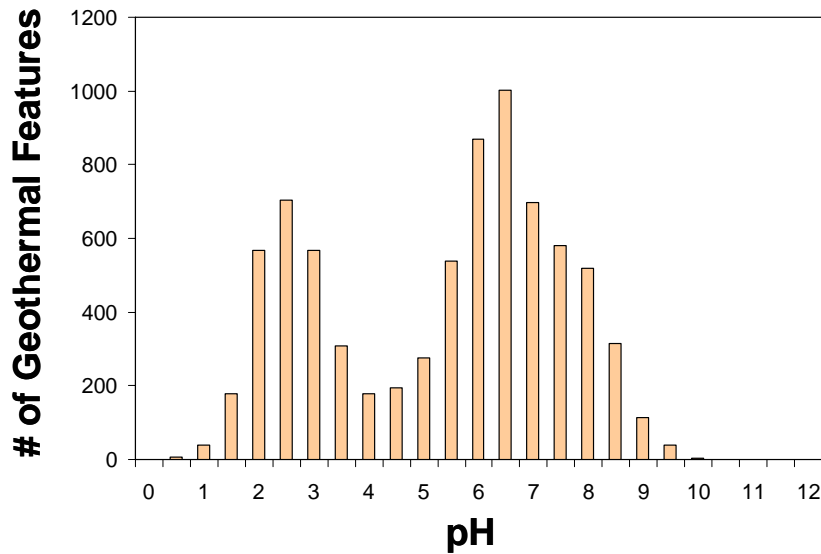


Figure 1.3. Histogram showing pH values of 7703 geothermal sites in YNP. The bimodal distribution supports the importance of low pH (2 - 3) and neutral pH (6 - 7) systems (Source: Yellowstone Center for Resources, NPS).

Three general classes of geothermal springs are often observed in YNP, namely, (i) *Acid-Sulfate-Chloride* (ASC) springs that are characterized by low pH (< 4) and high concentrations of dissolved SO_4^{2-} (~ 1 mM), and Cl^- (~ 13 mM), (ii) *Acid-Sulfate* (AS) springs that have low pH (< 4) and high dissolved concentrations of SO_4^{2-} (~ 7 mM), and (iii) *Alkaline-Chloride-Carbonate* (ACC) springs that exhibit higher pH (> 6), and mM concentrations of Cl^- (~ 10 - 20 mM) and dissolved inorganic carbon (DIC; ~ 0.5 mM) (Ball et al., 2002; Inskeep et al., 2005; McCleskey et al., 2005; Inskeep and McDermott, 2005; Nordstrom et al., 2005). Major dissolved ions from a variety of Yellowstone springs are plotted on the Piper diagrams shown in Figure 1.4. The diagram on the right shows three separate clusters that represent the ASC, AS, and ACC geothermal system types. The separation of these different geothermal system types is based primarily on Cl^- , SO_4^{2-} , and DIC concentrations. The different chemistries depicted in these diagrams

represent only one aspect of the diverse geochemical habitats that are available to chemosynthetic microorganisms in Yellowstone.

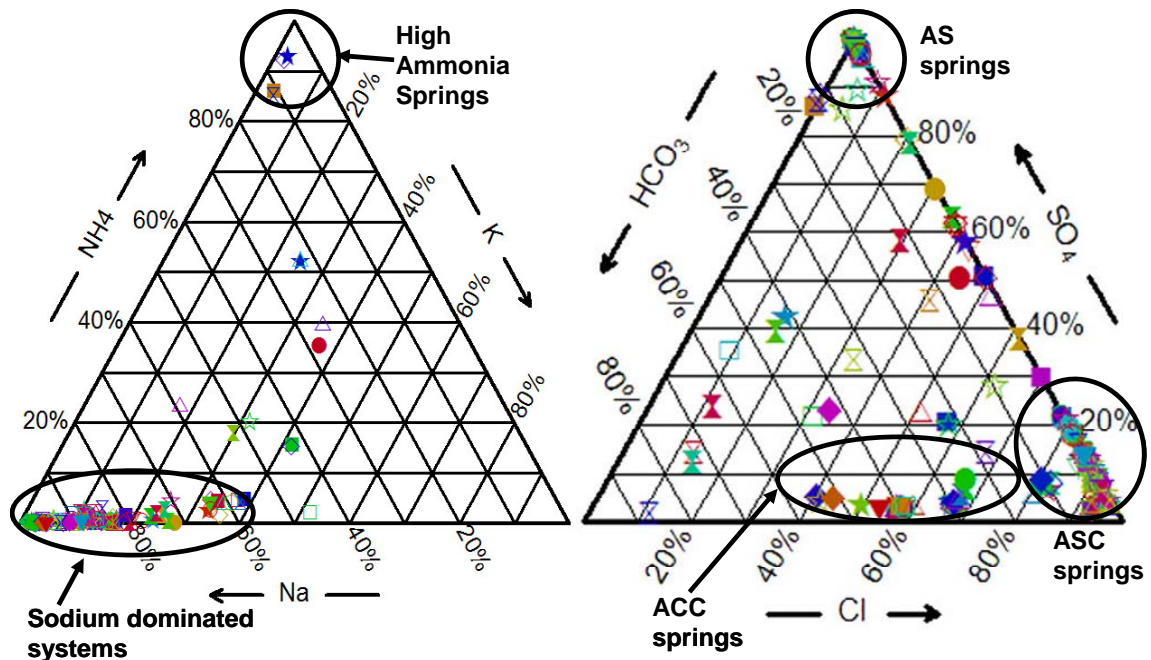


Figure 1.4. Piper plots of major dissolved cations (left) and anions (right) in geothermal source waters of YNP. Triangular graph displays the importance of a particular ion as a percent compared to other ions on opposing axis. Symbols represent sampling points from 166 locations within YNP showing the broad diversity in chemical makeup of geothermal fluids.

Geothermal source waters of YNP often contain elevated levels of specific trace-elements including As, Sb, Se, B, and Hg (Stauffer and Thompson, 1984; McCleskey et al., 2005; King et al., 2006). Significant research has focused on understanding the mechanisms by which microorganisms detoxify and or utilize these constituents for energy generation. In addition, the elevated levels of trace elements in these systems likely play an important role in microbial selection and adaptation. For example, the high

levels of As ($> 40 \mu\text{M}$) reported for a variety of springs throughout YNP suggest that microorganisms proliferating under these conditions possess some mechanism for As (Silver, 1996; Silver and Phung, 2005; Inskeep et al., 2002, 2005). Mercury is another toxic element that may drive microbial selection and levels of up to $3 \mu\text{M}$ have been documented in several thermal springs throughout the park (King et al., 2006). The potential metabolic capability to transform trace elements is currently of major interest in enzymology as well as microbiology, thus, many of the geothermal systems in Yellowstone provide important environments for studying microbial interactions with these toxic elements.

Chemosynthetic metabolisms involving different forms of sulfur are considered important to sulfur cycling in geothermal environments (Belkin et al., 1985; Blumentals et al., 1990; Xu et al., 1998, 2000; Amend and Shock, 2001; Druschel et al., 2003; Hoaki et al., 1995; Skirnisdottir et al., 2000; Meyer-Dombard et al., 2005; Donahoe-Christiansen et al., 2004). Researchers have suggested that microorganisms utilize a variety of reduced S species, and that thiosulfate ($\text{S}_2\text{O}_3^{2-}$) and polythionate ($\text{S}_x\text{O}_6^{2-}$) may be important in energy gain through either oxidation or reduction reactions supporting microbial metabolism in many sulfur containing systems (Blumentals et al., 1990; Jorgensen, 1990; Jorgensen and Bak, 1991; Vairavamurthy et al., 1993; Druschel et al., 2003). However, sulfur chemistry in geothermal waters is complex and is not completely understood. Attempts to measure thiosulfate, polythionate, polysulfides ($\text{H}_{2-x}\text{S}_x^{-x}$), and dissolved sulfide (H_2S) pose sampling problems due to the rapid degradation of reduced S species, especially upon brief exposure to oxygen (Xu et al., 1998). Consequently, the

importance of $S_2O_3^{2-}$ and $S_xO_6^{2-}$ in microbial metabolism may often be overlooked because H_2S and SO_4^{2-} are usually the only sulfur species measured in thermal fluids (Xu et al., 1998; Nordstrom et al., 2005). Xu and collaborators (1998) measured concentrations of $S_2O_3^{2-}$, $S_xO_6^{2-}$, H_2S , and SO_4^{2-} in thirty-nine geothermal springs throughout YNP. Thiosulfate concentrations ranged from below detection ($< 0.1 \mu M$) to $38 \mu M$, while polythionates were detected in only one spring, Cinder Pool ($8 \mu M$). Furthermore, they found that $S_2O_3^{2-}$ can only persist in neutral to alkaline waters and that $S_2O_3^{2-}$ may form by surface, near-surface, or subsurface oxidation of H_2S as well as other sulfur hydrolysis reactions. In general, little is known about *in situ* microbial interactions with sulfur species in thermal systems; consequently, additional studies would be extremely useful for understanding the chemistry of these potentially significant and metabolically relevant compounds.

Joseph's Coat Spring

Interest in the discovery of unique 16S rRNA gene sequences along with the isolation of novel organisms has been conducted predominantly in geothermal springs that are easily accessible by the road system throughout YNP. One of the broader goals of this work was to investigate unique geothermal systems containing high arsenic (As) and antimony (Sb). Although the acid-sulfate-chloride springs within Norris Geyser Basin contain significant levels of dissolved arsenite at the source ($30 - 70 \mu M$), this study was conducted in part to focus on higher pH systems containing both high As and Sb, as well as dissolved sulfide. Past geochemical analysis of springs within the Joseph's Coat geothermal complex (located in the center of the Northeast quadrant of YNP; Figure

2.1) suggested that these springs contain significant levels of As and Sb (Stauffer and Thompson, 1984). In fact, the geothermal spring chosen for this work was originally named ‘Scorodite Spring’ by Hague (1880). The earliest recorded data from this system comes from the first major USGS field campaign to characterize the chemical constituents present in a variety of geothermal systems (Hague, 1880). Hague sampled and analyzed solid phases from the source pool where analysis indicated scorodite [FeAsO₄·2H₂O] as one of the predominant mineral phases. However, analysis of the mineral phase by Hague gives no details on methods or materials used in the determination, and it appears that the solid phases analyzed in this study were actually external to the main source pool. Furthermore, no spring water was sampled at that time. Regardless, the current official name of this geothermal feature is Scorodite Spring (YNP Thermal Inventory No. JCS083). For purposes of this report, and due to the fact that our research detected no scorodite, we refer to this geothermal feature as Joseph’s Coat 3 (JC3). This near-neutral pH (6.1) spring may contain the highest soluble As (~ 130 μM), Sb (~ 1 μM), and S₂O₃²⁻ (~ 800 μM) concentrations measured in YNP. As will be shown, the concentrations of total As and Sb determined in this study are nearly identical to values reported by Stauffer and Thompson (1984) for an undisclosed geothermal site at Joseph’s Coat. The concentrations of total soluble As have remained nearly constant over four annual sampling trips (Ackerman, 2006) suggesting that this site is likely identical to that referenced in Stauffer and Thompson (1984). The high dissolved sulfide coupled with extremely high dissolved S₂O₃²⁻, As and Sb in this system represents an ideal environment for studying potential interactions of microbial metabolism with observed

redox transformations important in defining the fate of dissolved As, Sb and S species within the outflow channel.

Objectives

The overall goal of this thesis work was to determine predominant biogeochemical processes occurring within a near neutral, sulfidic, high-arsenic geothermal spring in YNP. More specifically, the objectives of this work were to:

- 1) To thoroughly characterize the aqueous and solid phase geochemistry within the source pool and outflow channel of a near-neutral, sulfidic geothermal system and evaluate the role of microorganisms in As, Sb and S cycling.
- 2) To evaluate the energetics of potentially important oxidation-reduction reactions that may be used for energy generation by thermophilic microorganisms.
- 3) To isolate and characterize novel microorganisms detected using 16S rRNA molecular approaches, using information on the measured geochemical composition as well as inferred physiologies of closest cultivated relatives to design appropriate cultivation media.

To accomplish these objectives, the aqueous and solid phase geochemistry, as well as the microbial community composition of the source pool and outflow channel of JC3 were extensively characterized using data and samples collected during four annual field trips. On site experiments were also conducted to examine the relative importance of biotic versus abiotic processes. To predict possible metabolisms occurring in the spring, the energetics of potentially important redox reactions were calculated using activity

values generated with the geochemical speciation model Visual MINTEQ. The Gibbs free-energy values (ΔG_{rxn}) for a variety of possible reactions were obtained using standard free-energy values ($\Delta G^{\circ}_{\text{rxn}}$) that correspond to spring temperatures. This thermodynamic information was coupled with 16S sequence data to predict microbial metabolisms occurring in the spring. Furthermore, this information was used to develop strategies for isolating relevant populations from the spring and enabled the isolation of two novel microorganisms, both within the Crenarchaea. These two archaea were shown to be dominant populations in the source pool and the warmer portion of the outflow channel (based on 16S rRNA gene sequence characterization) where they are likely involved in respiration of elemental sulfur. This extensive investigation of Joseph's Coat 3 represents a significant contribution to our understanding of the linkages between the geochemistry and microbiology in of one of the most interesting and unique geothermal springs in Yellowstone National Park.

CHAPTER 2

MATERIALS AND METHODS

Geothermal Site

There are approximately 155 different geothermal features in the Joseph's Coat (JC) Springs complex located roughly 8 km east of Canyon, Yellowstone National Park (YNP) (Figure 2.1A, B). Many of the springs are acidic, ranging in pH from ~ 2.0 to 3.0, and several contain relatively high concentrations of dissolved iron (~100 μM) [see Ackerman (2006) for a complete description of the geochemistry of high-ammonium acid-sulfate springs of this region, as well as descriptions found in Fournier (2005) and Lodge et al. (2003)]. The focus of this research, however, is a near-neutral geothermal spring (pH ~ 6.1) in the Joseph's Coat Springs geothermal basin (Figure 2.1C, D), unofficially referred to here as JC3 (44°44'21.4"N, 110°19'28.2"W; YNP Thermal Inventory Number JCS083).

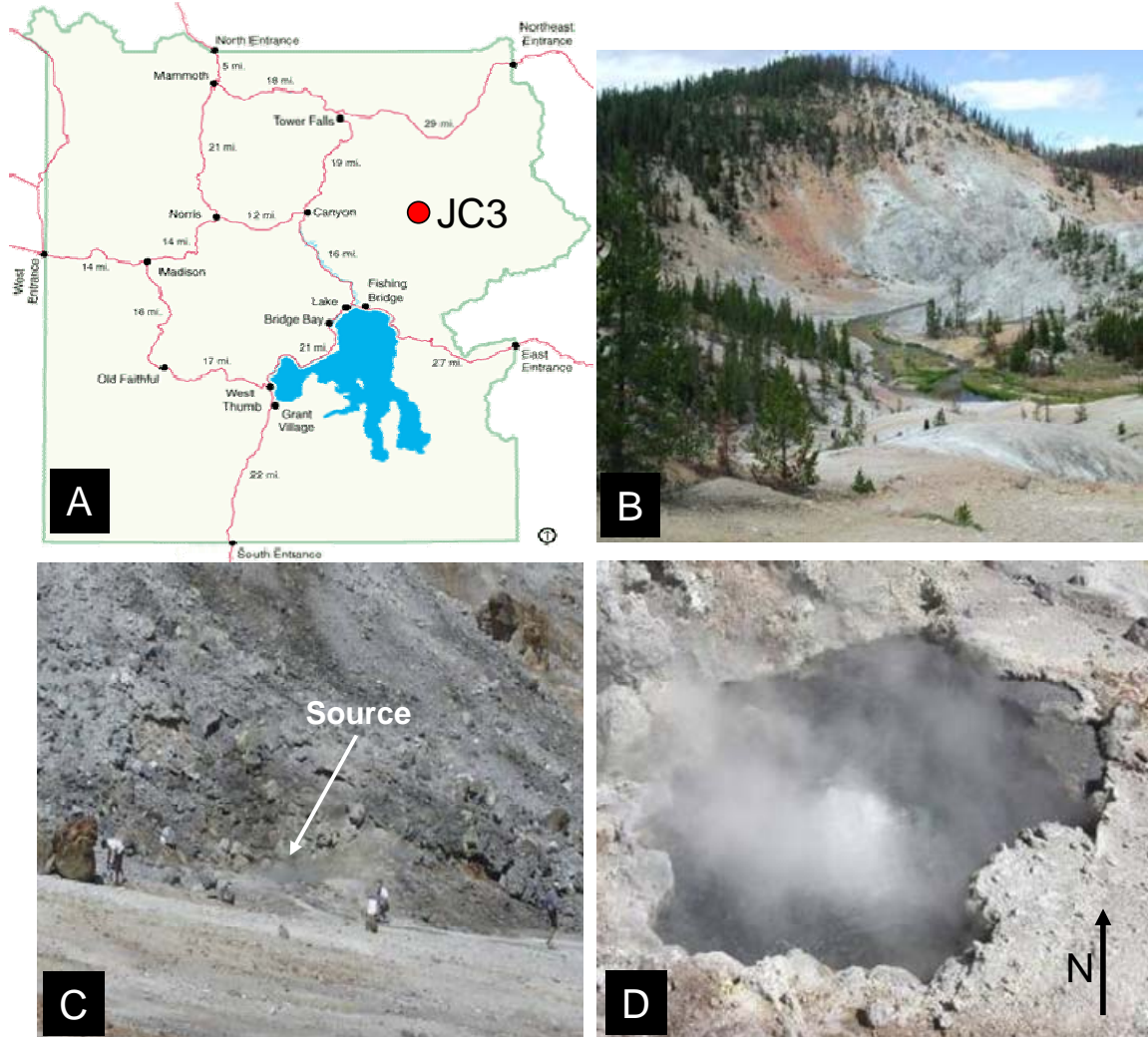


Figure. 2.1. A. Map of YNP showing major roads and the location of Joseph's Coat Springs (JC3; courtesy of <http://www.yellowstonenationalpark.com>). B. Photograph looking northwest into the Joseph's Coat Spring complex. C. Photograph showing location of JC3 source pool. D. Close up of JC3 source pool in August 2004.

This geothermal spring is unique in that it may contain the highest concentrations of arsenic (As), antimony (Sb), and thiosulfate ($S_2O_3^{2-}$) found in any known major geothermal feature of YNP. The geothermal source consists of a 3 - 4 m diameter, violently boiling pool whose water level is held constant by a small outflow channel located at the east edge (Figure 2.2A). The hottest regions of the source pool are lined

with a hard, 2-3 mm thick, lustrous, silver-colored solid phase which has been shown to consist of pyrite (FeS_2) and what appears to be a stibnite-like phase (Sb_2S_3) (Figure 2.2B). Visual inspection indicates that the source pool is at least two meters deep, and although the spring is perpetually boiling and frothing, no visual evidence was observed in our brief 2 - 4 day visits during 4 consecutive summers suggesting that this pool erupts as a geyser. A shelf of soft sediments is located on the east side of the spring approximately 1 m north of the outflow channel and encompasses roughly 15 % of the pool perimeter (Figure 2.2D). These shelf sediments are bathed in approximately 3 - 5 cm of geothermal spring water. Temperatures decline considerably towards the east edge of the source pool and the shallower sediments (< 3 cm) can exhibit temperatures as low as 70 - 75 °C. The temperature of the shelf sediments in deeper water (~ 5 cm) ranged from 80 - 88 °C. A top gray-black sediment layer (~ 1 - 2 mm) was underlain by orange, yellow, and gray interbedded layers. In some locations on this shelf, the total depth of the sediment layers was in excess of several cm thick. Orange and, to a greater extent, yellow subsurface sediment layers were also observed throughout the outflow channel (Figure 2.2D, E, F).



Figure 2.2. A. JC3 source pool showing the location of the outflow channel. B. Close-up of the unique metallic solid phases formed in the JC3 source pool. C. Photograph showing the outflow channel exiting the east side of the source pool. D. Sampling the source pool shelf sediments E. Core sample from shelf sediments showing stratification F. Stratified layers in outflow channel sediment. Photos were taken in August of 2004.

After multiple trips to this field site during the last four summers (2003 - 2006), there is no evidence that the water level varies to any significant degree, and flow volumes in the outflow channel have remained relatively constant at approximately 10 L min⁻¹, without noticeable pulsing. During the four year sampling period, source water temperatures averaged 91 °C (essentially boiling at this elevation and pressure: elevation = 2440 m, pressure = 0.73 atm). The first 12 meters of the outflow stream is confined to a narrow (~ 5 - 10 cm wide) channel, which opens into a broader fan further down gradient (Figure 2.3A, B). The source pool and outflow stream were sampled annually during the summers of 2003 through 2006. Aqueous and solid phase geochemistry in conjunction with microbial community composition (16S rRNA gene sequences) was analyzed as a function of distance from the source pool. Transects included six sampling positions originating at the source pool and continuing down gradient until water temperatures approached approximately 50 °C (Figure 2.3B).

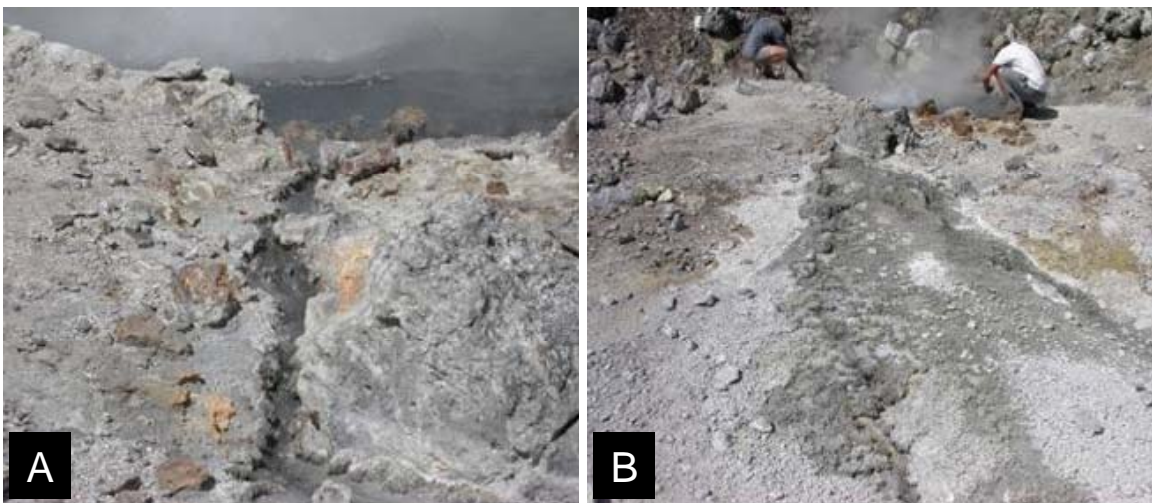


Figure 2.3. Photographs showing the outflow channel exiting the east side of the source pool (A) and extending down gradient (B) (August of 2004).

Aqueous geochemistry and dissolved gases

At each sampling location, filtered (0.2 μm) aqueous samples were obtained using sterile 60 mL syringes and transferred to two 50 mL sterile screw-cap FalconTM tubes. One sample was preserved using ultra-pure HNO_3 (to 1%) and analyzed for total dissolved Ca, Mg, Na, K, Si, Al, As, Fe and B and trace elements including Cd, Cr, Cu, Mn, Ni, Pb, Sb, Se and Zn using inductively coupled plasma atomic absorption spectrometry (ICP-AES). A second subsample that was not acidified was analyzed for inorganic anions (F^- , Cl^- , SO_4^{2-} , NO_3^- , CO_3^{2-} , $\text{S}_2\text{O}_3^{2-}$, AsO_4^{3-}) using anion exchange chromatography (Dionex Corp., Sunnyvale, CA, USA; AS16-4 mm column). This sample was also analyzed for aqueous NH_4^+ and NO_3^- using the phenolate colorimetric ($A_{630\text{nm}}$) procedure (APHA, 1998) performed on a flow injection analyzer (Lachat QuickChem FIA+ auto analyzer; Zellweger Analytics, Milwaukee, WI). A Dohrmann C-analyzer (Dohrmann DC-80; Teledyne, Mason, OH, USA) was used to determine dissolved inorganic C (DIC) and dissolved organic C (DOC; acidified to 70 mM H_3PO_3 and sparged with O_2 to remove DIC) in separate 0.2 μm - filtered samples obtained with no headspace in 30 mL glass serum bottles, crimped with butyl septa and Al rings. Several important redox sensitive species were analyzed (or preserved) in the field. Ferrous and ferric Fe were determined on site using the Ferrozine method (To et al., 1999). Total dissolved sulfide (DS) was determined on site using the amine sulfuric acid method (APHA, 1998) on unfiltered samples to circumvent rapid degassing of $\text{H}_2\text{S}(\text{aq})$ (this spring does not normally carry significant suspended loads and aqueous samples used for on-site sulfide analysis were generally free of major turbidity). Arsenic species

were preserved on site (As^{III} and As^{V}) using samples treated and untreated with Na-borohydride in the field, followed by laboratory analysis using hydride generation atomic absorption spectrometry (Langner et al., 2001). Briefly, the Na-borohydride procedure involves filtering 5 mL of sample into a 15 mL HDPE bottle containing 1 mL of 2 M Tris buffer (pH 6). While sparging the mixture with $\text{N}_2(\text{g})$, 1 mL of 0.25 M NaOH and 0.79 M NaBH_4 was added in 0.2 mL increments over 4 min to reduce As^{III} to arsine gas which was removed by sparging. The sample was immediately preserved in 1 % HCl and the remaining As^{V} was later analyzed using HG-AAS. Concentrations of As^{III} were determined by difference between As_{TS} and As^{V} . Dissolved O_2 (DO) was determined using an on-site, modified Winkler method (APHA, 1998). Briefly, the analysis was conducted using a DO Test Kit from Hach (Product # 146900, Hach Corp, Loveland, CO) with the exception that the initial reactions were conducted in a syringe. A 60 mL syringe was filled with 50 mL sample and capped with a rubber septum to avoid any contact with the atmosphere. Two 1 mL syringes with needles were used to inject 0.4 mL of 2.15 M MnSO_4 and 0.4 mL of alkali-iodide-azide solution (12.02 M NaOH, 0.869 M KI, 0.15 M NaN_3) respectively, through the septa. The sample was inverted several times to mix the suspension, and allowed to equilibrate for 3 - 5 min or until the resulting floc settled. This mixing and settling process was repeated before 0.4 mL concentrated H_2SO_4 was added via another needle and syringe. The syringe was inverted until the floc completely dissolved (~ 5 min), then 30 mL of the mixture was added to a 60 mL glass bottle. The solution was titrated with sodium thiosulfate (0.0101 M) to quantify DO. Aqueous pH and temperature were obtained using a Mettler-Toledo portable ion meter

(MA130) equipped with a temperature correcting probe; standardized buffers were calibrated at spring temperatures.

Headspace gas chromatography (GC) was utilized to determine dissolved H₂, CH₄, and CO₂. Samples for dissolved gas analysis were collected using an in-line 142 mm, 0.2 μm filter and peristaltic pump to fill 160 mL glass serum bottles. The bottles were purged with 3 - 4 pore volumes of sample, then capped with zero headspace using butyl stoppers and Al rings. Prior to GC analysis, known volumes of liquid were removed from serum bottles and replaced with an equivalent volume of N₂ (g). The bottles were then shaken at 150 cycles per min for 1 h at room temperature and the resultant headspace was analyzed using a Varian gas chromatograph (Model CP2900; Varian Inc., Palo Alto, CA) equipped with a dual channel thermal conductivity detector system using Ar and N₂ as carrier gases. Headspace gas concentration values were used to calculate the amount of dissolved gas in the equilibrium solution, as well as in the initial sample using Henry's Law constants for each gas (Amend and Shock, 2001) along with a mass balance equation for total dissolved gas prior to headspace equilibration:

$$\text{Henry's law: } K_H = c(\text{aq})/c(\text{g}) \quad (4)$$

$$\text{Mass balance: } [c(\text{aq})_{\text{sample}} V_{L, \text{initial}}] = [c(\text{g})_{\text{equil}} V_{g, \text{eq}}] + [c(\text{aq})_{\text{equil}} V_{L, \text{equil}}] \quad (5)$$

where K_H = Henry's Law constant at temperature of equilibration (K_H values adjusted for temperature from thermodynamic constants reported in Amend and Shock, 2001), c = concentration in either gas or aqueous phase (mol L⁻¹), and V = volume of liquid or gas.

Thiosulfate and polythionate analysis

Thiosulfate concentration was determined using ion chromatography (as described above) on samples collected using several protocols (Xu et al., 1998). Since the aqueous samples were obtained in the backcountry, IC analysis was not completed until 5 days after sampling. Consequently, several different methods of sample storage were compared, especially during the most recent sampling event in 2006. Aqueous samples obtained in 2003 - 2004 were collected with no headspace, stored at $\sim 4 - 10^\circ\text{C}$ and analyzed without exposure to ambient atmosphere. Additional closed headspace serum bottles were stored in an anaerobic chamber during travel back to the laboratory and compared directly with samples stored in serum bottles only. Finally, during 2006, samples were also preserved in the field by injecting 29 mL of spring water into 30 mL amber bottles containing 1 mL of a 1 M ZnCl_2 solution to fix dissolved sulfide, and minimize any conversion of sulfide to thiosulfate during sample storage. Polythionate analysis was conducted in 30 ml amber bottles containing 1 mL of 1 M ZnCl_2 , 1 mL of 1 M NaOH , and 1 mL of 1 M KCN solutions. Polythionates were then analyzed by determining the difference between cyanolyzed and uncyanolyzed samples using the same IC protocol as described above. If present, polythionates are cyanolysed, which generates thiocyanate and thiosulfate according to the reaction:



The composition of the chromatographic peak with a retention time matching that of standard $\text{S}_2\text{O}_3^{2-}$ was verified by collecting 1 mL volumes using a fraction collector and analyzing these solutions using ICP-AES. The calculated S concentration of the peak

corresponded to values expected for $S_2O_3^{2-}$ and no other elements such as arsenic (As) were detected.

Solid Phase Characterization

The composition, structure and mineralogy of solid phases deposited at the source and within the outflow channel were subjected to a suite of analytical procedures including: (i) X-ray diffraction (XRD), (ii) scanning electron microscopy along with energy dispersive analysis of X-rays (SEM/EDAX), (iii) field emission scanning electron microscopy (FESEM) coupled with small spot electron backscatter analysis, and (iv) acid digestion (HNO_3 - $HClO_4$ - HF at $110^\circ C$) of solid phases according to methods described in Inskeep et al. (2005). The composition of solid phases present in this system was used in combination with aqueous geochemical data to ascertain the primary chemical habitats available to microorganisms and to design appropriate media for cultivation of relevant thermophiles.

Chemical Speciation and Thermodynamic Calculations

To evaluate the potential for chemolithotrophic and chemoorganotrophic metabolism, the free energy values (ΔG_{rxn}) of numerous oxidation-reduction reactions were calculated using standard state Gibbs free energy values (ΔG_{rxn}°) corrected for temperature and predicted activities of chemical species using the expression:

$$\Delta G_{rxn} = \Delta G_{rxn}^\circ + RT \ln(Q_{rxn}) \quad (7)$$

where ΔG_{rxn}° is the temperature dependent standard state free energy of reaction ($kJ\ mol^{-1}$) and Q_{rxn} is the reaction quotient calculated using actual activities of chemical species (Stumm and Morgan, 1996; Amend and Shock, 2001; Amend et al., 2003;

Inskeep et al., 2005). Most temperature-dependent $\Delta G^{\circ}_{\text{rxn}}$ values were obtained from Amend and Shock (2001). Thermodynamic data for reactions with dissolved and solid phase Sb compounds were obtained from Filella and May (2003). Values of $\Delta G^{\circ}_{\text{rxn}}$ not provided in Amend and Shock (2001) or other literature were calculated from temperature corrected standard free energies of formation (ΔG°_f ; Amend and Shock, 2001). Measured values of total soluble chemical constituents were used as input to calculate the activities of chemical species with the aqueous equilibrium model, Visual MINTEQ (Ver 2.50, Allison et al., 1991). Solid phase, gas and redox equilibria were suppressed during chemical speciation calculations to specifically represent the solution as sampled.

Microbial Community 16S rRNA Gene Analysis

Analysis of 16S rRNA gene sequences from mat and sediment samples was used to assess the distribution of microbial populations across geochemical and temperature gradients observed in the source pool and outflow channel. Sediments were collected utilizing aseptic techniques into sterile 15 mL Falcon™ tubes, and immediately placed on dry ice for transport to a -80 °C freezer. The FastDNA SPIN Kit for Soil (Q-Biogene, Irvine, CA, USA) was used to extract total DNA from the samples, which served as template for PCR of 16S rRNA genes using both *Bacteria*-specific [Bac8f (5'-AGAGTTTGATCCTGGCTCAG-3')] and *Archaea*-specific [Arc2f (5'-TTCCGGTTGATCCYGCCGGA-3')] forward primers coupled with the universal reverse primer Univ1392r (5'-ACGGGCGGTGTGTAC-3'). Purified PCR products were cloned using the pGEM-T Vector System (Promega Corp., Madison, WI, USA), and the inserts

were sequenced using T7P and SP6 primers (TGEN, Phoenix, AZ or The Plant Microbe Genomics Facility at Ohio State University). DNA sequences were aligned using the Sequencher program (v.4.5, Gene Codes Corp, Ann Arbor, MI). Primer sequences were located and deleted from the consensus sequence, and then sequences were compared to others in the GenBank database using the BLAST algorithm search tool (Altschul et al., 1997). The DNA extraction, PCR amplification, cloning, and sequencing of 16S rRNA genes from JC3 were performed on samples collected during summers of 2003, 2004 and 2005 primarily by Ms. Sarah Korf a Research Associate employed in Dr. Inskip's laboratory. Forty-eight clones from each sampling position believed to contain proper sequence insertion were screened for correct insertion length (bp = 1300 – 1400) by running PCR amplified clones on an agarose gel. Clones determined to have the correct insertion size were sent for sequencing.

Ex-Situ Bioassay

Equal volumes of soft sediment were taken from a sampling point within the main outflow channel and transferred aseptically into three, 1000 ml, screw-top glass bottles. Immediately after inoculation, 500 ml of JC3 unfiltered source pool geothermal water was injected into the bottles with a 60 ml syringe. 5 ml of formaldehyde was added to the killed control bottle. A fourth bottle, containing only 500 ml filtered (0.22 μ M) source pool spring water was prepared as a blank. All four bottles were transferred to a nearby hot pool for incubation at 70 °C. Aliquots (20 mL) were taken from each bottle for sampling of As and Sb concentrations with a 30 mL syringe at sampling times of 0, 0.5, 2.5, and 24 hrs.

Isolation of Anaerobic Crenarchaea

Sediment samples (76 - 80 °C) were collected from the shallow shelf located on the east side of the source pool (August 2005 and 2006) using a sterile 60 mL syringe and injected immediately into a sterile 40 mL serum bottle. The serum bottle was filled with spring water, capped with a butyl rubber septum with no headspace, and stored at ambient temperatures (25 – 30 °C) for 5 d. Samples of the sediment suspension (0.5 mL) were used as inoculum into 10 mL serum bottles containing 5 mL of synthetic growth media, and serially diluted to 10^{-6} in triplicate. The serum bottles were incubated at 75 °C \pm 2° without shaking. The synthetic growth media used for cultivation of anaerobic thermophiles contained 4.4 mM KCl, 6.2 mM NH₄Cl, 2.4 mM KH₂PO₄, 1.62 mM MgCl₂, 2.2 mM CaCl₂, 2.1 mM Na₂S, 1 g L⁻¹ starch, 0.2 g L⁻¹ yeast extract (Difco), 15 µg mL⁻¹ Kanamycin, 15 µg mL⁻¹ Vancomycin, 1 mL L⁻¹ trace element solution (Pfennig and Lippert, 1966), 1 mL L⁻¹ vitamin solution (Wolin et al., 1963) and 1 mg L⁻¹ resazurin supplemented with 0.05 g L⁻¹ elemental sulfur. Media pH was adjusted to 7.0 with HCl or NaOH before addition to serum bottles. The headspace (5 mL) was purged with 99.96 % N₂ (g) for 30 minutes prior to addition of 100 µL 0.1 M cysteine, added to scavenge remaining O₂. The addition of cysteine lowered the pH to ~ 6.0. CO₂ (g) was added during initial isolation (10 % v/v) but was omitted after ascertaining the isolates grew heterotrophically. These culture conditions were designed to be consistent with anaerobic zones in the source pool sediments of JC3, and targeted microorganisms capable of heterotrophic growth and respiration on elemental S⁰.

The concentration of H₂S was measured after 5 days, using a modified version of the amine-sulfuric acid method (APHA, 1998). The modified low-volume method utilized 33 μL of amine sulfuric acid reagent and 10 μL of FeCl₃ reagent mixed in a 1.5 mL centrifuge tube. A 50 μL aliquot of sample was injected beneath the surface of the mixture to minimize loss of H₂S, followed by addition of 450 μL deionized H₂O. Blanks received 500 μL H₂O. Di-hydrogen phosphate reagent (3.79 M H₂PO₄) was added (107 μL) and the tubes were vortexed for 30 s, then centrifuged at 13,000 x g for 1 min to remove precipitate. Approximately 600 μL of the supernatant was used to measure absorbance ($A_{664 \text{ nm}}$) on an Ocean Optics Spectrophotometer (CHEMUSB4-VIS-NIR, Dunedin, Florida, USA). The most dilute cultures showing H₂S production were transferred to the same media and serial diluted to 10⁻⁷. Successive cycles of dilution to extinction resulted in the isolation of a single organism and a co-culture. Both the pure culture and the co-culture were transferred every 10 - 15 d using the above described media and methods.

Microbial populations present in the cultures were monitored a combination of optical microscopy and denaturing gradient gel electrophoresis (DGGE) of partial 16S rRNA gene fragments (Muyzer et al., 1993). The FastDNA SPIN Kit for Soil (Q-Biogene, Irvine, CA, USA) was used to extract total DNA from the serum bottle cultures. This DNA served as template for PCR using *bacteria*-specific [Bac1070f (5'-ATGGCTGTCGTCAGCT-3')] and *archaea*-specific [Arc931f (5'-CACCCCTTGTGGTGC-3')] forward primers coupled with the universal reverse primer Univ1392r (5'-ACGGGCGGTGTGTRC-3'), which incorporated a 40 bp GC-clamp

(Macur et al., 2004a, b). The primers were added to the PCR mixture at a concentration of 0.5 μ M, along with 10 mM Tris-HCl (pH 8), 50 mM KCl, 4.0 mM MgCl₂, 800 μ M dNTP's, 1.25 U *Taq* DNA polymerase (Promega, Madison, WI), and 1-5 μ L DNA template (2 – 20 ng). Thermocycler protocol was 94 °C for 5 min, followed by 32 cycles of 94 °C, 52 °C, and 72 °C each for 45 s, with a final 7 min extension period at 72 °C. To ensure purity, negative control reactions were performed with all PCR reagents along with positive controls using *Escherichia coli* DNA (*E. coli* is amplified by both bacterial and archaeal primer sets). DGGE gels consisting of 8 % acrylamide and a 35 – 65 % urea/formamide denaturing gradient were used to separate the 16S rRNA fragments (~ 90 ng total PCR product per lane). A DCode System (Bio-Rad, Hercules, CA) was utilized for electrophoreses at 60 V and 60 °C for 17 h. The resultant gel was stained with SYBR Green II (Molecular Probes, Eugene, OR) for 30 minutes prior to imaging using UV transillumination. To identify the organisms in culture, clone libraries of near-full length 16S rRNA gene sequences from cultures were sequenced using the methods described above.

Fluorescence Microscopy

Cultures were examined using fluorescence microscopy after staining with an equal volume of 10x SYBR-Green II (Molecular Probes, Eugene, OR) for 5 minutes. A 10 μ L aliquot of the stained media was placed on a glass slide and heat fixed (10 min at 85 °C). A Zeiss Axioskop 2+ fluorescent microscope (Carl Zeiss Inc., Germany) was used to identify morphology, to confirm isolate purity, and to monitor growth (cell numbers).

Growth Curves and Growth Optima

Several cycles of dilution to extinction on different replicate cultures inoculated with JC3 source pool sediments and incubated at 75 °C resulted in two cultures. One culture exhibited only rods while the other was a co-culture exhibiting cocci and rods. By process of elimination, rod-shaped organisms in each culture had identical 16S rRNA gene sequences (1336 bp) and was designated strain WP28t, while the cocci was designated WP29d. Growth curves were generated for strain WP28t in triplicate using the above described standard media at pH 6.0, T = 75 °C, and 0.2 g/L yeast extract. Bottles used for growth curve experiments were initially inoculated with 10^3 cells mL⁻¹ based on direct counts using a Zeiss phase-contrast microscope and a Petroff-Hausser Counting Chamber (Hausser Scientific). Experiments designed to determine the optimum temperature for growth of strain WP28t were performed using cells inoculated during log phase growth (10ml serum bottles; 10^5 cells mL⁻¹) into fresh media (described above). A custom-made, water jacketed aluminum heat-block was utilized to generate a thermal gradient of 45.7 - 99.5 °C (std. dev. \pm 0.2 °C) over the length of the block. Holes were drilled into the block to allow placement of triplicate serum bottles at equally spaced positions across the thermal gradient. After five days, H₂S concentrations and cell numbers were determined as a function of temperature. The pH optimum of strain WP28t was determined by adjusting the pH of the growth media with either HCl or NaOH after the addition of 5 mM HEPES, 5 mM MES, and 10 mM H₃BO₃ buffers to obtain 7 pH values ranging from 4 to 10. Three replicate serum bottles per pH treatment were inoculated with 10^5 cells mL⁻¹ and incubated at 75 °C. After 5 d, H₂S concentrations

and cell counts were determined for each serum bottle along with a final pH measurement. Uninoculated serum bottles were used to check for pH stability before and after the start of each experiment, and for use as a H₂S blank for dissolved sulfide measurements. The maximum pH variation between initial and final measurements was < 0.3 pH units. To test for growth under microaerobic conditions, one mL of sterilized air (5 ml headspace) was injected into inoculated serum bottles, creating a 2 % O₂ headspace environment.

Isolate Metabolism

Unless otherwise stated, the pure culture (strain WP28t) and the co-culture isolate were grown in triplicate in standard synthetic media (see above) under a N₂ (g) atmosphere at 75 °C. After 5 d, growth was monitored by direct counting (cells mL⁻¹, final conc. minus initial conc.) using phase-contrast light microscopy and by measuring dissolved sulfide concentrations using the low-volume sulfide method described above. The ability of strain WP28t to utilize various substrates as a C and energy source was evaluated including D-glucose (J.T. Baker Chemical Co., Phillipsburg, N.J.), lactose (Sigma Aldrich Chemical Co., Milwaukee, W.I.), soluble starch (Sigma Aldrich Chemical Co., Milwaukee, W.I.), and acetate (J.T. Baker Chemical co., Phillipsburg, N.J.) added at 4% (w/v). Various amounts of yeast extract (YE) and tryptic soy broth (TSB) were also tested to ascertain potential carbon and energy sources for strain WP28t and the co-culture (0.0, 0.002, 0.02, and 0.2 g L⁻¹). To check for autotrophic growth, 1.25 mL of 99.96 % CO₂ (g) was added to the headspace (final headspace composition of 25 % CO₂ and 75 % N₂) in the absence of any potential organic carbon sources; a trace

amount of YE (0.002 g L^{-1}) shown to be required for growth was utilized. The ability to ferment YE was determined by the addition of 0.2 g L^{-1} YE to the media, while all other potential electron acceptors were excluded from the media. Possible electron acceptors other than elemental S^0 were tested by excluding S^0 from the media and adding either As^{V} (5 mM ; $\text{Na}_2\text{HAsO}_4 \cdot 7\text{H}_2\text{O}$; Aldrich Chemical Co. Milwaukee, W.I.), Fe^{III} (0.02 g L^{-1} ; Fe_2O_3 ; J.T. Baker Co., Phillipsburg, N.J.) or Sb^{V} (0.02 g L^{-1} ; Sb_2O_5 ; Acros Organics, New Jersey, USA). Finally, given the high thiosulfate levels observed in JC3 strain WP28t was evaluated for thiosulfate usage as an electron acceptor by the addition of a final concentration of $10 \text{ mM S}_2\text{O}_3^{2-}$ (Sigma Aldrich Chemical Co., Milwaukee, W.I.) to the standard media

Archiving Isolates

To preserve pure-culture isolates and co-cultures, 0.25 mL of DMSO was injected into 10 mL serum bottles containing 5 mL of actively growing organisms (final DMSO concentration = 5%). After 30 min , 1 mL of the solution was withdrawn from the serum bottle and injected into $2 \text{ mL N}_2(\text{g})$ filled screw-cap serum vials (butyl septa) containing $100 \mu\text{L}$ of 0.1 M cysteine. The 2 mL vials were submerged directly into liquid $\text{N}_2(\text{g})$ for several minutes to rapidly freeze the suspension. The vials were then placed in a $-80 \text{ }^\circ\text{C}$ freezer for storage. To test for revivability after 30 d , the frozen cultures were allowed to thaw at room temperature and aliquots (0.5 mL) were injected into prepared serum bottles containing synthetic media and incubated as described above. In all cases, growth resumed after 72 h .

CHAPTER 3

RESULTS

Aqueous Geochemistry

One of the primary goals of this study was to characterize the geochemistry and geomicrobiology of a unique, near-neutral pH, high-temperature geothermal spring (JC3) in Joseph's Coat Basin. Extensive on-site and laboratory analyses of aqueous and solid phases within the source pool and outflow channel were conducted during four annual summer sampling trips from 2003 through 2006. Source pool temperatures and pH averaged 91 ± 2 °C and 6.1 ± 0.07 , respectively (Figures 3.1 and 3.2). Temperatures decline from approximately 90 °C at the source pool to 44 °C at 12 m down gradient in the outflow channel. The pH values increased from 6.1 ± 0.07 at the source to 6.5 ± 0.2 by 12 m, due likely to the outgassing of H₂S and or CO₂, which at the pH of the spring, will consume protons according to the following reactions (Nordstrom et al., 2005):



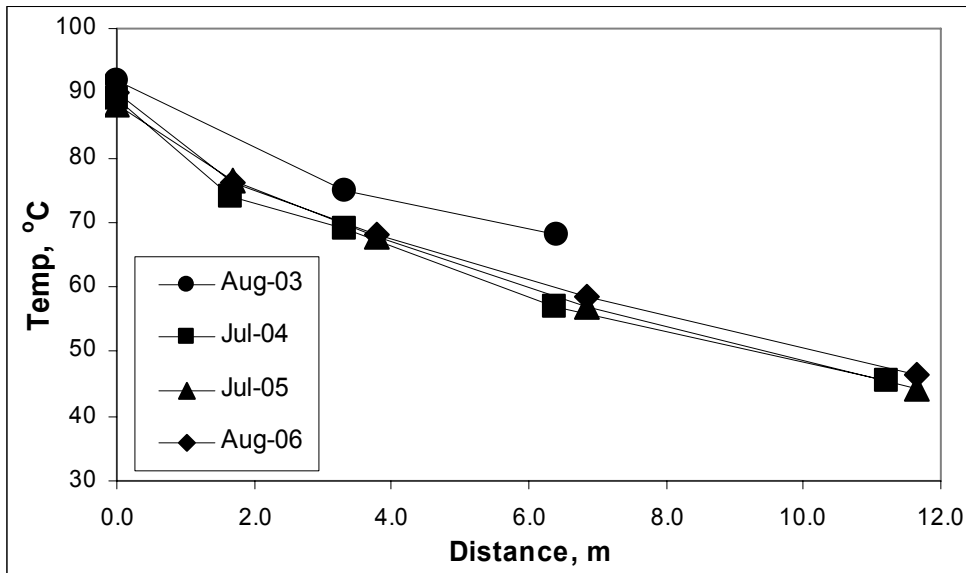


Figure 3.1. Temperature values within the outflow channel of geothermal spring JC3 measured as a function of distance from the source pool (results shown for four annual sampling trips).

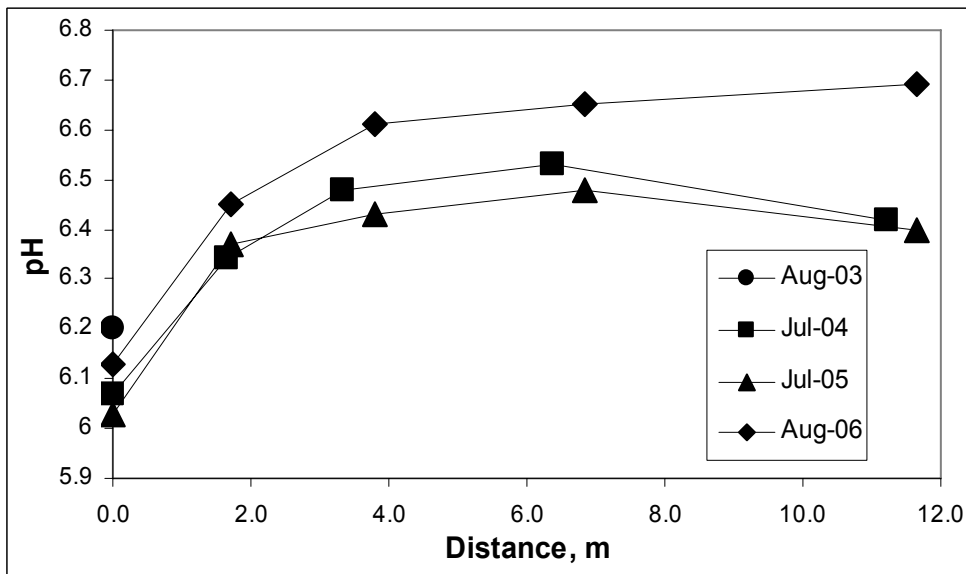


Figure 3.2. Aqueous pH values measured as a function of distance from the geothermal source for annual sampling events during 2003 - 2006 (only source water pH is reported for 2003).

Dominant Cations and Anions

Extensive analysis of aqueous phase chemistry over the duration of this study showed that the concentrations of nearly all inorganic chemical constituents were quite stable and generally varied less than 10 percent over four annual sampling trips (Table 3.1; see Appendix A, Table A.1 for complete data set for all transect positions). Cations are dominated by Na^+ ($11.4 \pm 0.2 \text{ mM}$), NH_4^+ ($5.6 \pm 0.3 \text{ mM}$), and K^+ ($2.1 \pm 0.04 \text{ mM}$), while dominant anions included Cl^- ($10.3 \pm 1.2 \text{ mM}$), SO_4^{2-} ($4.2 \pm 0.2 \text{ mM}$), $\text{S}_2\text{O}_3^{2-}$ ($0.75 \pm 0.09 \text{ mM}$), F^- ($0.4 \pm 0.03 \text{ mM}$), and HCO_3^- ($0.07 \pm 0.03 \text{ mM}$). The dominant ions in the system, Na^+ and Cl^- , were present at a molar ratio of nearly 1:1. Measurable increases in the concentrations of the major cations and anions such as Cl^- , F^- , Na^+ , and SO_4^{2-} of approximately 11 percent down gradient of the source (Appendix A, Table A.1) are likely due to evaporation (Nordstrom et al., 2005). Ammonium (NH_4^+) was the second most important cation detected in the spring, while in comparison, NO_3^- represented only about 0.1 % of the total N. The high ammonium levels in geothermal springs in this region of YNP apparently originate from the distillation of buried hydrocarbon sediments (Fournier, 2005), and suggest that oxidation reactions where NH_4^+ serves as an electron donor may be energetically favorable in this system. However, no changes in down gradient concentrations of either NH_4^+ or NO_3^- were observed (Appendix A, Table A.1).

Table 3.1 Average total dissolved concentrations and standard deviations of predominant chemical constituents measured in the source water of Joseph's Coat Spring (JC3) over four annual sampling events (2003 – 2006).

Parameter	Unit	Value	Parameter (continued)	Unit	Value
Temperature	°C	89.9 ± 1.6	B	mM	5.6 ± 0.08
pH		6.1 ± 0.1	Si	mM	3.9 ± 0.2
Na ⁺	mM	11.4 ± 0.2	As ^{III}	μM	107 ± 11
NH ₄ ⁺	mM	5.6 ± 0.3	As ^V	μM	22 ± 4
K ⁺	mM	2.1 ± 0.04	Mn	μM	4.6 ± 0.3
Ca ⁺²	mM	0.4 ± 0.004	Sb ^{III}	μM	0.6 ± 0.5
Mg ⁺²	μM	40 ± 2	Sb ^V	μM	0.3 ± 0.1
Al ⁺³	μM	1.2 ± 0.6	Ba	μM	0.8 ± 0.09
Fe ^{II}	μM	0.5 ± 0.2	Zn	μM	0.2 ± 0.1
Fe ^{III}	μM	<0.2 ± na ⁶	CO ₂ (aq)	mM	0.2 ± 0.09
Cl ⁻	mM	10.3 ± 1.2	¹ CO ₂ sat. index	μM	2.0
SO ₄ ²⁻	mM	4.2 ± 0.2	² DS	μM	22 ± 7
S ₂ O ₃ ²⁻	mM	0.75 ± 0.09	CH ₄	μM	0.9 ± 0.1
F ⁻	mM	0.4 ± 0.03	H ₂	nM	108 ± 53
NO ₃ ⁻	μM	9.6 ± 5.7 ⁶	³ DOC	μM	58.0
P	μM	3.2 ± 1.5	⁴ DIC	mM	0.35
			⁵ Ionic strength	mM	23.4

1 CO₂ saturation index =
 $\log[\text{CO}_2(\text{aq})/\text{CO}_2(\text{aq}, p\text{CO}_2 = 0.00035\text{atm})]$.

2 DS = total dissolved sulfide.

3 DOC = total dissolved organic carbon.

4 DIC = total dissolved inorganic carbon.

5 Ionic strength at spring temperature calculated using MINTEQA (Allison et al., 1991)

6 Constituents exhibiting high standard deviations were often close to detection e.g. (NO₃⁻, Sb, Fe, P and Zn)

Gas Exchange: Foundation for Understanding Outflow Channel Processes

The concentrations of dissolved CO₂, CH₄, H₂S, and H₂ in the geothermal source waters of JC3 are significantly supersaturated with respect to atmospheric conditions

(Table 3.1). Consequently, when these geothermal waters come into contact with the atmosphere, they are immediately subject to degassing of supersaturated constituents, as well as ingassing of atmospheric O₂ (Figure 3.3).

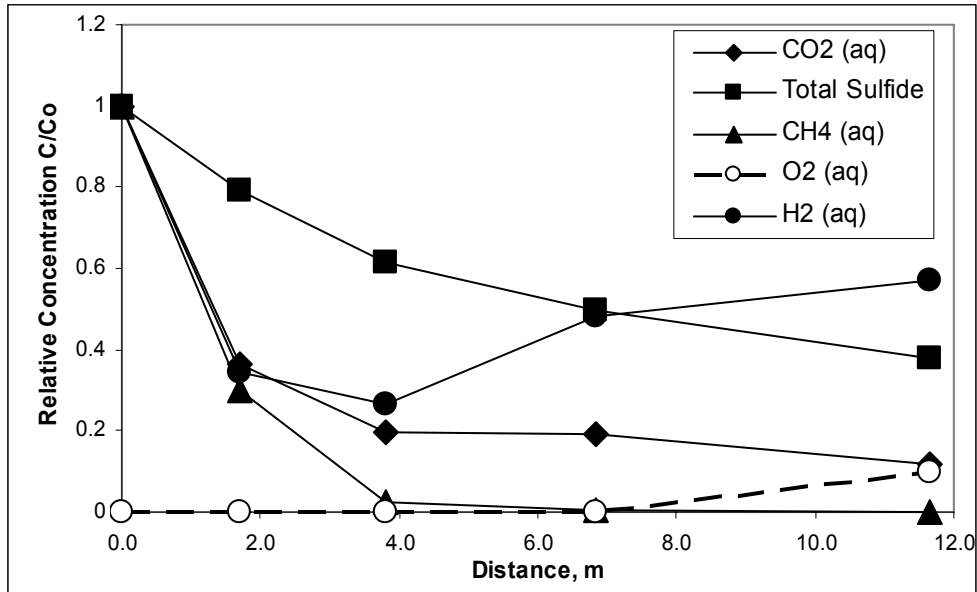


Fig. 3.3. Relative concentrations of dissolved gases plotted as a function of distance (cm) from the geothermal source (n=4). The relative concentrations of H₂, CO₂, H₂S, and CH₄ are calculated based on C₀ values measured within the source pool (Table 3.1). Conversely, dissolved O₂ values are calculated as a fraction of theoretical saturation values (theoretical saturation = 143 μM at 75 °C).

The rates of degassing depend on a number of factors including initial aqueous concentration of dissolved species, atmospheric concentrations, pH, temperature and hydrodynamic processes influencing boundary layer dynamics at the air-water surface.

The concentration of total dissolved inorganic C (DIC) in the source waters of JC3 (0.35 ± 0.2 mM) represents all carbonate species including CO₂ (aq) (or H₂CO₃, depending on nomenclature), HCO₃⁻ and CO₃²⁻. The concentration of CO₂ (aq) in the source pool corresponds to a CO₂ saturation index ($\log[\text{CO}_2(\text{aq})/\text{CO}_2(\text{aq}, 0.00035 \text{ atm})]$) of

2.0 (calculated using Visual Minteq). This represents a $p\text{CO}_2$ value that is more than 100 times greater than the $p\text{CO}_2$ value predicted for waters in equilibrium with atmospheric CO_2 (g) (0.00035 atm). Concentrations of DIC drop rapidly down gradient to 0.2 mM by 4 m, then more gradually to 0.1 mM by 12 m (Appendix A). The gradual decline in DIC throughout the outflow channel of JC3 is in contrast to more rapid losses of DIC observed in acidic geothermal springs (Langner et al., 2001; Ackerman, 2006). The differences in DIC disappearance rates between the near-neutral JC3 and the acidic springs ($\text{pH} < 4$) is due in part to the impact of pH on the chemical speciation of inorganic carbonate. Aqueous CO_2 (H_2CO_3) is the dominant carbonate species at pH values < 5 , but the HCO_3^- species increases in importance as the pH approaches the pK_a ($\text{pK}_a = \text{acid dissociation constant}$) of H_2CO_3 (6.32 at 85 °C; Amend and Shock, 2001). Consequently, it is plausible to expect CO_2 degassing rates to be considerably lower in higher pH springs where concentrations of the anionic forms of carbonate increase relative to the neutrally-charged CO_2 (aq). Lower concentrations of CO_2 (aq) decrease the gradient for degassing to the atmosphere. Finally, the presence of CO_2 (aq) in the source pool and outflow channel of JC3 may be an important source of inorganic C for autotrophic organisms.

Concentrations of total dissolved sulfide (DS) in source waters of JC3 averaged $22 \pm 7 \mu\text{M}$ over four sampling events and remained relatively high throughout the outflow channel of the near-neutral pH spring (Figure 3.3). Values of DS decline by $\sim 60\%$ at 12 m; however, compared to acidic (e.g., $\text{pH} < 4$) geothermal outflow channels, the disappearance rates of DS are considerably lower in the near-neutral systems such as JC3

(Inskeep et al., 2005; Inskeep and McDermott, 2005; Nordstrom et al., 2005). Lower sulfide disappearance rates at higher pH are again consistent with the influence of pH on the speciation of soluble sulfide. As with the carbonate system, the pK_a of H_2S (aq) is 6.52 at 85 °C, consequently at pH 6.5, HS^- represents a more significant proportion of DS and disappearance rates are lower. Lower concentrations of H_2S generates a lower concentration gradient therefore disappearance rates of H_2S (aq) is slower. Other studies in higher pH outflow channels such as Ojo Caliente and Angel Terrace also show lower sulfide disappearance rates compared to acidic systems (Nordstrom et al., 2005; Inskeep and McDermott, 2005). A complicating factor regarding the speciation of soluble S in Joseph's Coat spring (JC3) is the potential presence of As-S complexes, which would also impact degassing rates by further lowering the concentration of H_2S (aq).

The presence of DS plays a significant role in maintaining anoxic conditions within the outflow channel of JC3 since DS effectively scavenges O_2 as illustrated in one of the possible overall reactions explaining the abiotic reaction of dissolved sulfide with O_2 :



Dissolved oxygen values shown in Figure 3.3 are plotted as a fraction of theoretical saturation calculated for the elevation and pressure at JC3 (saturation = 143 μM at 75 °C and 153 μM at 45 °C). By 12 m, the O_2 concentration was still less than 20 % of theoretical saturation (Figure 3.3). Conversely, numerous acidic systems in YNP often exhibit very rapid loss of DS and more rapid O_2 ingassing as geothermal waters flow down gradient (Ackerman, 2006; Inskeep et al., 2005).

Significant concentrations of dissolved methane ($0.9 \pm 0.13 \mu\text{M}$) were detected in the source waters of Joseph's Coat spring (JC3) relative to earth surface conditions. The disappearance of CH_4 (aq) occurred rapidly in the outflow channel, dropping to near detection levels by 4 m (Figure 3.3). The more rapid disappearance rates for CH_4 relative to DS and DIC in the same spring may in part be due to the fact that CH_4 (aq) is the dominant species comprising the total dissolved methane (e.g. no complexation or dissociation).

Dissolved H_2 (aq) was detected at nanomolar concentrations ($108 \pm 53 \text{ nM}$) in the source pool, dropped to $\sim 40 \text{ nM}$ by 4 m, then increased to greater than $\sim 50 \text{ nM}$ at 7 – 12 m. This pattern was consistent over the last two sampling dates (2005-2006). The increase in H_2 (aq) concentrations after 4 m could possibly be due to H_2 production via microbial activity. However, this hypothesis has not been confirmed. The concentrations of H_2 (aq) detected in JC3 are significant, and thus, H_2 represents a potentially important energy source for chemotrophic metabolism in JC3 (Spear et al., 2005). The higher standard deviations for dissolved H_2 appear to reflect true variation in source water composition, as values near 100 nM are well above the effective detection of 2 nM .

In summary, gas exchange is one of the most important processes controlling the environmental conditions supporting various thermophilic metabolisms. For example, many geothermal springs are supersaturated with respect to atmospheric levels of H_2 , DIC, H_2S and CH_4 at the point of discharge, but undergo gas exchange reactions as well as O_2 ingassing reactions that ultimately drive the types of communities present within the source pool or outflow channel sediments. The near-neutral pH value of Josephs Coat

spring (JC3) is likely responsible for a slower apparent degassing rate relative to low pH systems, which also suppresses measurable dissolved O₂ until considerable distances down gradient (12 m). The dissolved gas profiles within the outflow channel suggest that anaerobic to microaerobic environments predominate in the source pool and within much of the outflow channel > 50 °C.

Iron

Total soluble concentrations of Fe (Fe_{TS}) measured in JC3 source waters were near the detection limit for the FerroZine method (DL = 0.2 μM ± 0.1; To et al., 1999), but were consistently low over the four sampling dates (2003 – 2006). Low concentrations of Fe would be expected in this system since the solubility of potential Fe controlling Fe-oxyhydroxide solids is extremely low at pH 6.1 (Stumm and Morgan, 1996). Concentrations of Fe_{TS} were essentially constant throughout the outflow channel averaging 0.6 μM ± 0.1 across all sampling locations. Ferrous iron (Fe^{II}) was the dominant Fe species detected in JC3 source waters (Table 3.1). However, although traces of Fe^{III} were consistently detectable in JC3 source waters, the concentrations of total soluble Fe were also essentially near detection, consequently, the absolute and relative abundance of Fe^{II} versus Fe^{III} must be considered an estimate. Interestingly, pyrite (Fe^{II}S₂) deposition is occurring in the source pool of JC3 even though saturation indices indicated undersaturation with respect to FeS, the only ferrous sulfide solid phase included in the MINTEQA2 database. As will be discussed further, it is difficult to conclude whether the formation of pyrite is attributable to long-term abiotic depositional processes or microbial biomineralization. However, the importance of pyrite in this

system is consistent with the high sulfide and low dissolved oxygen values observed in the source pool and majority of the outflow channel.

Arsenic

To our knowledge, the source waters of Joseph's Coat spring (JC3) contain the highest concentration of total soluble As ($130 \pm 8 \mu\text{M}$) measured in any geothermal spring in YNP. In comparison, values of As in other springs range from 2 to $80 \mu\text{M}$ (Stauffer and Thompson, 1984; Langner et al., 2001; Ball et al., 2002; Inskeep et al., 2005). Significant oxidation of arsenite to arsenate occurred in the outflow channel of JC3. Arsenate increased from $22 \pm 4 \mu\text{M}$ at the source to $\sim 70 - 120 \mu\text{M}$ at 10 to 12 m, depending on the year (Figure 3.4).

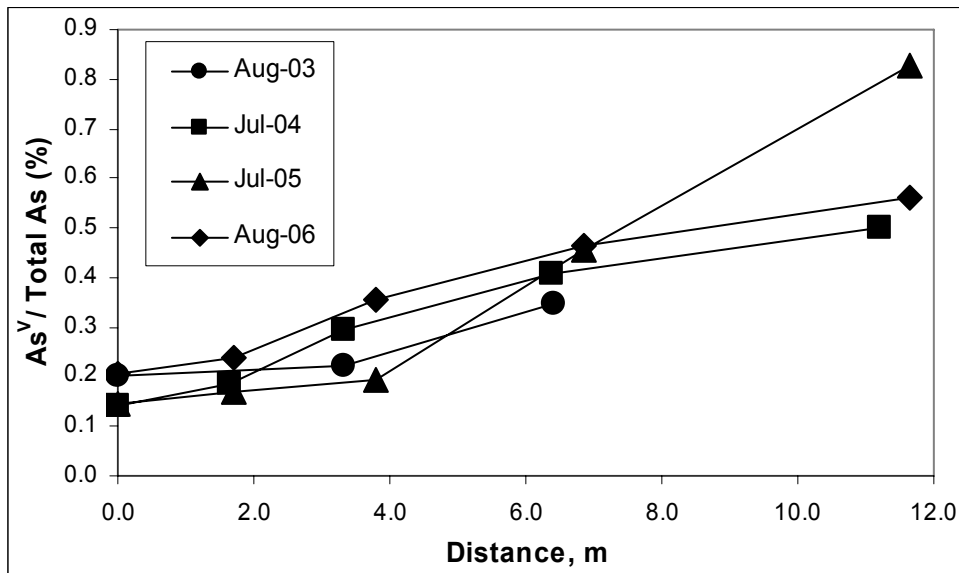


Figure 3.4. The oxidation of arsenite as function of distance from the geothermal source is shown as a ratio of As^{V} to total soluble As concentration (As_{TS}). Total soluble As remains essentially constant throughout the outflow channel at $\sim 130 \mu\text{M}$. Consequently, arsenate increases from as low as $10 \mu\text{M}$ at the source to as high as $100 \mu\text{M}$ at 12 m.

Experiments comparing arsenite oxidation rates in serum bottles inoculated with sediment from the source pool of JC3 and serum bottles containing sterilized sediment indicate that arsenite oxidation is at least in part biotically mediated (Figure 3.5).

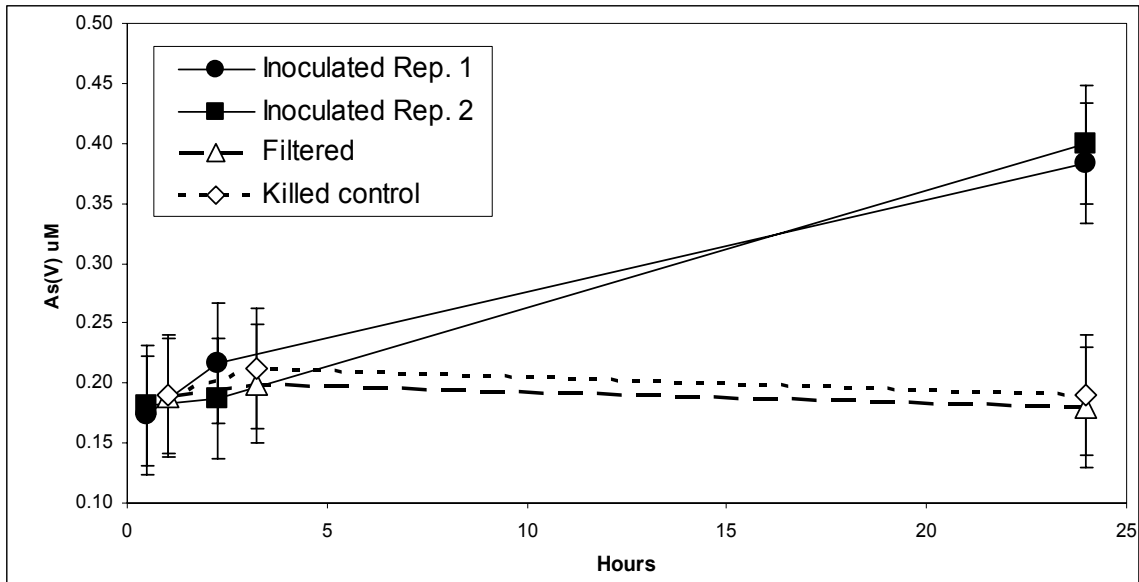


Figure 3.5. Concentrations of arsenate (As^{V}) as a function of time in an ex situ bioassay experiment conducted with JC3 outflow channel sediments at 75 °C. Relative to killed or filtered controls, replicated inoculated treatments show arsenite oxidation.

Other studies conducted in conjunction with this work found that arsenite oxidase genes (*aroA*) are expressed in JC3 outflow channel sediments (Inskeep et al., 2007), providing supporting evidence that arsenite oxidation is biotically mediated. Arsenite oxidation in other geothermal springs in YNP has been attributed to biological processes (Langer et al., 2001; Gihring et al., 2001; Macur et al., 2004; Inskeep et al., 2004; Inskeep et al., 2005). The lower rate of arsenite oxidation observed in Joseph's Coat spring (JC3) compared to past observations in acidic systems is consistent with the lower sulfide disappearance rates and correspondingly lower oxygen ingassing rates in JC3. It could

also suggest that other electron acceptors besides O_2 may be important in the oxidation of arsenite.

Thiosulfate

Source water thiosulfate concentrations averaged $751 \pm 92 \mu M$ over the four year study with a maximum value of $830 \mu M$ measured in August, 2006. To our knowledge, Champagne Pool in New Zealand is the only other geothermal spring with similarly high thiosulfate concentrations ($705 - 875 \mu M$; Druschel et al., 2003). Prior to our measurements in JC3, the highest reported values for thiosulfate in YNP were $37 \mu M$ in Cinder Pool (Norris Geyser Basin) (Xu et al., 1998). Interestingly, while thiosulfate concentrations are quite high in JC3, H_2S concentrations are significantly lower ($\sim 22 \mu M \pm 6.7$) in comparison. Molar ratios of total dissolved sulfide: thiosulfate for the Joseph's Coat geothermal system averaged ~ 0.03 , whereas Cinder Pool and Champagne Pool exhibit ratios of 1.25 and 2.5, respectively. One of the mechanisms of thiosulfate production involves the oxidation of dissolved sulfide, and this is plausible in springs with higher dissolved sulfide: thiosulfate ratios. However, the extremely low dissolved sulfide: thiosulfate ratio suggests that high thiosulfate levels in JC3 do not originate from H_2S oxidation after geothermal discharge.

Geothermal waters enriched in dissolved sulfide often contain elevated thiosulfate concentrations. Three primary pathways are thought to generate thiosulfate in hydrothermal systems: i) $H_2S - SO_2$ interactions, ii) H_2S oxidation, and iii) temperature driven hydrolysis of elemental sulfur (Xu et al., 1998). Magmatic gases that contain SO_2 (g) can react rapidly with H_2S in solution to form $S_2O_3^{2-}$. However, there is little evidence

supporting magmatic SO₂ degassing into YNP hydrothermal waters (Xu et al., 1998). Contact of H₂S rich geothermal waters with oxygenated groundwater prior to discharge could be responsible for the elevated S₂O₃²⁻ concentrations measured in JC3. However, due to the relatively low concentrations of H₂S in the system, it is more likely that hydrolysis reactions with elemental sulfur (S⁰) at temperatures between 100 and 200 °C and at pH values between 4 and 8 are responsible for the high concentrations of S₂O₃²⁻ in JC3 (Xu et al., 1998; 2000) The interaction of hydrothermal waters and elemental sulfur may explain the high concentrations of S₂O₃²⁻ and the significantly lower concentrations of dissolved sulfide according to the following reaction:



When the acidity generated from the hydrolysis of S⁰ exceeds the buffering capacity of the hydrothermal fluid, the stability of S₂O₃²⁻ is reduced. However, the high concentrations of H₃BO₃ (5.5 mM) and DIC (0.35 mM) in JC3 waters and other solid phase reactions buffer this system at a solution above pH ~ 6.0. Importantly, the high thiosulfate values in this particular spring are of great interest to geomicrobiologists and geochemists due to the highly reactive nature of intermediate S species. Thiosulfate may be important as an oxidant or as a reductant, and may undergo disproportionation reactions under specific conditions. For the same reasons, thiosulfate may participate in a diverse range of metabolic strategies for chemotrophic organisms inhabiting the sediments of this environment.

Antimony and boron

Total soluble Sb in the source waters of JC3 was variable over the 2004 - 2006 sampling period and ranged from 0.5 to 1.2 μM . These values correspond favorably to a value of 1.4 μM Sb reported by Stauffer and Thompson (1984), which based on Cl/Sb, Cl/As, Cl/B, and Cl/F molar ratios, appears to have been measured in the same spring. To our knowledge, this is the highest Sb concentration reported for a YNP geothermal spring. Consequently, this unique geothermal spring has high Sb and As, providing opportunities to study microbial interactions with what are normally considered toxic levels of these trace elements (Fillela et al., 2002; Silver and Phung, 2005). The oxidation of antimonite (i.e., Sb^{III}) was measurable within the outflow channel of this spring; antimonate increased from approximately 40 to 68% of the total soluble Sb by 7 m (Figure 3.6). Consequently, although measurable, the oxidation of Sb^{III} was not as significant as arsenite oxidation (Figure 3.4)

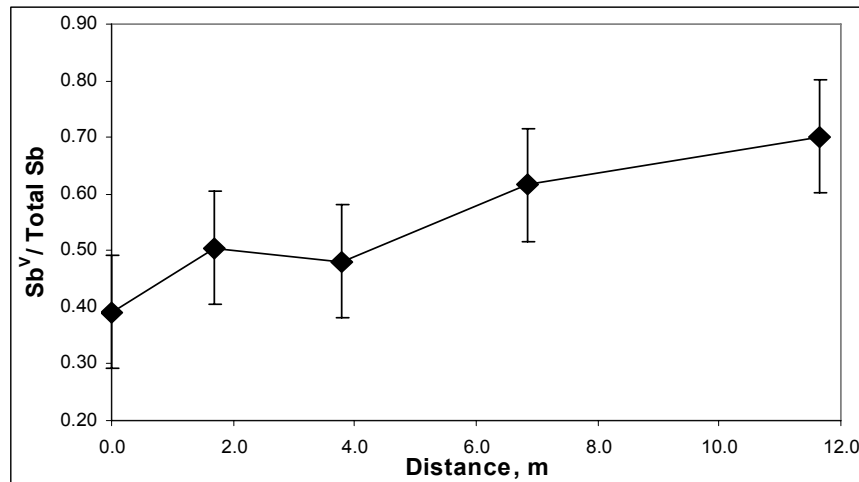


Figure 3.6. Oxidation of antimonite in Joseph's Coat spring (JC3) as a function of distance from geothermal source. The production of antimonate is shown as a ratio to Sb^{V} to total soluble Sb concentrations (TS). Data presented here are averages over annual sampling events in 2005 and 2006.

The mechanism of Sb^{III} oxidation remains unclear, but Sb^{III} -sulfide solid phases are an important part of the microbial environment in this system. Although pyrite is the predominant solid phase lining the source pool and accumulating in sediments, the separate Sb-sulfide phases are clearly an important component of this geothermal system.

Boron (B) concentrations were detected at levels of over $5.5 \pm 0.1 \text{ mM}$ in JC3 source waters. At these pH values (6.1 - 6.5), B is predicted to exist primarily as the protonated boric acid (H_3BO_3^0 , $\text{pK}_a = 9.24$). Although no solid phases containing B were detected in JC3, other studies have shown that biomineralization to form an iron-carbonate precipitate containing boron can occur at concentrations of 4.8 mM B (Hazen et al., 2002). Boron toxicity to microbial function has also been implicated at levels as low as 1.6 mM (Ahmad et al., 2004; Woods, 1994; Hoffmann et al., 1981). However, there is very little information available regarding the impacts of high B concentrations on microbial activity and it is difficult to speculate whether the concentrations observed in Joseph's Coat spring (JC3) impact microbial community structure and or other important geochemical processes.

Other important soluble constituents

Concentrations of total dissolved Si (predominately H_4SiO_4^0 under spring conditions) are relatively high in JC3 source waters ($3.9 \pm 0.2 \text{ mM}$). Saturation indices [$\text{SI} = \log \{ \text{ion activity product (IAP) / solubility product (K}_{\text{SP}}) \}$] calculated using Visual Minteq (Allison et al., 1991) indicate that soluble Si was oversaturated with respect to quartz ($\text{SI for SiO}_2 \text{ (quartz)} = 0.89$) and near equilibrium with respect to amorphous SiO_2

(SI for $\text{SiO}_2(\text{am}) = -0.14$). Thus, these calculations suggest the potential importance of SiO_2 -like solid phase mineralization in this system.

Low but significant concentrations of dissolved organic C (DOC) relative to other geothermal systems measured in YNP, were detected in the source waters of JC3 ($\sim 20 \mu\text{M}$). The compounds contributing to DOC were not determined and this was not the scope of the current study; however, these sources of organic C may represent important C sources or electron donors for microbial growth. The two crenarchaeal isolates obtained in this study (discussed below) are obligate heterotrophs, and thus would require some form of C other than CO_2 .

Energetic Analysis of Potential Chemotrophic Metabolisms

An aqueous geochemical equilibrium model (Visual MINTEQ; Allison et al., 1991) was used to calculate the distribution of ion activities, an accurate ionic strength, charge balances, and saturation indices with respect to various solid phases within the source pool and outflow channel of JC3. Anion and cation charge balance calculations for all samples analyzed from this spring show less than 10 % disparity between total anionic and cationic charge, supporting the assumption that all predominant anions and cations were accounted for and measured accurately (see Appendix A). The calculated activities of a variety of aqueous chemical species were also used in free energy calculations (Equation # 7, page 32) specific to source pool and outflow channel conditions. Modeling the potential energy sources available to microorganisms in hot spring environments is essential for elucidating those chemical constituents supporting primary productivity in non-photosynthetic environments.

The absence of photosynthesis at temperatures $> 70-74\text{ }^{\circ}\text{C}$ (Cox and Shock, 2003; Allewalt et al., 2006) supports the assumption that primary productivity in much of this geothermal system is fueled by reduced inorganic constituents. Dissolved redox-active elements that could potentially be utilized as electron donors or acceptors in chemotrophic metabolisms (either anaerobic or aerobic) include: $\text{As}^{\text{III}, \text{V}}$, $\text{Sb}^{\text{III}, \text{V}}$, $\text{S}^{-\text{II}, \text{O}, \text{II}, \text{VI}}$, $\text{Fe}^{\text{II}, \text{III}}$, $\text{C}^{-\text{IV}, \text{IV}}$, $\text{H}^{0, \text{I}}$, $\text{N}^{-\text{III}, \text{V}}$, and $\text{O}^{-\text{II}, 0}$. Calculated Gibbs free energy values (ΔG_{rxn}) for 55 oxidation-reduction reactions involving a representative range of constituent combinations ranged from near equilibrium (i.e., $\Delta G_{\text{rxn}} \sim 0$) to almost $-100\text{ kJ mole electron}^{-1}$ (Table 3.2).

Table 3.2. Oxidation-reduction reactions considered in the energetic analyses of potential chemosynthetic metabolisms occurring in the geothermal environment of Joseph's Coat Spring (JC3). Reactions are written with the electron donor as the first reactant followed by the electron acceptor. The standard state free energy value ($\Delta G^{\circ}_{\text{rxn}}$, $\text{kJ mol}^{-1} \text{ e}^{-1}$) for each reaction is given at 85°C .

Rxn. No.	Reaction Written as donor + acceptor	ΔG_{rxn} ($\text{kJ mol}^{-1} \text{ e}^{-1}$)
1	$\text{H}_2(\text{aq}) + 0.5\text{O}_2(\text{aq}) = \text{H}_2\text{O}$	-96.5
2	$\text{CH}_4(\text{aq}) + 2\text{O}_2(\text{aq}) = \text{CO}_2(\text{aq}) + 2\text{H}_2\text{O}$	-95.3
3	$\text{S}_2\text{O}_3^{2-} + 2\text{O}_2(\text{aq}) + \text{H}_2\text{O} = 2\text{SO}_4^{2-} + 2\text{H}^+$	-95.1
4	$\text{S}^0 + 1.5\text{O}_2(\text{aq}) + \text{H}_2\text{O} = \text{SO}_4^{2-} + 2\text{H}^+$	-93.2
5	$\text{H}_2\text{S}(\text{aq}) + 2\text{O}_2(\text{aq}) = \text{SO}_4^{2-} + 2\text{H}^+$	-88.9
6	$5\text{S}_2\text{O}_3^{2-} + 8\text{NO}_3^- + \text{H}_2\text{O} = 10\text{SO}_4^{2-} + 4\text{N}_2(\text{aq}) + 2\text{H}^+$	-88.6
7	$\text{H}_2\text{S}(\text{aq}) + 0.5\text{O}_2(\text{aq}) = \text{S}^0 + \text{H}_2\text{O}$	-75.9
8	$\text{H}_3\text{AsO}_3 + 0.5\text{O}_2(\text{aq}) = \text{H}_2\text{AsO}_4 + \text{H}^+$	-70.9
9	$\text{S}^0 + 0.75\text{NO}_3^- + \text{H}_2\text{O} + 2\text{H}^+ = 0.75\text{NH}_4^+ + \text{SO}_4^{2-}$	-66.1
10	$5\text{S}_2\text{O}_3^{2-} + 4\text{O}_2(\text{aq}) + \text{H}_2\text{O} = 6\text{SO}_4^{2-} + 2\text{H}^+ + 4\text{S}^0(\text{s})$	-65.3
11	$\text{Fe}^{2+} + 0.25\text{O}_2(\text{aq}) + 2.5\text{H}_2\text{O} = \text{Fe}(\text{OH})_3(\text{s}) + 2\text{H}^+$	-58.8
12	$4\text{H}_2(\text{aq}) + \text{NO}_3^- + 2\text{H}^+ = \text{NH}_4^+ + 3\text{H}_2\text{O}$	-56.6
13	$\text{CH}_4(\text{aq}) + \text{NO}_3^- + 2\text{H}^+ = \text{NH}_4^+ + \text{CO}_2(\text{aq}) + \text{H}_2\text{O}$	-55.7
14	$\text{S}_2\text{O}_3^{2-} + \text{NO}_3^- + 2\text{H}_2\text{O}(\text{l}) = 2\text{SO}_4^{2-} + \text{NH}_4^+$	-55.2
15	$\text{H}_2(\text{aq}) + 2\text{Fe}^{3+} = 2\text{Fe}^{2+} + 2\text{H}^+$	-54.8
16	$\text{CH}_4(\text{aq}) + 8\text{Fe}^{3+} + 2\text{H}_2\text{O} = \text{CO}_2(\text{aq}) + 8\text{Fe}^{2+} + 8\text{H}^+$	-53.7
17	$\text{S}^0 + 6\text{Fe}^{3+} + 4\text{H}_2\text{O} = 6\text{Fe}^{2+} + \text{SO}_4^{2-} + 8\text{H}^+$	-51.6
18	$\text{H}_2(\text{aq}) + \text{Sb}(\text{OH})_6^- + \text{H}^+ = \text{Sb}(\text{OH})_3^0 + 3\text{H}_2\text{O}(\text{l})$	-51.2
19	$\text{CH}_4(\text{aq}) + 4\text{Sb}(\text{OH})_6^- + 4\text{H}^+ = \text{CO}_2(\text{aq}) + 4\text{Sb}(\text{OH})_3^0 + 10\text{H}_2\text{O}(\text{l})$	-50.0
20	$\text{S}_2\text{O}_3^{2-} + 8\text{Fe}^{3+} + 5\text{H}_2\text{O}(\text{l}) = 2\text{SO}_4^{2-} + 8\text{Fe}^{2+} + 10\text{H}^+$	-46.7

TABLE 3.2 CONTINUED

21	$\text{Sb(OH)}_3^0 + 0.5\text{O}_2(\text{aq}) + 2\text{H}_2\text{O(l)} = \text{Sb(OH)}_6^- + \text{H}^+$	-45.3
22	$\text{H}_2\text{S(aq)} + 4\text{Sb(OH)}_6^- + 2\text{H}^+ = \text{SO}_4^{2-} + 4\text{Sb(OH)}_3^0 + 8\text{H}_2\text{O(l)}$	-43.6
23	$\text{NH}_4^+ + 2\text{O}_2(\text{aq}) = \text{NO}_3^- + 2\text{H}^+ + \text{H}_2\text{O}$	-39.9
24	$5\text{Sb(OH)}_3^0 + 2\text{NO}_3^- + 9\text{H}_2\text{O(l)} = \text{N}_2(\text{aq}) + 5\text{Sb(OH)}_6^- + 3\text{H}^+$	-38.8
25	$2\text{Fe}^{2+} + 0.5\text{O}_2(\text{aq}) + 2\text{H}^+ = 2\text{Fe}^{3+} + \text{H}_2\text{O}$	-37.5
26	$\text{H}_2\text{S(aq)} + 0.25\text{NO}_3^- + 0.5\text{H}^+ = 0.25\text{NH}_4^+ + 0.75\text{H}_2\text{O} + \text{S}^0$	-36.0
27	$\text{S}^0 + 6\text{Fe(OH)}_3 + 10\text{H}^+ = 6\text{Fe}^{2+} + \text{SO}_4^{2-} + 14\text{H}_2\text{O}$	-35.0
28	$\text{C}_3\text{H}_6\text{O}_6 + 6\text{S}^0 + 3\text{H}_2\text{O(l)} = 3\text{CO}_2(\text{aq}) + 6\text{H}_2\text{S(aq)}$	-34.3
29	$\text{H}_2\text{S(aq)} + \text{Fe}^{3+} = 2\text{Fe}^{2+} + 2\text{H}^+ + \text{S}^0$	-34.2
30	$4\text{H}_3\text{AsO}_3 + \text{NO}_3^- + \text{H}_2\text{O} = 4\text{H}_2\text{AsO}_4^- + \text{NH}_4^+ + 2\text{H}^+$	-30.8
31	$\text{H}_3\text{AsO}_3 + 2\text{Fe}^{3+} + \text{H}_2\text{O} = 2\text{Fe}^{2+} + \text{H}_3\text{AsO}_4 + 2\text{H}^+$	-29.3
32	$2\text{C}_3\text{H}_6\text{O}_6 + 3\text{S}_2\text{O}_3^{2-} + 6\text{H}^+ = 6\text{H}_2\text{S(aq)} + 6\text{CO}_2(\text{aq}) + 3\text{H}_2\text{O(l)}$	-29.3
33	$\text{CH}_3\text{COOH} + 4\text{S}^0 + 2\text{H}_2\text{O} = 2\text{CO}_2(\text{aq}) + 4\text{H}_2\text{S(aq)}$	-27.8
34	$\text{H}_2(\text{aq}) + \text{H}_3\text{AsO}_4 = \text{H}_3\text{AsO}_3 + \text{H}_2\text{O}$	-25.6
35	$\text{H}_3\text{AsO}_3 + \text{Sb(OH)}_6^- + \text{H}^+ = \text{Sb(OH)}_3^0 + 2\text{H}_2\text{O(l)} + \text{H}_3\text{AsO}_4$	-25.6
36	$\text{CH}_4(\text{aq}) + 4\text{H}_2\text{AsO}_4^- + 4\text{H}^+ = \text{CO}_2(\text{aq}) + 4\text{H}_3\text{AsO}_3 + 2\text{H}_2\text{O}$	-25.6
37	$\text{CH}_4(\text{aq}) + \text{SO}_4^{2-} + 2\text{H}^+ = \text{H}_2\text{S(aq)} + \text{CO}_2(\text{aq}) + 2\text{H}_2\text{O}$	-25.5
38	$\text{S}_2\text{O}_3^{2-} + 4\text{H}_2\text{AsO}_4^- + \text{H}_2\text{O(l)} + 2\text{H}^+ = 2\text{SO}_4^{2-} + 4\text{H}_3\text{AsO}_3$	-24.3
39	$\text{S}^0 + 3\text{H}_2\text{AsO}_4^- + \text{H}_2\text{O} + \text{H}^+ = 3\text{H}_3\text{AsO}_3 + \text{SO}_4^{2-}$	-22.3
40	$\text{S}^0 + 3\text{H}_3\text{AsO}_4 + \text{H}_2\text{O} = 3\text{H}_3\text{AsO}_3 + \text{SO}_4^{2-} + 2\text{H}^+$	-22.3
41	$\text{CH}_3\text{COOH} + \text{S}_2\text{O}_3^{2-} + 2\text{H}^+ = 2\text{H}_2\text{S(aq)} + 2\text{CO}_2(\text{aq}) + 2\text{O}_2(\text{aq})$	-21.1
42	$\text{H}_2(\text{aq}) + \text{S}^0 = \text{H}_2\text{S(aq)}$	-20.6
43	$\text{Fe}^{2+} + 0.125\text{NO}_3^- + 2.625\text{H}_2\text{O} = 0.125\text{NH}_4^+ + \text{Fe(OH)}_3(\text{s}) + 1.75\text{H}^+$	-18.6
44	$4\text{H}_2(\text{aq}) + \text{S}_2\text{O}_3^{2-} + 2\text{H}^+ = 2\text{H}_2\text{S(aq)} + 3\text{H}_2\text{O(l)}$	-13.1
45	$\text{CH}_4(\text{aq}) + \text{S}_2\text{O}_3^{2-} + 2\text{H}^+ = \text{CO}_2(\text{aq}) + 2\text{H}_2\text{S(aq)} + \text{H}_2\text{O}$	-12.9
46	$\text{S}_2\text{O}_3^{2-} + \text{H}_2\text{O(l)} = \text{SO}_4^{2-} + \text{H}_2\text{S(aq)}$	-12.5
47	$2\text{H}_2\text{S(aq)} + 4\text{H}_2\text{AsO}_4^- + 2\text{H}^+ = 4\text{H}_3\text{AsO}_3 + \text{S}_2\text{O}_3^{2-} + \text{H}_2\text{O}$	-11.8
48	$\text{H}_3\text{AsO}_3 + 2\text{Fe(OH)}_3 + 3\text{H}^+ = 2\text{Fe}^{2+} + \text{H}_2\text{AsO}_4^- + 5\text{H}_2\text{O}$	-11.5
49	$\text{SO}_4^{2-} + \text{H}_2(\text{aq}) + 2\text{H}^+ = \text{H}_2\text{S(aq)} + 4\text{H}_2\text{O}$	-7.6
50	$4\text{Sb(OH)}_3^0 + \text{NO}_3^- + 9\text{H}_2\text{O(l)} = \text{NH}_4^+ + 4\text{Sb(OH)}_6^- + 2\text{H}^+$	-5.4
51	$\text{H}_2\text{S(aq)} + \text{H}_2\text{AsO}_4^- + \text{H}^+ = \text{H}_3\text{AsO}_3 + \text{H}_2\text{O} + \text{S}^0$	-5.0
52	$\text{H}_2\text{S(aq)} + \text{H}_3\text{AsO}_4 = \text{H}_3\text{AsO}_3 + \text{S}^0 + \text{H}_2\text{O}$	-5.0
53	$\text{Sb(OH)}_3^0 + 2\text{Fe}^{3+} + 3\text{H}_2\text{O(l)} = 2\text{Fe}^{2+} + \text{Sb(OH)}_6^- + 3\text{H}^+$	-3.7
54	$\text{NH}_4^+ + 8\text{Fe}^{3+} + 3\text{H}_2\text{O} = 8\text{Fe}^{2+} + \text{NO}_3^- + 10\text{H}^+$	-2.4
55	$4\text{H}_2(\text{aq}) + \text{CO}_2(\text{aq}) = \text{CH}_4(\text{aq}) + 2\text{H}_2\text{O}$	-0.9

The distribution of free energy values for this system can be thought of as a customized redox ladder for this specific site, and exhibits a redox profile of the potential reactions that may be important in supporting the microbial metabolism of thermophilic organisms.

The distribution of free energy values for the oxidation-reduction reactions evaluated in this study demonstrate that reactions involving O_2 as the electron acceptor (reactions 1 - 5, 7 and 8; see Figure 3.7, upper left) exhibit the greatest amount of energy

available per electron transferred. In general, nitrate reduction represents the next most favorable electron acceptor followed by Fe^{III} , Sb^{V} and As^{V} .

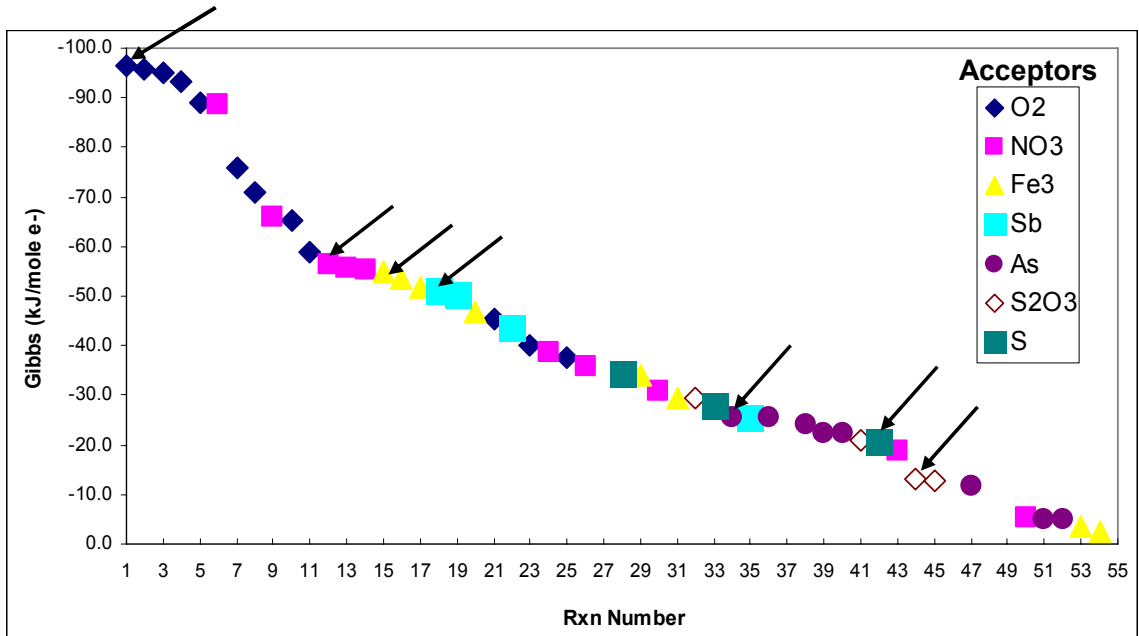


Figure 3.7. Reaction free energy (ΔG_{rxn} , kJ mol^{-1}) profile for the geothermal system at Joseph's Coat springs (JC3) showing Gibbs free energy values ($\text{kJ mol}^{-1} \text{e}^{-1}$) for individual oxidation-reduction reactions (Reaction Numbers, Table 3.2) based on 7 differing terminal electron acceptors, indicated in legend. Arrows highlight the reactions with a fixed electron donor, in this case H_2 , and the effect changing electron acceptors has on free energy.

Reactions where thiosulfate or S^0 serve as an electron acceptor are generally less thermodynamically favorable, and these reactions are distributed near the bottom right portion of the energy profile (Figure 3.7). When comparing electron donors, H_2 is the most favorable electron donor followed by H_2S , CH_4 , $\text{S}_2\text{O}_3^{2-}$, S^0 , H_2S , Sb^{III} , As^{III} , Fe^{II} , and NH_4^+ . Several reactions included in this analysis suggest that the oxidation of reduced organic C using anaerobic electron acceptors such as S or $\text{S}_2\text{O}_3^{2-}$ are favorable, albeit at significantly lower free energy values than many other reactions (e.g. Reactions 28, 32, 33, 41; Table 3.2). The trends depicted in this free energy profile are familiar

concepts in redox chemistry, and reveal the hierarchy of electron donors and acceptors typically observed in redox ladders presented at standard state conditions or customized to pH 7 (e.g., Rogers and Amend, 2005; 2006; Amend and Shock, 2003; Stumm and Morgan, 1996; Brock and Madigan, 1991).

Free energy values calculated under source pool conditions do not change considerably moving down gradient along outflow channel sampling locations (data not shown). Despite the fact that outflow channel processes are indeed occurring (e.g. slow O₂ ingassing, H₂S, CO₂ and CH₄ disappearance, As^{III} oxidation), free energy values are not particularly sensitive to these changes. The actual free energy value for any redox couple is highly poised near the standard state free energy value by virtue of its definition (e.g. see Equation #7). The reaction quotient can modify the calculated free energy value, but at reasonably constant pH within this system, the calculated free energy values of the majority of the 55 reactions considered are generally stable throughout the outflow channel. In fact, ΔG_{rxn} values generally vary by less than 5 kJ mol⁻¹ e⁻¹ throughout the outflow channel (see also Inskeep et al., 2005; Ackerman, 2006). Even though the decline in temperature and changes in dissolved gas concentrations in the outflow channel are accounted for in these calculations, the relative consistency of ΔG_{rxn} values do not provide significant insight regarding potential changes in microbial habitats occurring across gradients within the source pool and or outflow channel.

Solid Phase Analysis

The Joseph's Coat spring (JC3) was initially chosen for study by Dr. Inskeep's laboratory because of the interesting submerged solid phases that line the source pool.

This strikingly lustrous-metallic solid phase lining the majority of the rim of this violently boiling pool (Figure 3.8) varied in thickness from approximately 1 to 3 mm, and overlies a white, porous Si-rich precipitate; the phase boundary is abrupt and the surface pyritic phase naturally cracks at this boundary during sampling.

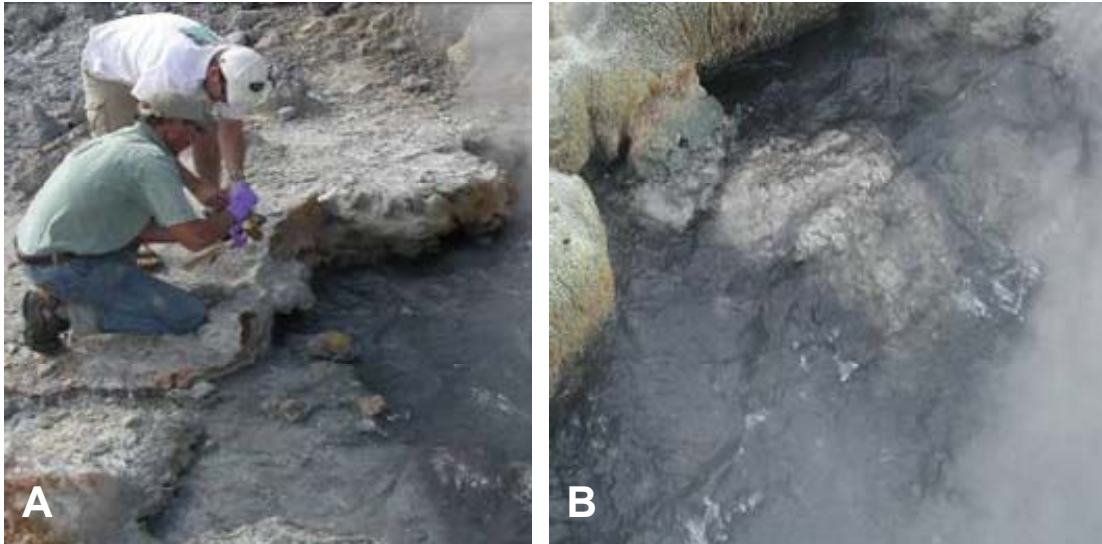


Figure 3.8. Site photographs showing (A) sample collection at the southeast rim of the main source pool of Joseph's Coat Spring (JC3), and (B) a close-up view of the pyritic, stibnite-rich 'metallic' solid phase submerged below the water surface.

One of the primary goals of this study was to elucidate the mineralogy of these and other solid phases in JC3 by employing a host of analytical techniques including SEM, SEM-EDAX, FEM-EBSD, XRD, and total dissolution (Table 3.5). In addition, the processes involved in the formation of these phases were investigated.

Solid phase identification

Saturation indices (SI) based on the activities of aqueous constituents are useful for understanding abiotic precipitation and biomineralization processes. Calculations using Visual MINTEQ indicated that JC3 source and outflow channel waters were

oversaturated with respect to quartz, ferrihydrite ($\text{Fe}(\text{OH})_3$), goethite (FeOOH), K-jarosite ($\text{KFe}_3(\text{OH})_6(\text{SO}_4)_2$) and hematite (Fe_2O_3), and near saturation with respect to amorphous SiO_2 (Table 3.3). The formation of SiO_2 -like phases was confirmed by SEM-EDAX observations, which revealed that SiO_2 phases are ubiquitous within the outflow channel. Further, a bleached-white Si-rich solid phase is present just below the 2 to 3 mm-thick metallic-pyritic phase in the source pool.

Although calculations indicated that the aqueous phase is oversaturated with respect to ferrihydrite ($\text{Fe}(\text{OH})_3$), goethite (FeOOH), K-jarosite ($\text{KFe}_3(\text{OH})_6(\text{SO}_4)_2$), and hematite (Fe_2O_3), these Fe solid phases were not observed in the JC3 system. Conversely, FeS_2 was the only Fe-containing solid phase detected in JC3 thermal sediments even though saturation indices show that the waters were significantly undersaturated with respect to FeS (calculated $\text{SI} = -3.9$). This discrepancy indicates the nonequilibrium nature of the geothermal source waters, and the fact that the source pool appears considerably anoxic based on dissolved gas measurements. The role of microorganisms in the deposition of pyrite in this system is not clear, but will be discussed further below. SEM images of the FeS_2 phase lining the source pool show what are likely microbial cells embedded within the pyritic surface (Fig 3.9 D, see page 66); consequently, microorganisms may be directly involved in the precipitation or dissolution of pyrite and other sulfidic phases (Sb-S, As-S).

Table 3.3. Saturation indices ($[\log(IAP/K_{SP})]$) with respect to various mineral phases calculated using measured total soluble concentrations after chemical speciation using the aqueous equilibrium program, MINTEQA2 (IAP=ion activity product; K_{sp} = solubility product constant).

Alunite $KAl_3(SO_4)_2(OH)_6$	Ferrihydrite $Fe(OH)_3$	Iron Sulfide FeS	Goethite $FeOOH$	Magnetite Fe_3O_4	K-jarosite $KFe_3(OH)_6(SO_4)_2$
-3.8	+4.1	-3.9	+5.6	+15.7	+0.1

Quartz SiO_2	Am. Quartz $SiO_2(am)$	Stibnite Sb_2S_3	Realgar As_4S_4	Orpiment As_2S_3	Hematite Fe_2O_3
+0.9	-0.1	-14.2	-8.6	-7.8	+13.8

Compositional data from small-spot SEM-EDAX supported the presence of both pyrite (FeS_2) and stibnite (Sb_2S_3) in the metallic solid phase that lines the source pool (Table 3.4). Average, atomic (mole) ratios of Fe:S taken at several locations were close to the theoretical value of 0.5 for pyrite. Conversely, average Sb:S ratios of the stibnite like phase were ~ 0.55 , slightly lower than the theoretical value of 0.66 for Sb_2S_3 . Mean angular diffraction values (MAD) measured by FEM-EBSD corresponded to values for pyrite and stibnite, and thus, definitively confirmed the presence of these minerals. Total dissolution analysis of metallic solid phases from the source pool, soft sediments from source pool shelf, and sampling positions from the head of the source pool down gradient (JC3B – JC3E; Table 3.5). Total dissolution analysis were consistent with these observations and revealed that the metallic deposits contained significant concentrations of Fe, Sb, and S, and to a lesser extent As (Table 3.5).

Table 3.4. Small-spot energy dispersive analysis of x-ray (EDAX) compositional data of the brittle metallic phase lined the source pool of Joseph's Coat Spring (JC3). Data presented are averages over separate spots (n = 3). Pyrite and Stibnite standards (Wards) generated the same ratios respectively as environmental samples.

Figure 3.9A		Figure 3.9C	
element	atom %	element	atom %
Fe	24.4	Sb	25.1
S	48.2	S	46.2
ratio Fe:S	0.51	ratio Sb:S	0.55

Table 3.5 Total chemical composition of solid phases and sediments sampled from the source pool and outflow channel (2004) of Joseph's Coat spring (JC3). Si and O were not measured in this analysis.

Sample	Sb	As	S	Fe	Al	K	Ca	Na	Mg	P
	wt%									
JC3A Metallic phase	10.22	0.80	26.500	18.600	0.290	0.081	0.113	0.047	0.011	0.005
JC3A Metallic phase	19.06	1.01	27.900	13.900	0.775	0.134	0.069	0.062	0.013	0.009
JC3A Bottom, SiO ₂ phase	0.02	0.00	0.015	9.524	0.239	0.002	0.021	0.019	0.002	0.001
JC3A soft sediment	0.55	0.07	0.748	0.400	0.928	0.219	0.039	0.055	0.018	0.004
JC3B >0.5cm	0.27	0.06	0.591	0.292	0.426	0.138	0.034	0.085	0.011	0.002
JC3B 0 - 0.5 cm	0.49	0.08	1.139	0.715	0.530	0.141	0.034	0.063	0.017	0.003
JC3C 0 - 1 cm	0.30	0.11	3.572	0.321	0.702	0.200	0.030	0.053	0.020	0.003
JC3D 0 - 1 cm	0.18	0.17	0.721	0.193	0.468	0.128	0.032	0.069	0.013	0.003
JC3D 1 - 2 cm	0.18	0.39	0.526	0.155	0.526	0.151	0.028	0.060	0.014	0.002
Sample	Ti	Mn	Ba	Se	Zn	Mo	Ni	Cd	Cr	Cu
	mg/kg									
JC3A Metallic phase	1003.4	517.0	163.6	889.2	90.4	40.0	40.2	26.6	29.7	6.2
JC3A Metallic phase	952.3	452.8	109.9	1401.8	61.0	31.2	39.3	30.5	22.6	4.8
JC3A Bottom, SiO ₂ phase	6278.1	14.6	182.8	9.5	0.5	4.1	5.6	1.0	11.7	1.5
JC3A soft sediment	6708.1	57.4	841.3	49.5	5.7	41.4	7.2	2.5	10.8	5.9
JC3B >0.5cm	2894.1	33.3	1925.4	29.2	3.2	34.6	7.6	2.9	8.6	3.1
JC3B 0 - 0.5 cm	6696.0	45.7	3976.7	86.0	4.0	31.4	19.3	5.0	22.7	7.1
JC3C 0 - 1 cm	3534.1	48.0	567.6	32.2	4.2	42.7	15.9	5.9	22.5	5.1
JC3D 0 - 1 cm	2699.7	28.1	953.6	37.7	1.3	25.8	16.2	10.3	21.9	3.9
JC3D 1 - 2 cm	3040.4	32.7	976.1	23.5	2.1	22.7	12.7	14.1	18.8	3.3

Compositional data of metallic solid phases and sediments from JC3 clearly indicate a shift in mineral composition as a function of location within this geothermal system (Table 3.5). The high percentages of Sb, Fe, and S in the JC3A metallic phase corroborate the XRD and SEM conclusions that pyrite and stibnite are the dominant minerals comprising this mineralized formation. In one replicate sample, the amount of Sb (%) was actually higher than the Fe content (Table 3.5). Analysis of the bleached-white Si-rich phase found beneath the pyritic layer confirmed the abrupt boundary between these phases observed in the field, and the concentrations of most constituents (e.g. Sb, S, Fe, As) are significantly lower in this phase with the notable exception of Ti (Table 3.5).

Scanning electron micrographs (SEM) of the stibnite phases show rod-like orthorhombic structures projecting from a central point (Fig. 3.9 B, C). These structures are found on a background of pyrite (Fig. 3.9 A). The morphology of these structures are strikingly similar to stibnite crystals generated in the laboratory (An et al., 2003; Fig. 3.10). The calculated saturation index (SI) for stibnite in the source pool was -14.2, indicating significant undersaturation. Previous studies have linked the formation of stibnite to biomineralization (Phoenix et al., 2005). Rapid adsorption of reactive aqueous metal species onto microbial cell walls may be operating in JC3 to produce many of the mineral phases detected.

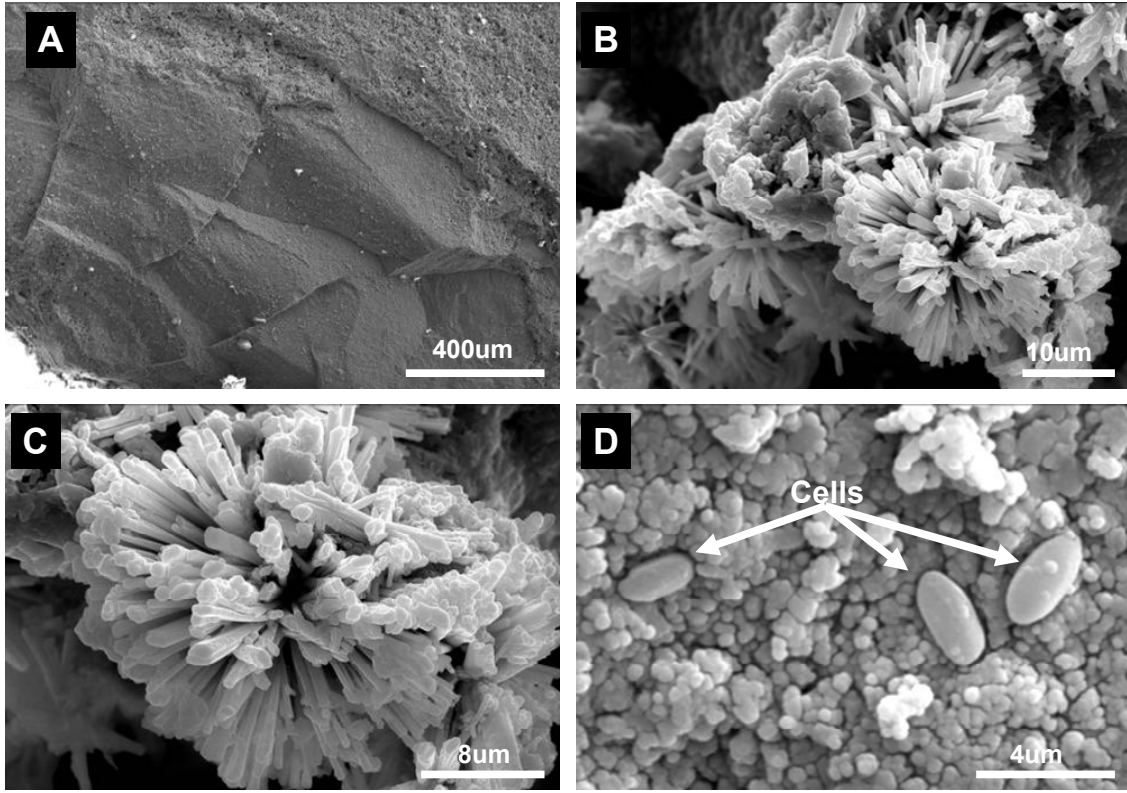


Fig. 3.9. Scanning electron micrographs (SEM) of JC3 source pool mineral deposits. Low magnification image (A) shows the edge and top surface of the 2 mm thick FeS_2 mineral deposit. Higher magnification images (B, C) reveal the presence of highly structured Sb-S crystals forming on the top of the FeS_2 surface. High magnification image of what are most likely individual cells imbedded into surrounding pyritic material (D).

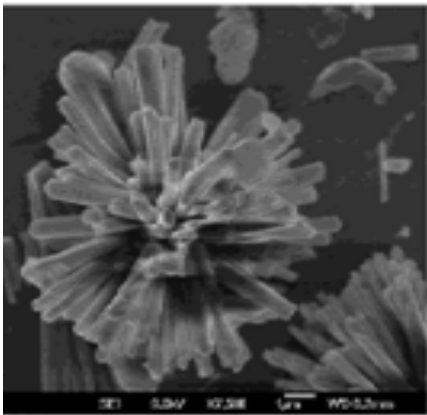


Fig. 3.10. SEM image of stibnite (Sb_2S_3) generated synthetically under laboratory conditions (An et al., 2003).

Soft sediments obtained from the 75-78 °C shelf on the east side of the source pool contained an assemblage of solid phases identified using EDAX and XRD including pyrite, stibnite, alunite [$\text{KAl}_3(\text{SO}_4)_2(\text{OH})_6$], As_2S_3 , S^0 , and SiO_2 . Consequently, total dissolution data from sediment samples reflects the contribution of each of these phases (unfortunately, Si is lost during the acid digestion procedure). Analysis of outflow channel sediments (SEM/EDAX) revealed that elemental S^0 was present as a minor component at all sampling positions. As discussed above, the formation of solid phase S^0 can occur abiotically as a result of the oxidation of dissolved sulfide within the outflow channel (Reaction 6; Xu et al., 1998; Inskeep and McDermott, 2005; Macur et al., 2004a). The abiotic formation of elemental S^0 at this pH is considered slow due to the slow rate of diffusion for O_2 . However, it is also possible that microorganisms within this system also contribute to the oxidation of $\text{S}^{-\text{II}}$ to S^0 .

Alunite [$\text{KAl}_3(\text{SO}_4)_2(\text{OH})_6$] was also identified in source pool and outflow channel sediments using SEM-EDAX (Figure 3.11). Formation of alunite in thermal acid-sulfate waters is common in many Yellowstone locations (Nordstrom et al., 2005); however, saturation indices for alunite in JC3 were significantly undersaturated (SI = -3.8) with respect to this mineral phase.

Separate attempts were made in collaboration with Dr. R. Macur (Montana State University) to identify the mineral phases responsible for the alternating yellow, orange, and grey layers with variable thickness (~1-2 mm) observed in the source pool (shelf zone) and outflow channel. Analysis of small (< 50 uL) samples containing colored sediment were analyzed using SEM-EDAX and results suggest that the predominant

color generally correlated with the percent of As and Sb within each layer. Yellow layers contained an average of 1.25 atom % As, orange layers contained approximately 0.12 atom % As, and grey layers contained less than 0.03 atom % As. Conversely, Sb concentrations were significantly higher in orange layers (0.48 atom %) in comparison to yellow layers (0.18 atom %), and grey layers contained less than 0.06 atom % Sb. In addition, solid phases matching the composition of orpiment (As_2S_3), which has a characteristic yellow color, were more numerous in the yellow layers in comparison to the orange and grey layers.

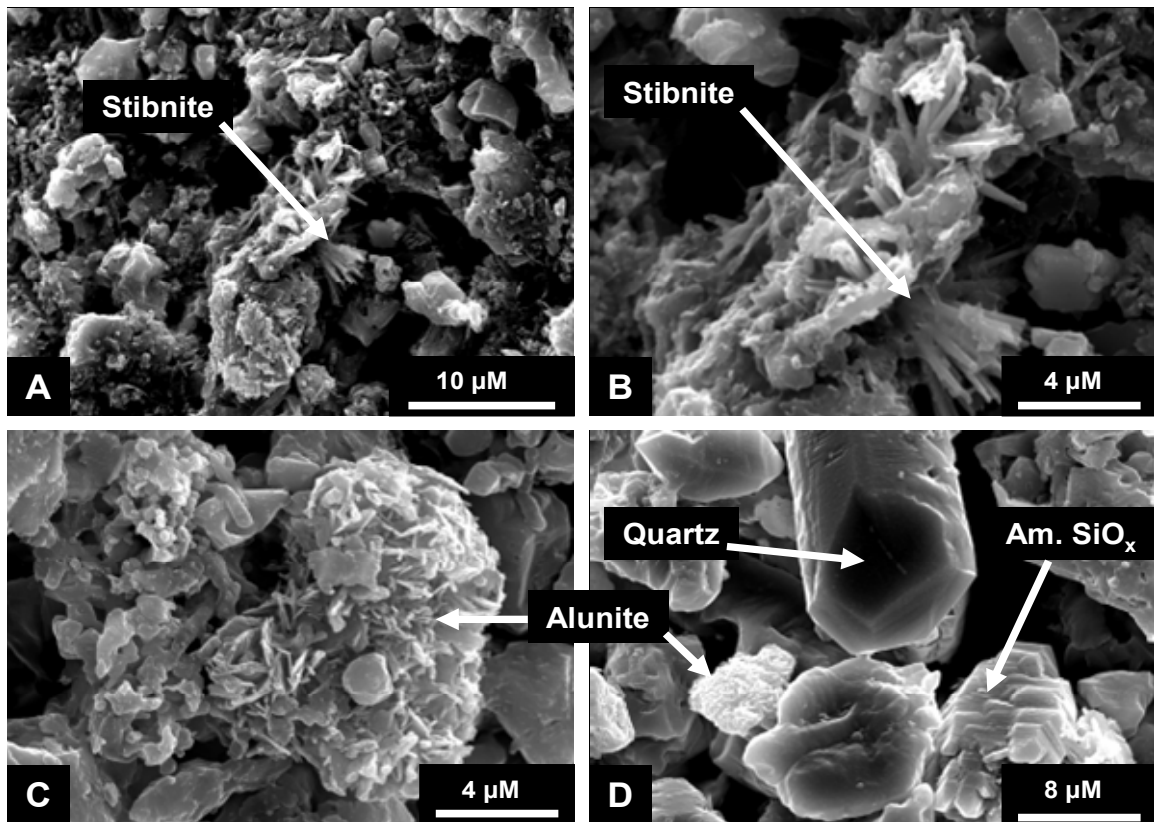


Figure 3.11. Scanning electron micrographs (SEM) of JC3 source pool mineral stibnite deposits, low magnification (A), and higher magnification (B) of stibnite crystals. Alunite is clearly seen and identified in panel (C) from JC3B position within the outflow channel. Quartz, alunite, and amorphous SiO_x are identified in samples taken from JC3B (D).

Microbial community structure

To develop a comprehensive understanding of the geobiology and microbial ecology in Joseph's Coat spring (JC3), it was important to compare geochemical observations and energetic analyses with microbial community composition. Archaeal and bacterial 16S rRNA gene sequences were characterized using DNA extracted from multiple locations within Joseph's Coat spring (JC3) including sediments and solid phases from the source pool, as well as sampling positions throughout the outflow channel positions (B, C, D, and E), where temperatures ranged from 75 °C (JC3B) down to 45 °C (JC3E).

The sequence data revealed that the JC3 system is apparently dominated by relatively few genera (Figures 3.12, 3.13). Bacterial diversity of dominant populations was inversely related to temperature, with an increase in the number of bacterial populations as temperatures decreased with distance from the source (Figure 3.12). Apparent archaeal diversity also increased with distance from the source until the temperature declined to 69 °C at position JC3C (Figure 3.13).

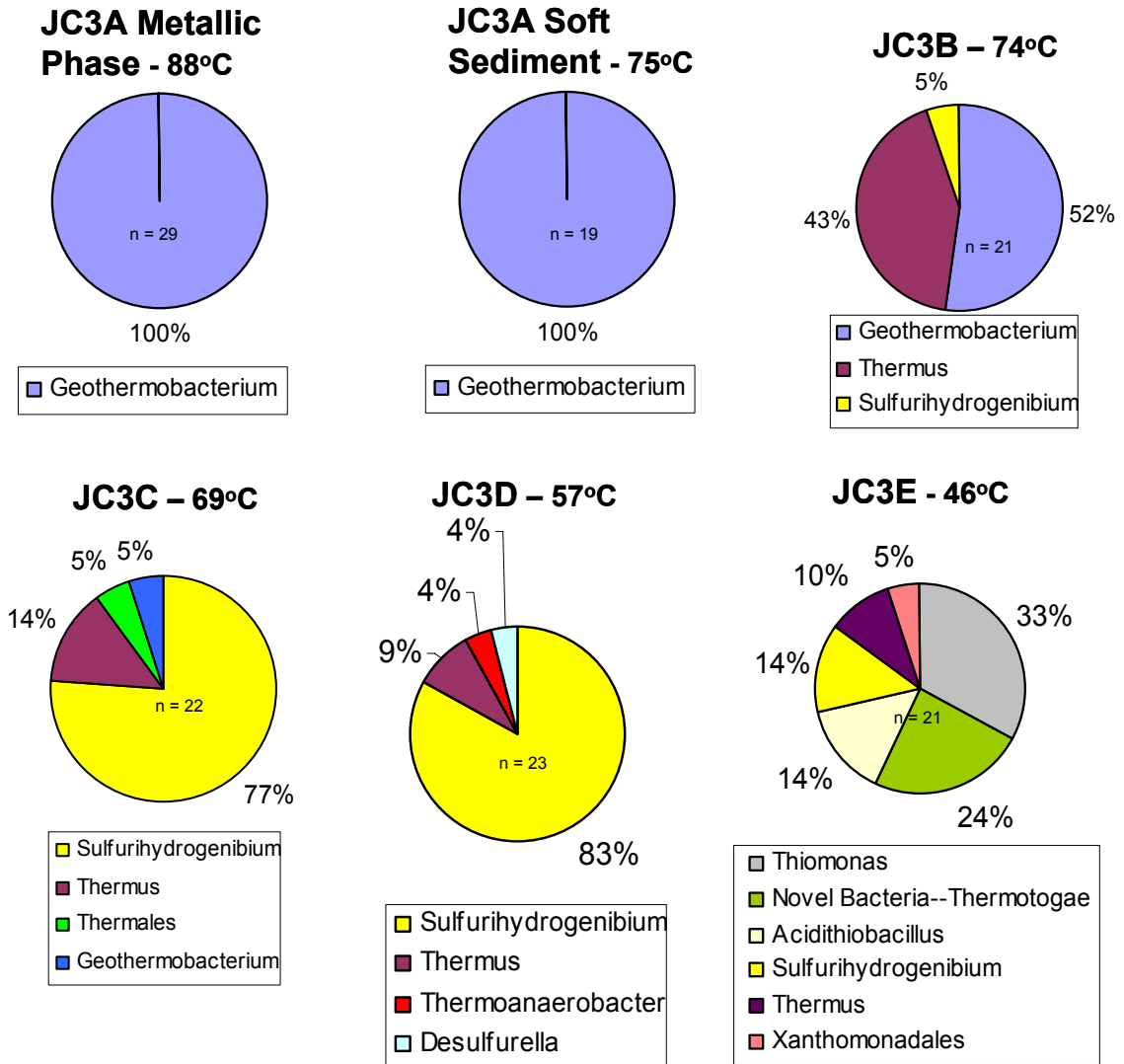


Figure 3.12. Pie charts showing bacterial community composition based on 16S rRNA gene sequences detected at each sampling position in JC3 (2004 samples only). Names of the sequences are based on sequences of nearest cultivated relatives obtained using BLAST alignment (Altschul et al., 1997; <http://www.ncbi.nlm.nih.gov/blast/>). Closest relatives are indicated with genera names when sequences are > 95 % similar. Family names when sequences are only 90 – 94 % similar and phylum level when < 90 %. (Clone sequence data collected by S. Korf, Inskeep laboratory).

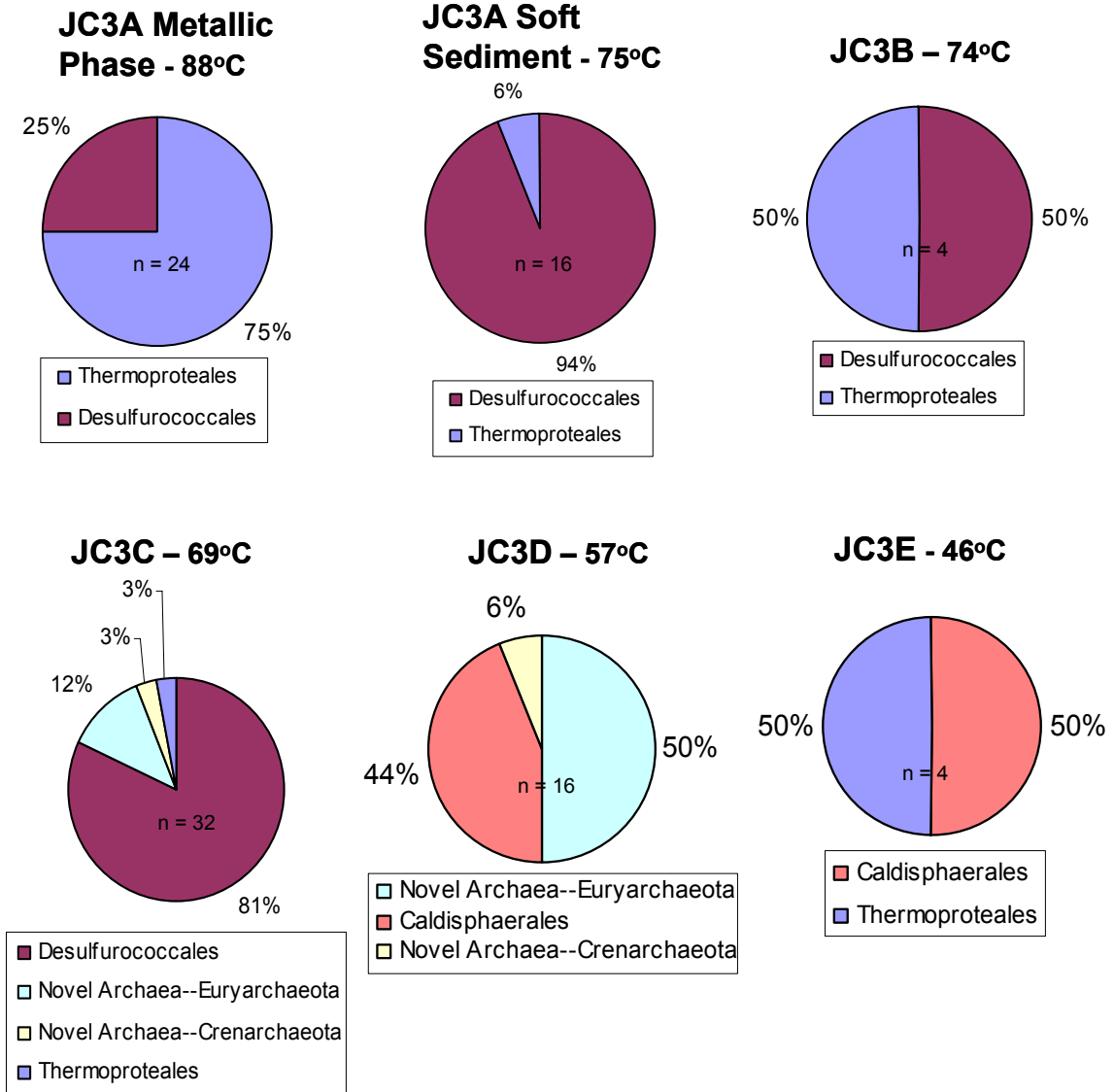


Figure 3.13. Pie charts showing archaeal community composition based on 16S rRNA gene sequences detected at each sampling position in JC3 (2004 samples only). Names of the sequences are based on sequences of nearest cultivated relatives obtained using BLAST alignment (Altschul et al., 1997; <http://www.ncbi.nlm.nih.gov/blast/>). Closet relatives are indicated with genera names when sequences are > 95 % similar. Family names when sequences are only 90 – 94 % similar and phylum level when < 90 %. (Clone sequence data collected by S. Korf, Inskeep laboratory).

Predominant sequences detected in the metallic phase within the source pool (88 - 90 °C) are highly related to the sequences of the Fe^{III} reducing, H₂ oxidizing bacterium *Geothermobacterium ferrireducens* (99%) and the S-respiring Crenarcheota, *Vulcanisaeta* sp. (97%) and *Caldococcus* sp. (97%). *Geothermobacterium ferrireducens* was the only bacterial sequence detected in the metallic phase as well as the lower temperature (75 - 78 °C) soft sediments of the source pool (Kashefi et al., 2002; Aoshima et al., 1996; Itoh et al., 2002). Archaeal sequences detected in the soft sediments and the cooler outflow channel sediments at JC3B (74 °C) corresponded to the sequences found in the metallic phase but also included *Thermofilum pendens* (95%), a heterotrophic S-reducer (Zillig et al., 1983; Itoh et al., 1998). The apparent bacterial diversity increased at JC3B with the detection of sequences highly related to the H₂-oxidizing *Sulfurihydrogenibium azorense* (98%) and a heterotrophic fermenting *Thermus* sp. (99%) (Aguilar et al., 2004; Gihring et al., 2001; Nakagawa et al., 2005). Bacterial diversity continued to increase with distance down the outflow channel (JC3D; 57 °C) where sequences similar to those of a fermenting, S-reducing *Thermoanaerobacter* sp. (98%), and a heterotrophic, S-reducing *Desulfurella* sp. (98%) were detected (Cayol et al., 1995; Miroshnichenko et al., 1998). The broadest bacterial diversity was observed at the coolest sampling position (JC3E; 46 °C). Sequences detected at JC3E correlated to a thiosulfate reducing *Thermosipho* sp. (85%) and a possible denitrifying *Thermomonas* sp. (94%). In addition, sequences closely related to *Thiomonas* sp (97%) and *Acidithiobacillus* sp. (98%), both aerobic Fe-oxidizers, were detected at JC3E (Ravot et al., 1996; Katayama et al., 2006; Inskeep et al., 2004). Archaeal populations detected at JC3D and JC3E were

highly related to the heterotrophic S-reducer *Caldisphaera* sp. (97%). In addition, a *Thermoproteus* sp. (85%) –like sequence was detected at JC3E (Itoh et al., 2003; Stetter and Zillig, 1989). Several novel archaeal sequences that are only distantly related to any cultured organisms (< 90 % similar) were detected at both JC3C and JC3D. These sequences appear to cluster with the Euryarchaeota, but again are < 90 % similar. Consequently, inferring metabolisms from the phylogeny of these distantly related organisms was not possible.

Phylogenetic trees were generated using representative bacterial and archaeal 16S rRNA gene sequences obtained from JC3 samples collected during the 2003 and 2004 field trips (a total of 902 archaeal plus bacterial clones were evaluated). However, 16S rRNA gene sequences indicating > 99 % similarity to one another were grouped and represented on the phylogenetic trees as one entry (Figures 3.14, and 3.15). Sequences identified from various sampling positions within JC3 as well as important thermophilic microorganisms isolated from other geothermal systems were also included in the trees. Sequences obtained from JC3 clustered with the Thermatoga, Thermodesulfurococci, Aquificales, and Deinococcus bacterial orders and the Desulfurococcales, Sulfolobales, Thermoproteales, and Thermoplasmatales archaeal orders. Various bacterial sequences highly related to the *Thermus* were only obtained from down-gradient positions in the outflow channel (JC3B - JC3E). Sequences treeing within the *Thermocrinis* and *Sulfurihydrogenibium* clades (*Aquificales*) were also only detected in the outflow channel. Other bacterial sequences obtained from the spring, including the *Geothermobacterium* –like organism also observed in co-cultures from the soft

sediments, grouped within the *Thermodesulfurococci* or the *Thermotoga* clades. High temperature archaea detected in the spring were members of either the Desulfurococcales or Thermoproteales. The phylogenetic trees and the pie-charts generated in this study are both useful for examining patterns in microbial community structure. Phylogenetic trees provide a useful tool for examining relationships of cloned 16S rRNA gene sequences with other cultured organisms. In contrast, sequences from the pie charts (Figures 3.12 and 3.13) highlight changes in species composition as a function of temperature and position.

Isolation and Characterization of Numerically Relevant Archaea

Isolation

Three microorganisms from JC3 source pool sediments were initially obtained in a tri-culture after several cycles of serially diluting inoculum in serum bottles containing anaerobic synthetic media with a N₂(g) headspace. The tri-culture consisted of two *Archaea* and one *Bacteria*. The two archaea were members of the Crenarchaeota and were 95 % similar to *Thermofilum pendens* and 88 % similar to *Desulfurococcus mobilis*, respectively. The *Thermofilum pendens*-like organism (referred to here as strain WP28t) and the *Desulfurococcus mobilis*-like organism (referred to here as strain WP29d) were present with a bacterium closely related to *Geothermobacterium ferrireducens* (98 % similar). After determining the composition of the tri-culture, antibiotics (kanamycin and vancomycin) were added at 15 µg mL⁻¹ to eliminate the bacterium. Several additional cycles of dilution to extinction with antibiotics resulted in a pure culture of WP28t (*Thermofilum pendens*-like), and a co-culture of the two archaea.

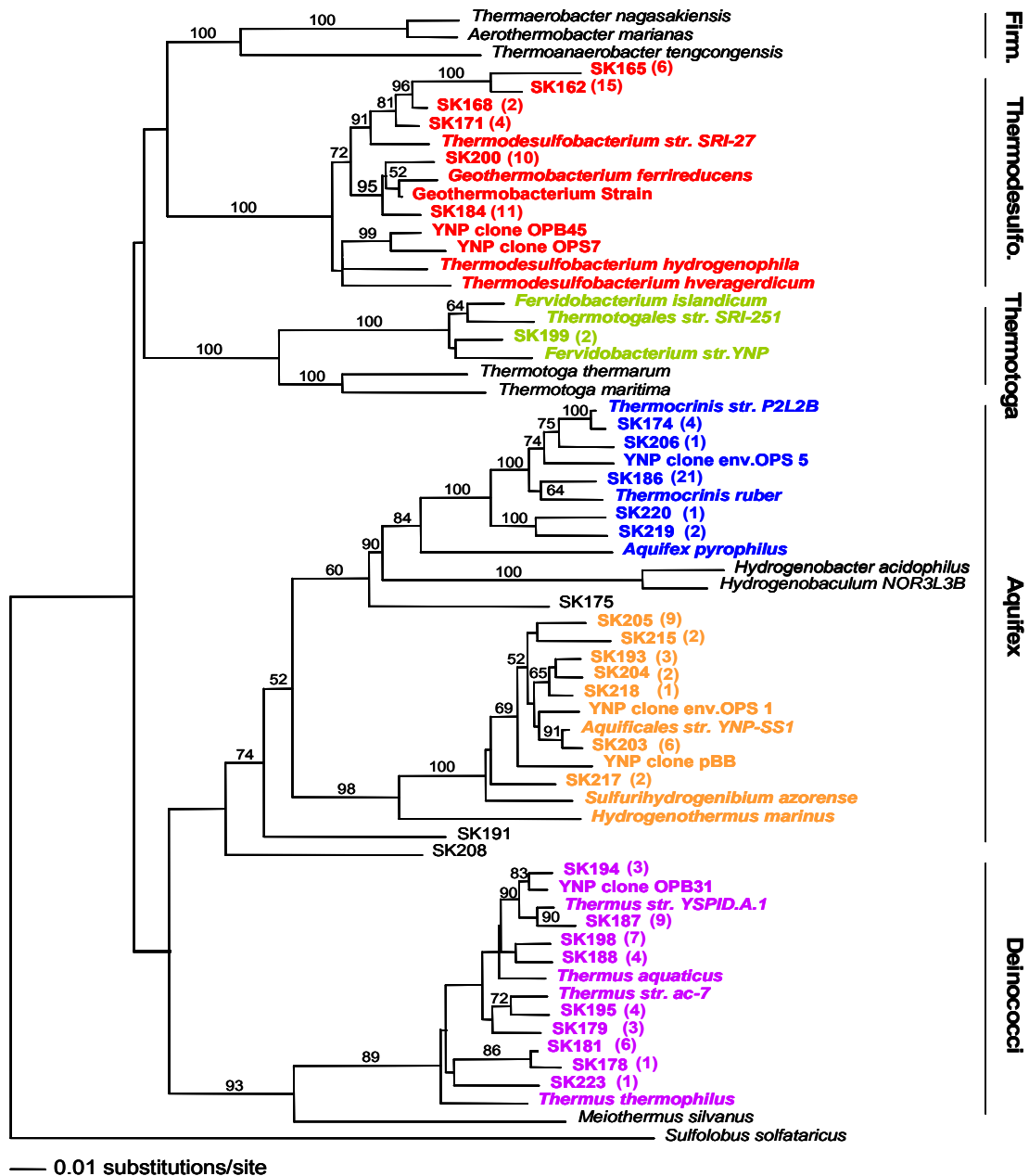


Figure 3.14. Rooted phylogenetic tree based of bacterial 16S rRNA gene sequences detected in Joseph's Coat Spring (JC3) showing environmental clones, microorganisms isolated from JC3, important related microorganisms, and taxonomic clades. The trees were constructed using the neighbor joining method (scale bar indicates one estimated substitution per 100 nt; absolute bootstrap values per 100 bootstraps). Numbers in parentheses indicate the number of closely related sequences.

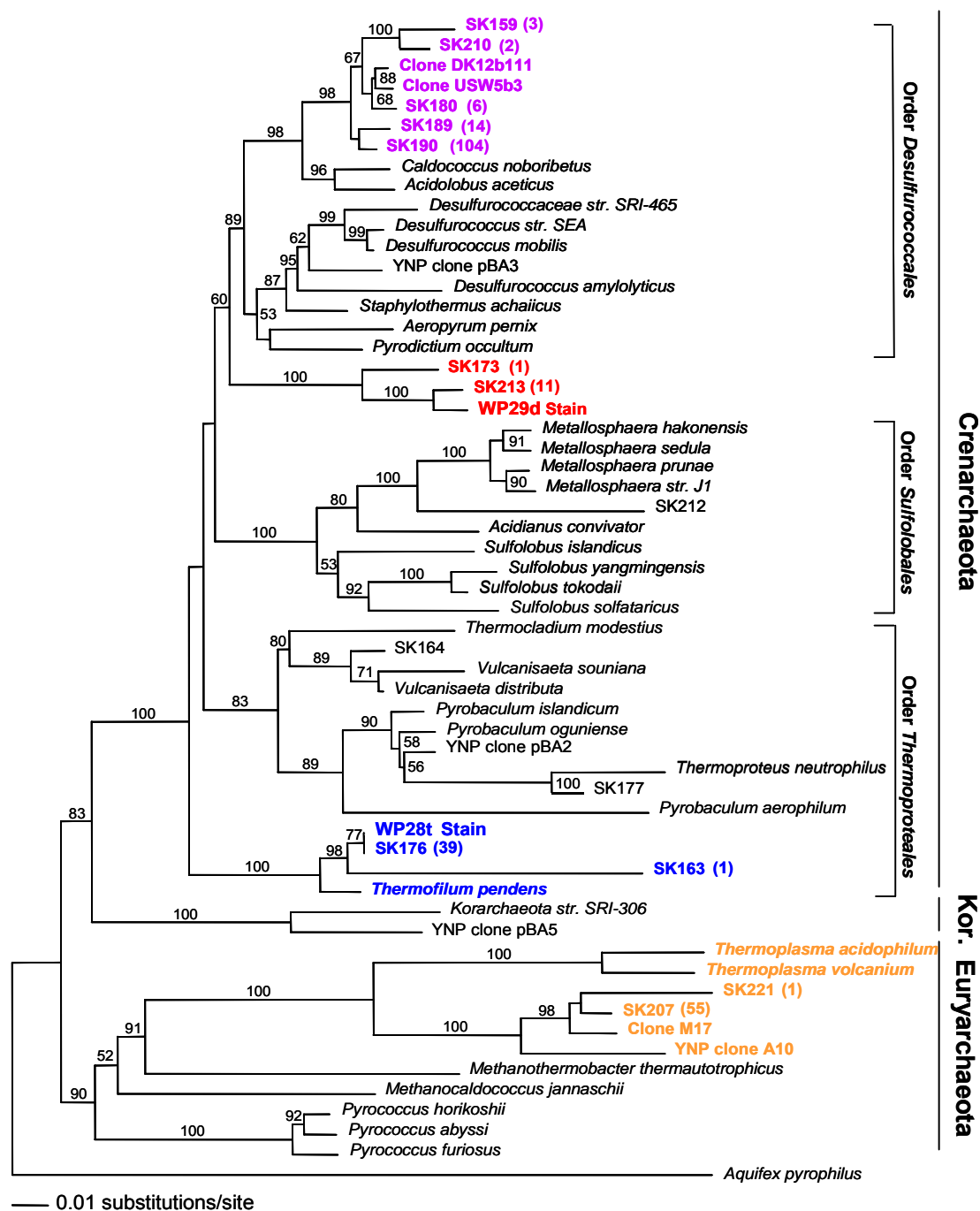


Figure 3.15. Rooted phylogenetic tree based on archaeal 16S rRNA sequences detected in Joseph's Coat Spring (JC3) showing environmental clones, microorganisms isolated from JC3, important related microorganisms, and taxonomic clades. The trees were constructed using the neighbor joining method (scale bar indicates one estimated substitution per 100 nt, absolute bootstrap values per 100 bootstraps). Numbers in parentheses indicate the number of closely related sequences.

Numerous attempts to separate WP29d from WP28t in the co-culture were not successful. These treatments included utilization of different C sources and spent-media extracts coupled with repeated dilution to extinction. The difficulty in separating these two organisms suggests that WP29d may require compound(s) produced by WP28t. The requirement of a specific growth factor from another organism is not uncommon among archaea and was also determined to be important for the successful isolation of *Thermocodium modestius* and *Thermofilum pendens* (Zillig et al., 1983; Itoh et al., 1998). Both organisms required addition of polar lipids from a distantly related crenarchaeote for isolation. The inability to separate WP29d from WP28t necessitates that interpretation of the physiology of WP29d be made in the context of a co-culture with isolate WP28t.

Highly-related 16S rRNA gene sequences (99 - 100%) to each of these isolates were detected in clone libraries from JC3, indicating that the *Thermofilum* and *Desulfurococcus*-like isolates represented what are likely numerically relevant populations in the spring. Certainly, the biases inherent in DNA extraction, amplification and cloning must be recognized as potentially influencing the relative frequency of specific 16S rRNA gene sequences within a clone library. However, the combination of traditional isolation with cultivation-independent molecular approaches provides a foundation necessary for further elucidating primary community members and their physiological role and connection to geochemical processes.

Morphology

Fluorescent microscopy of WP28t cells stained with SYBR-green II revealed straight regular rods of $\sim 0.5 \mu\text{m}$ in diameter with infrequent branching. Average cell length was between 3 and 5 μm (Figure 3.16 A, B) however, it appeared that some cells were up to 50 μm in length (Figure 3.16 C, D). Cells were often arranged in aggregates and in some cases; the cells were bent at up to 10 degrees (Figure 3.16 C, D, E). Cells bearing globular bodies ($\sim 10\%$ of cells) were observed toward the end of the exponential growth phase (Figure 3.16 E, F). The globular bodies were formed at all points along the cell wall and appeared to be very similar to the *golf club* features formed by *Thermofilum pendens* (Zillig et al., 1983), *Thermocladium modestius* (Itoh et al., 1998), *Caldivirga maquilingsis* (Itoh et al., 1999) and *Pyrobaculum aerophilum* (Volkl et al., 1993). Strain WP29d exhibited regular cocci morphology, with average diameters of approximately 1 μm (Perevalova et al., 2005; Figure 3.17 A, B). WP29d occurred as single cells but were also rarely observed in diplococci form. Neither of the organisms appeared to be motile under optical microscopy.

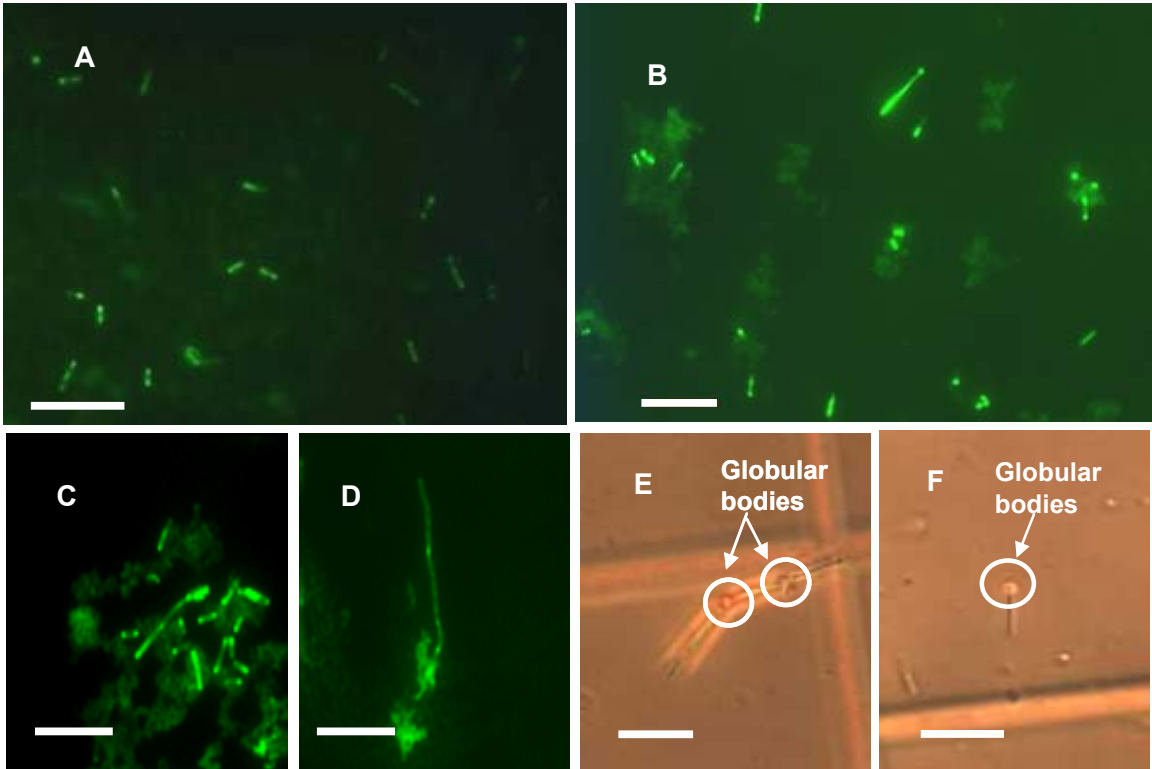


Figure 3.16. Images of isolate WP28t obtained using SYBR-green II stained cells and phase contrast microscopy. Cells were rod-shaped, 3 - 8 μm in length (A, B), but occasionally grew to lengths of 20 μm or more (C, D). Aggregates of cells were common (C). Cells are shown with globular bodies (E, F). Bars are 10 μm .

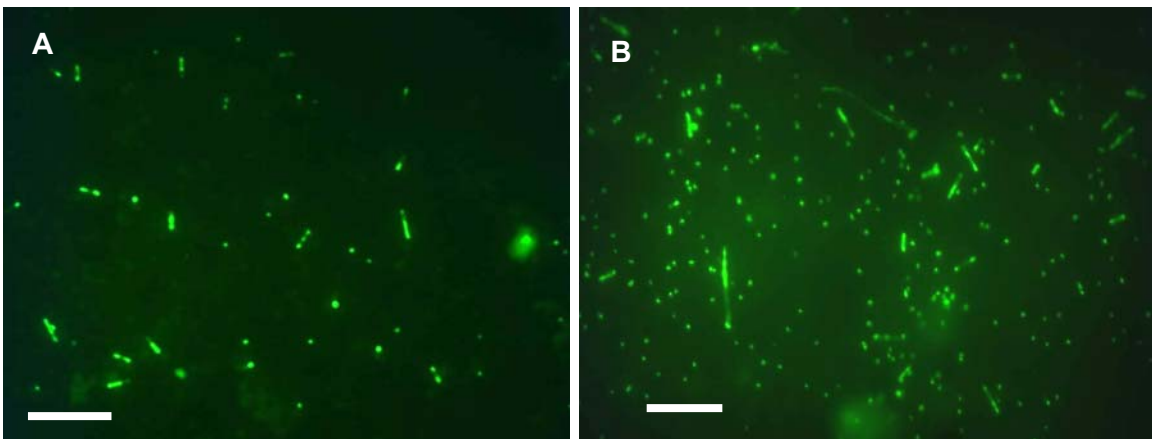


Figure 3.17. Light microscopy using SYBR-green II of a co-culture containing WP28t and WP29d. Strain WP29d appears as a regularly-shaped cocci 1 μm in diameter (A, B). Bars are 10 μm .

Growth optima

High concentrations of sulfide were produced during growth of both the pure culture containing only strain WP28t and the co-culture containing both strains WP28t and WP29d (Figure 3.17). At optimal conditions (pH 6.1, 75 °C, yeast extract = 0.2 g/L), isolate WP28t grew to cell densities of 7.0×10^6 cells ml⁻¹ exhibiting doubling times under optimum conditions of 5.9 h (Figure 3.18). The temperature range for growth of strain WP28t was 58 to 95 °C, with optimum growth occurring at 75 °C (Fig. 3.19; pH 6.0). Growth was observed over a wide pH range of 3.6 - 9.0, but maximum growth occurred between pH values of 4.6 - 6.6 at 75 °C (Fig. 3.20; 75 °C). Sulfide production by WP28t correlated closely with cell growth, although maximum sulfide concentrations were measured after cells reached stationary phase (0.38 mM DS after 11 days).

Due to the difficulties in differentiating strain WP29d from elemental S⁰ particles in the media, accurate cell counts of WP29d could not be obtained. Consequently, pH and temperature optima for growth of WP29d in the presence of strain WP28t are not known at this time. However, H₂S production from the co-culture mirrored that observed in experiments conducted in pure cultures of strain WP28t (data not shown). Co-culture cell densities of strain WP28t mimicked cell counts and growth curves observed in pure culture (e.g. Figure 3.18). To determine the effects of WP29d on growth of WP28t, the co-culture was subjected to the same temperature and pH treatments applied to the pure isolate. No changes in the growth optima for strain WP28t were noted in the presence or absence of strain WP29d.

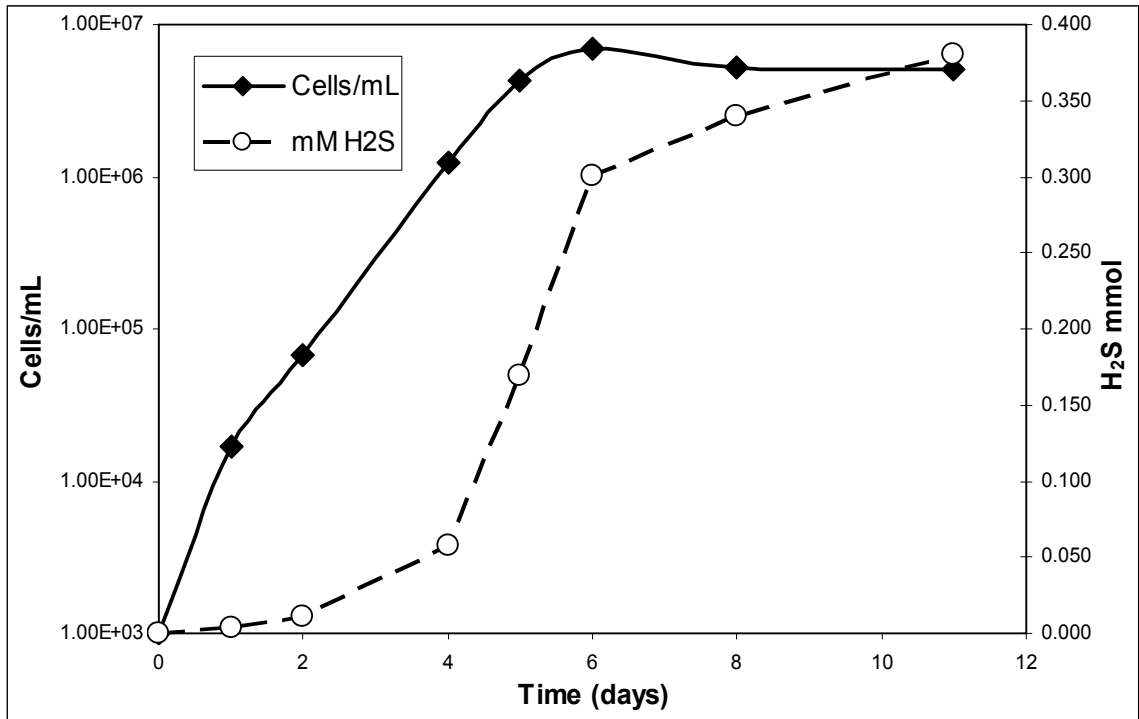


Figure 3.18. Growth (cells/mL) of *Thermofilum*-like strain WP28t at optimum growth temperature and media conditions (75 °C, pH 6.1) plotted along with the concentrations of dissolved sulfide as a function of time.

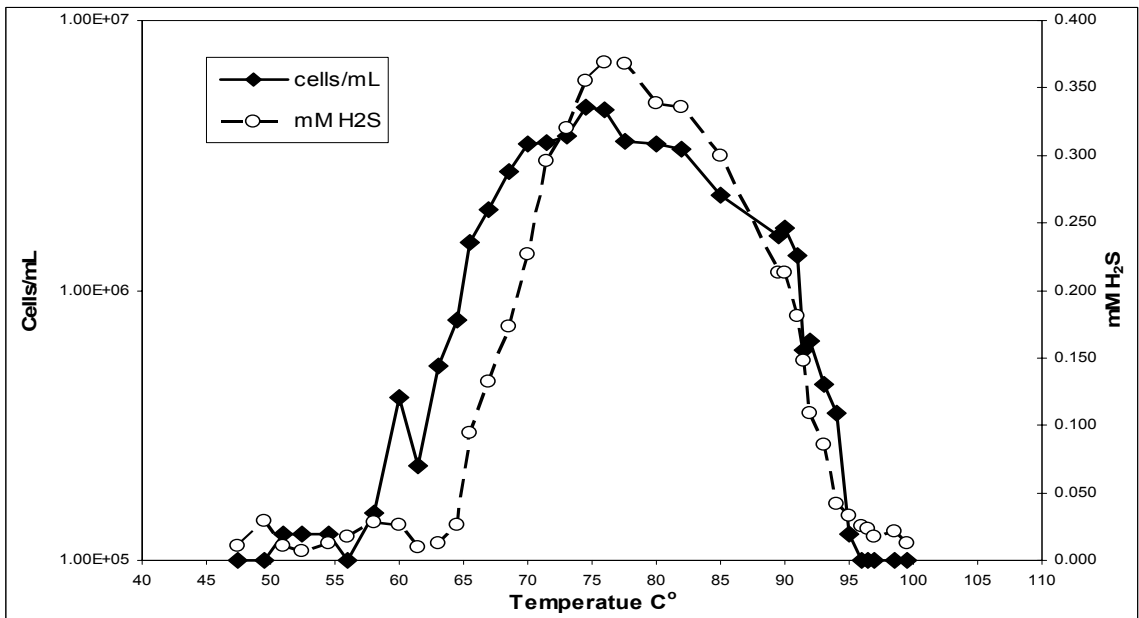


Figure 3.19. Growth (cells/mL) and dissolved sulfide production of *Thermofilum*-like strain WP28t as a function of temperature. Cell counts and sulfide production were assessed after 5 days in cultures inoculated with 10^5 cells mL⁻¹ at a pH = 6.1.

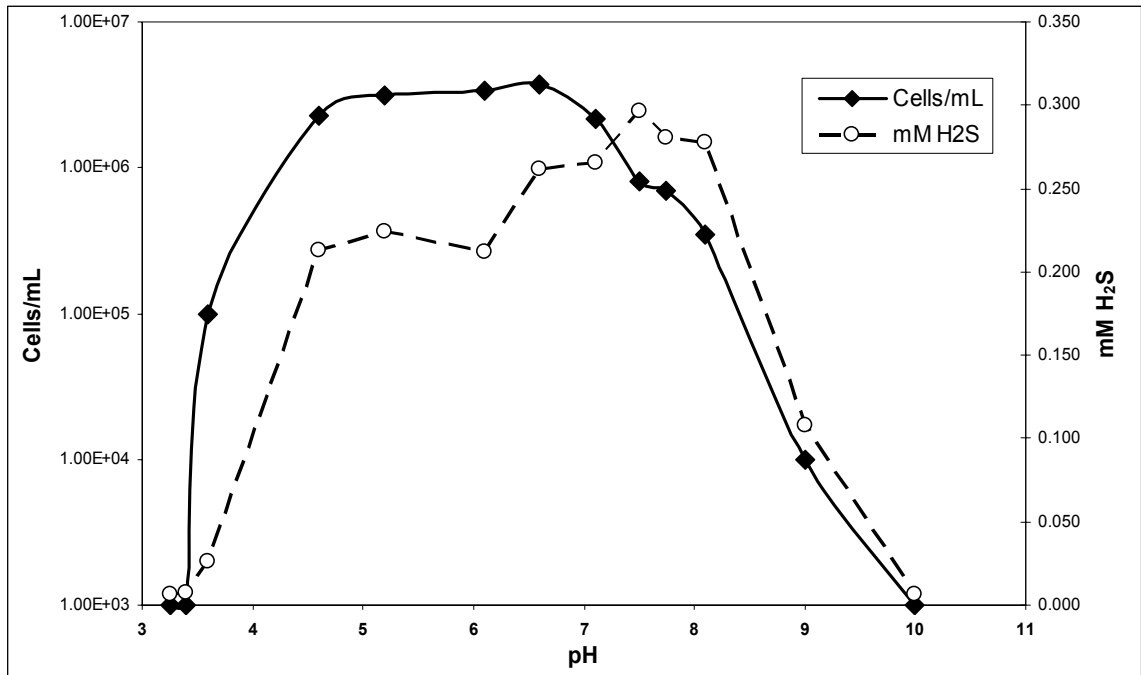


Figure 3.20. Growth (cells/mL) and dissolved sulfide production of *Thermofilum*-like strain WP28t as a function of pH. Cell counts and sulfide production were assessed after 5 days in culture inoculated with 10^3 cells mL^{-1} at a $T = 75^\circ\text{C}$.

Metabolism

Strain WP28t grew under strictly anaerobic conditions using either S^0 or $\text{S}_2\text{O}_3^{2-}$ as an electron acceptor (Table 3.6, Treatments 4, 17). Neither the WP28t isolate nor the co-culture grew autotrophically under a $\text{N}_2:\text{CO}_2$ (4:1, v/v) atmosphere (Table 3.6; Treatment 1). The growth conditions yielding the greatest production of DS and the greatest increase in cell numbers included 0.2 g/L yeast extract with elemental S^0 as an electron acceptor (Treatment 4). Maximum cell densities of strain WP28t were achieved with yeast extract (0.2 g/L), where in addition to any vitamins or growth promoting substances, C compounds present in YE served as a readily available C and energy source. In fact, the growth of WP28t was directly correlated with YE concentration (Treatments 2 - 4). Lactate, acetate, starch and glucose did not appear to enhance growth over the

background 0.002 or 0.02 g/L yeast extract treatments of with strain WP28t (Treatments 5 – 13). A minimum concentration of at least 0.002 g/L yeast extract (YE) was required for growth with other simple carbon sources (e.g. starch, lactate, acetate, and glucose) and was included in all experiments (Treatments 5 - 8). The addition of thiosulfate (5 and 10 mM) in the presence of YE (0.02 and 0.2 g/L) respectively produced low cell counts (Treatment 10 and 16). When the standard N₂ headspace was replaced with H₂ (g), at a yeast extract concentration of 0.02 g/L cell counts of isolate WP28t remained similar but sulfide production increased (Treatment 14). The presence of 2 % O₂ in the headspace completely inhibited growth of both the isolate and co-culture strains (Treatment 15). Several other relevant electron acceptors were applied in the absence of S⁰ with no growth detected (Treatments 18 – 20). Finally, the ability to utilize YE as a C source for fermentation was evaluated using treatments with the addition of no major electron acceptors; no growth occurred (Treatment 17).

Table 3.6. Evaluation of potential carbon sources and possible electron acceptors supporting growth of *Thermofilum*-like strain WP28t. Experiments were conducted in 100% synthetic media contained in 10 mL serum bottles at 75 °C and pH 6.1. nd = not detectable. YE = yeast extract.

Treatment #	C source	Yeast Extract (g/L)	Electron Acceptor	H₂S mM	Cells/mL (final-initial)
1.	CO ₂	0	S ⁰	nd	0.0E+00
2.	YE	0.002	S ⁰	0.07	1.85E+04
3.	YE	0.02	S ⁰	0.16	2.64E+05
4.	YE	0.2	S ⁰	0.26	1.23E+06
5	Starch	0.002	S ⁰	0.09	1.08E+05
6	Lactate	0.002	S ⁰	0.08	3.63E+04
7	Acetate	0.002	S ⁰	0.06	6.97E+04
8	Glucose	0.002	S ⁰	0.08	3.0E+03

TABLE 3.6 CONT.

Treatment #	C source	Yeast Extract (g/L)	Electron Acceptor	H₂S mM	Cells/mL (final-initial)
10	Starch	0.02	S ₂ O ₃ (5mM)	0.03	1.47E+04
11	Lactate	0.02	S ⁰	0.14	4.73E+04
12	Acetate	0.02	S ⁰	0.18	1.14E+05
13	Glucose	0.02	S ⁰	0.12	0.0E+00
14	H ₂	0.02	S ⁰	0.25	3.11E+05
15	YE	0.2	O ₂ (1%)	nd	0.0E+00
16	YE	0.2	S ₂ O ₃ (10mM)	0.17	1.03E+05
17	YE	0.2	None	nd	0.0E+00
18	YE	0.2	Sb ^V	nd	0.0E+00
19	YE	0.2	As ^V	nd	0.0E+00
20	YE	0.2	Fe ^{III}	nd	0.0E+00

CHAPTER 4

DISCUSSION

Geochemistry: Foundation for Understanding Chemotrophy

One of the predominant geothermal features in the Joseph's Coat Springs complex (referred to in this study as JC3) currently exhibits the highest average ($n = 4$) thiosulfate ($S_2O_3^{2-}$, $750 \mu M$), arsenic (As, $130 \mu M$), and antimony (Sb, $1.0 \mu M$) concentrations of any known analyzed geothermal feature in YNP. The aqueous concentrations of major cations and anions in the near-neutral ($pH=6.1$), boiling ($T=90^\circ C$) source pool remained quite stable (standard deviations $< 10 \%$) over 4 annual sampling events (2003-2006). This spring has a unique chemical signature including high chloride ($10.3 mM$), sodium ($11.4 mM$), ammonium ($5.6 mM$), sulfate ($4.2 mM$), boron ($5 mM$), total dissolved arsenic ($130 \mu M$), thiosulfate ($750 \mu M$) and total dissolved sulfide ($22 \mu M$), accompanied with low total soluble iron ($0.6 \mu M$) (Table 3.1). Concentrations of dissolved gases (e.g. CO_2 , H_2 , H_2S , CH_4) in the source waters of this spring were more variable (standard deviations ranging from 10 to 50 %) across sampling events than the major ions. However, predominant trends in outflow channel processes as inferred from changes in aqueous and solid phase chemistry down gradient were very stable across the 2003 to 2006 monitoring period (Figures 3.1, 3.2, 3.3 and 3.4).

The geothermal source waters of Joseph's Coat spring (JC3) exhibit significant thermal and chemical nonequilibrium with respect to atmospheric conditions. The concentrations of dissolved gases (H_2S , CH_4 , H_2) and CO_2 are significantly oversaturated

with respect to atmospheric conditions, and dissolved oxygen values are below detection. The simultaneous presence of numerous reduced species establishes significant nonequilibrium among individual half-cell reactions (i.e. calculated values of electron ‘activity’), and with respect to atmospheric levels of O_2 (0.16 atm at this elevation and pressure). The number of possible electron donor/acceptor pairs that may be important in microbial metabolism is significant as demonstrated from energetic analyses. This nonequilibrium drives a variety of important abiotic and biotic processes occurring within the outflow channel including degassing and ingassing, as well as the oxidation of chemical species such as arsenite. Combined with a 40 °C decline in temperature, the chemical and physical gradients establish a continuum of possible microbial habitats within stream sediments and or biomineralized solid phases (Figure 3.3).

The degassing of dissolved sulfide is considerably slower at pH 6.1 - 6.5 than observed in acid-sulfate systems, and can be explained based on the pH dependence of S speciation (H_2S $pK_a = 6.52$). Slower apparent O_2 ingassing within JC3 is a direct result of slower H_2S degassing than observed in lower pH systems, and results in a more reduced environment for a greater distance within the outflow channel as inferred from dissolved O_2 measurements in the aqueous phase. The same is true for the disappearance of dissolved inorganic C (DIC) in the JC3 system, where at pH 6.1 - 6.5 HCO_3^- becomes a more significant species, slowing the rates of H_2CO_3 (i.e. $CO_2(aq)$) degassing. However, $CH_4(aq)$ remains a neutrally charged species at this pH and shows rapid disappearance down gradient.

Energetics and Chemotrophy

Numerous oxidation-reduction reactions involving different combinations of electron donors and acceptors are exergonic in JC3 (Table 3.2). The 55 oxidation-reduction reactions considered in this study represent a small subset of the possible energy generation reactions that could be utilized by microorganisms in JC3. Several of the exergonic reactions considered here are the basis for chemolithotrophy observed in cultivated microorganisms (Amend and Shock, 2001). Furthermore, the reactions yielding the greatest amounts of energy (kJ/mole electron) are often singled out as providing the basis for primary production in geothermal systems (Spear et al., 2005). While this may be convenient, it does not necessarily provide an accurate assessment of the microbial physiologies actually operating *in situ*. For example, the oxidation of H₂ with O₂ will always yield a significant amount of energy per mole electron (~70 - 95 kJ mol⁻¹ electron⁻¹) down to extremely low activities (e.g., 10⁻¹⁵M) of these species (Inskeep et al., 2005). Although microbial oxidation of hydrogen in the source pool may indeed be an important process in JC3 source water environments, the electron acceptors responsible for primary productivity in JC3 may instead be Fe^{III} or elemental S⁰, which yield considerably less energy (only 20-35 kJ mol⁻¹ electron⁻¹). Likewise, oxidation reactions using reduced forms of S with O₂ as an electron acceptor will always yield significant energy, provided detectable levels of sulfide (or elemental S⁰) and oxygen are at least at detection limits. However, the importance of organisms whose close relatives are implicated in S⁰ and or S₂O₃²⁻ reduction in the source and outflow channel also suggest that the flux of oxygen into the source pool and early outflow channel sampling

locations (e.g. 0 – 6.5 m) is too low to support oxygen-based metabolism. The majority of 16S rRNA gene sequences obtained from the JC3 source pool sediments; for example, represent organisms that are known heterotrophic sulfur reducers. The energy yields from reactions involving the oxidation of organic C sources with S^0 or $S_2O_3^{2-}$ (reactions 28, 32, 33, 41) are generally fairly low, but are similar to energy yields from anaerobic chemolithotrophy (H_2/Fe^{III} , H_2/S^0 ; reactions 15 and 42), (Rogers and Amend, 2006).

When considering a representative range of electron donor-acceptor combinations, the amount of free energy available follows a systematic pattern of established thermodynamic hierarchy often depicted as an electron ladder where O_2 as a terminal electron acceptor (TEA) yields the highest energy followed by NO_3^- , Fe^{III} , Sb , S^0 , As , $S_2O_3^{2-}$ (figure 3.7). The analysis of Gibbs free energy values (ΔG_{rxn}) combined with 16S rRNA gene sequence data is useful for determining possible sources of chemical energy that are responsible for microbial community structure in geothermal environments (Rogers and Amend, 2005, 2006; Inskeep and McDermott, 2005; Inskeep et al., 2005; Spear et al., 2005; Meyer-Dombard et al., 2005). The calculated free energies based on actual spring conditions provide a *free energy profile* (Figure 3.7) useful for direct comparison with inferred metabolic properties based on the 16S rRNA gene phylogeny of clones obtained from the spring sediments. This combined approach can be utilized to develop a better understanding of the geochemical processes that may define microbial population distribution and physiology *in situ*, and lead to stronger hypotheses regarding metabolisms of specific phylogenetic clades. Moreover, a comparison of actual physiologies occurring *in situ* with the distribution of free energy values provides an

energetic context for ecological hypotheses related to strategies for energy conservation. However, the reliance on energetic data alone can lead to false assumptions about energy sources driving primary productivity in geothermal systems. While exergonic reactions are required for microbial energy conservation, other important factors determine which of the many energy yielding reactions are ultimately utilized by native microorganisms.

Possible Microbial Metabolisms Inferred from 16S rRNA Gene Sequence Distribution

Support for chemolithotrophic primary productivity in the source pool of JC3 is based on the presence of 16S rRNA gene sequences whose close relatives are known H₂ oxidizers (e.g. *Geothermobacterium*-like sequences) (Kashefi et al., 2002). In addition, the presence of chemoorganotrophs respiring on either S⁰ or S₂O₃²⁻ is inferred from the identification of numerous clones whose close relatives are known S reducers (e.g., *Thermofilum* and *Desulforococcus*-like sequences) (Perevalova et al, 2005; Itoh et al., 1999). Several oxidation-reduction reactions where S or S₂O₃²⁻ serves as electron acceptors were shown to be energetically favorable in this system (Reactions 28, 32, 33, and 41 from Table 3.2). Together with inferred metabolisms of microorganisms represented in 16S rRNA gene clone libraries, these results indicate the important linkage between reduced forms of S and microbial community structure in the low O₂ environments of JC3.

Solid phase precipitation-dissolution reactions occurring within and across JC3 geothermal gradients also provide clues regarding possible linkages among specific microbial phyla and their respective metabolisms. Biomineralization occurring due to the discharge of supersaturated hydrothermal fluids from hot-spring systems is well

documented (Konhauser et al., 2001; Phoenix et al., 2006, Inskeep et al., 2004; Langer et al., 2001). Microbial cells in these hydrothermal systems can serve as nucleation sites for the precipitation of dissolved constituents and or utilize redox reactions for chemosynthetic metabolisms, which result in the precipitation of minerals on cell surfaces. Detailed microscopic analyses of solid phases present in the source pool and outflow channel reveal deposition of solid phases including pyrite, stibnite, orpiment and elemental S. The relative abundance of orpiment-like phases appears to be in part responsible for distinct orange and yellow layers within the sediments of this system. Reduced conditions in the source pool of JC3 and the lack of detectable O_2 (aq) in the down-stream (up to 11 m) transect positions accounts for the formation of pyrite (FeS_2) as well as the absence of oxidized Fe^{III} -solid phases. Stibnite (Sb_2S_3) was also confirmed as a major solid phase occurring in the JC3 source pool (Figure 3.9 B and 3.7C). However, Sb_2S_3 saturation indices calculated from aqueous geochemistry were well under-saturated for this mineral phase (Table 3.3). Although the mechanisms responsible for stibnite mineralization in JC3 cannot be definitively established, the potential exists for microorganisms to act as nucleation sites for the formation of metal-sulfides and amorphous silica phases (Phoenix et al., 2005). It has been hypothesized that cell membranes (e.g. S-layers) and or other cellular components act as nucleation sites for mineralization of orpiment and stibnite like phases in Champagne Pool (New Zealand) (Phoenix et al., 2005), and this may contribute to the formation of these phases within JC3. Total dissolution analysis showed that these minerals dominate the composition of the thin (~2 - 3 mm thick) brittle “metallic” phase lining the hottest regions of the source

pool (see Figures 3.8 A and 3.8 B), and reveal that these solids contain nearly 16, 14, 27, and 1 wt. % Fe, Sb and S and As, respectively.

The most frequent 16S rRNA gene sequences detected in the source pool solids and sediments included *Geothermobacterium*-like, *Caldococcus*-like and *Thermofilum*-like organisms (Figure 3.12 and 3.13). The closest cultivated relative of the *Geothermobacterium*-like sequences is *Geothermobacterium ferrireducens*, an obligate anaerobic chemolithotroph capable of oxidizing H₂ using Fe^{III} as an electron acceptor (Table 3.2, reaction 11; Kashefi et al., 2002). This is consistent with the mineralization of FeS₂ observed in the source pool of JC3. In addition, rod-shaped structures reminiscent of cells were observed on the pyrite surface (Figures 3.9 D). Conversely, the metabolism of *Caldococcus noboribetus* (Aoshima et al., 1996), and other relatives of the Desulfurococcales (*Staphylothermus* sp., *Desulfurococcus* sp.) involves reduction of elemental S⁰ with organic C sources (e.g., peptides, yeast extract) serving as a C and energy source (Perevalova et al., 2005; Arab et al., 2000). Nearly every 16S rRNA gene sequence detected across all sampling positions within JC3 has as its closest phylogenetic relative, an organism whose metabolism involves S cycling. Specifically, *Thermofilum*, *Desulfurococcus*, *Caldococcus*, *Caldisphaera*, *Vulcanisaeta* and *Desulfurella*-like sequences suggest the importance of S⁰, S₂O₃²⁻ or potentially SO₄²⁻ reduction in the majority of both outflow channel and source pool sampling sites.

It is not until further down gradient when members of the Aquificales and Thermales emerge as important microbial community members (Figure 3.12, Figure 3.13). The predominant Aquificales relatives were *Sulfurihydrogenium*-like and

Thermocrinus-like sequences. The fact that cultivated relatives of these sequences are generally microaerobic to aerobic suggests that O₂ ingassing is beginning to influence microbial community structure by even 4 m in the outflow channel, despite the fact that dissolved O₂ remains below detection until 8 m. Alternatively, the organisms represented by these sequences may utilize electron acceptors besides O₂ (e.g. NO₃⁻), but even microaerobic conditions may allow these thermophilic organisms to colonize environments close to the air-water surface. Sulfur (either S^{-II} or S⁰) oxidation is a likely metabolic niche for the *Sulfurihydrogenibium*-like sequences, especially given that *Sulfurihydrogenibium yellowstonse* is a known S⁰ oxidizer isolated from the Calcite Springs area (Reysenbach et al., 2000) and similar sequences have been observed in other S-rich environments in YNP (Spear et al., 2005, 2006; Fouke et al., 2003). Curved-rods were observed in the orange and yellow sediment layers from transect positions further down gradient using SEM (e.g. 10-12 m; Figure 4.1 A, B). However, the relatively high concentrations of cells observed in yellow or orange layers of JC3 sediments were not obvious in mixed-sediment or grey-sediment samples. The exact identity of these organisms cannot be ascertained from SEM micrographs; however, the morphology appears consistent with members of the Aquificales or the Thermus-like organisms isolated in other experiments (Reysenbach et al., 2000, 2005; Gihring et al., 2001), which are closely related to sequences observed in these samples. The presence of *Thermocrinus*-like sequences observed at transect locations B, C, D and E suggest that H₂ oxidation may also be an important energy source supporting these populations under microaerobic conditions (Huber et al., 1998). Unlike *Sulfurihydrogenibium* sp.,

Thermocrinus sp. appear to prefer hydrogen rather than S as an electron donor (Huber et al., 1998, 2000; Meyer-Dombard et al., 2005; Reysenbach et al., 2005; Spear et al., 2005).

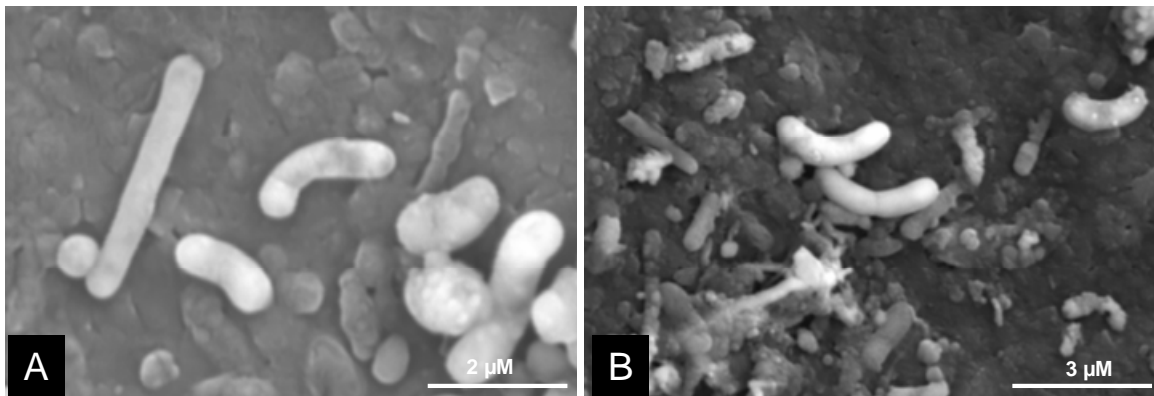


Figure 4.1. SEM images of curved rods and rods observed in the yellow sediment layers of JC3E (A, B).

One of the most dramatic and important geochemical changes occurring in the outflow channel is the oxidation of arsenite (As^{III}) to arsenate (As^{V}) (Figure 3.4). This exergonic process may be catalyzed by organisms for energy gain (Figure 3.5). Previous work has shown that members of the Aquificales and Thermales are known arsenite oxidizers (Gihring et al., 2001; Reysenbach et al., 2005; Aguiar et al., 2004). However, there is uncertainty whether these organisms mediate this redox transformation for energy gain or as a detoxification strategy (Inskeep et al., 2007). Arsenite oxidase genes (*aroA*) have been detected in the outflow channel of JC3 and these sequences appear to cluster near the *Thermus*-like AroA oxidases. Further work will be necessary to elucidate the role of As in microbial metabolisms in this system, but the expression of *aroA* genes clearly links microbial processes with geochemical changes.

Several potentially important bacterial and archaeal sequences detected across JC3 sampling locations were not closely related (e.g. less than 90%) to 16S rRNA gene

sequences of cultivated microorganisms. Furthermore, several of the sequences detected in the spring have close relatives exhibiting more than one potential metabolism that could be utilized *in situ* (Figures 3.12 – 3.15). Therefore, it is critical to obtain actual pure culture isolates that can be shown to be relevant members of the community via cultivation-independent methods, and whose physiologies can be confirmed in the laboratory. In the current study, cultivation strategies were designed based on knowledge of spring geochemistry and 16S rRNA gene phylogeny.

Isolation of Relevant Microorganisms

Sediments from a 75-78 °C location within the source pool of Joseph's Coat spring (JC3) were used as inoculum to successfully obtain a pure culture (strain WP28t) of a novel crenarchaeote within the order Thermoproteales. Sequence analysis (1336 bp) of the rod-shaped strain WP28t place this novel organism in the phylum Crenarchaeota, order Thermoproteales, family Thermofilaceae, and would likely be considered a new species of the *Thermofilum* genera (Figure 3.15). DNA sequence and subsequent phylogenetic analysis indicate that the closest 16S rRNA relative of isolate WP28t is *Thermofilum pendens* (95 % sequence similarity). The physiology, morphology (including 'golf-club' appendages) and optimum growth temperatures (75 °C) of strain WP28t are fairly consistent with those established for *T. pendens* (Zillig et al., 1983; Itoh et al., 1998, 1999). Specifically, the obligate requirement for organic C (organoheterotrophy) and anaerobic respiration on S⁰ appear to be a consistent physiological niche for these closely related crenarchaeotes (Zillig et al., 1983; Itoh et al., 2003). Like many isolates from the order Thermoproteales, strain WP28t utilized complex

proteinaceous compounds such as yeast extract as a carbon source and sulfur and or thiosulfate as an electron acceptor (Itoh et al., 1998; 1999; Zillig et al., 1983).

A co-culture of the *Thermofilum*-like strain (WP28t) plus an additional novel crenarchaeote within the order Desulfurococcales (strain WP29d) was also obtained from the source pool sediments. Sequence analysis of the two organisms present in the co-culture indicates that strain WP29d has the highest 16S rRNA gene sequence similarity to various species within the order Desulfurococcales, family Desulfurococcaceae; however, BLAST alignments indicate that strain WP29d is only distantly related (88%) to *Desulfurococcus mobilis*, and likely represents a new genera within this family. Strain WP29d is a thermophilic, organoheterotrophic, obligate anaerobe exhibiting cocci morphology. All these characteristics are consistent with other isolated members of the Desulfurococcaceae family (Jannasch et al., 1988; Zillig et al., 1982; Perevalova et al., 2005; Itoh, 2003). However, the inability to fully isolate WP29d along with only a distant relationship to known cultivated microorganisms makes it difficult to definitely assign a physiological function to the *Desulfurococcus*-like organism. Although the co-culture also yielded copious amounts of H₂S, strain WP28t may have been responsible for all of the S respiration as was noted in pure culture. Other cultivated relatives within the Desulfurococcales (e.g. *D. mobilis*, *Staphylothermus* sp.etc.) have been shown to oxidize reduced forms of C and even ferment, while reducing elemental S to sulfide (Jannasch et al., 1998; Arab et al., 2000). The two stains of the co-culture appeared to respond differently to simple and complex carbon sources and S⁰, but repeated attempts to separate WP29d from WP28t were not successful.

It is possible that strain WP29d requires a specific substrate or growth factor produced by strain WP28t. This idea is supported by the fact that both populations were detected in the same geothermal spring sediment samples. This dependent relationship may be similar to the relationship observed between *Thermofilum pendens* and another *Desulfurococcus* sp. (Zillig et al., 1983). Although *Thermofilum pendens* could grow in co-culture with the *Desulfurococcus* species, growth in pure culture required the addition of a polar lipid fraction obtained from a distantly related *Archaea* (Zillig et al., 1983). In contrast, growth of WP29d could not be stimulated with addition of spent media obtained from a co-culture of WP29d and WP28t. Consequently, additional experiments with spent media or culture extracts should be tested in further attempts to purify WP29d. Successful isolation of WP29d will provide a better understanding of the interspecies relationship between these two dominant Crenarchaea in JC3.

The role of chemical energy gradients in establishing the microbial community structure observed in JC3 was examined in this study. It is clear that energetics is not necessarily the only factor controlling the distribution of microbial populations in this geothermal system. The isolation and characterization of relevant microorganisms also provides important information for developing a full understanding of species requirements and interspecies relationships that control microbial community structure in geothermal systems. Future work will utilize this dataset as a guide for culturing other unique thermophiles to further define metabolic capabilities and interactions among JC3 inhabitants. As additional connections are made between specific microbial populations

and the geochemistry of geothermal environments, a comprehensive conceptual model will be developed that includes physiochemical requirements of community members.

Summary and Conclusions

Geothermal systems are excellent model environments for studying linkages between geochemical gradients and microbial community structure. The results of this study support the fundamental assumptions that (i) primary C and energy sources link prokaryotic life and biological productivity to geochemical cycling, (ii) geochemical gradients are an important determinant of microbial community structure, and (iii) interspecies interactions may be important in defining community metabolic networks.

The overall goals of this thesis work were to determine predominant biogeochemical processes occurring within a near neutral, sulfidic, high-arsenic geothermal spring in the Joseph's Coat Springs complex of YNP (JC3), and to link these processes with microbial community structure. This objective was accomplished by extensive analysis of aqueous and solid phase geochemistry, as well as microbial community composition of the source pool and outflow channel sediments within JC3. Gibbs free energy calculations indicate that most oxidation-reduction reactions analyzed in this work are viable microbial energy conservation strategies based on a threshold of approximately -5 to -20 kJ mole^{-1} electron (Jackson and McInerney, 2002). Shifts in microbial community structure were observed as a function of distance throughout the outflow channel. Source pool pyritic phases and Sb and S rich sediments were dominated by *Geothermobacterium*, *Desulfurococcus*, and *Thermofilum*-like 16S sequences whose cultivated relatives are all obligate anaerobes. Changes in microbial community structure

were observed within the outflow channel including appearance of 16S sequences whose close relatives are members of the Aquificales and Thermales sequences. Cultivation strategies designed and based on spring geochemistry along with energetic analysis were successful in isolating two novel thermophilic Crenarchaeota with high 16S rRNA gene sequence similarity to sequences characterized within the spring sediments. An anaerobic, heterotrophic, S-respiring *Thermofilum*-like strain (WP28t) exhibits characteristics consistent with spring geochemistry, and confirms the importance of microbial reduction of elemental S⁰ in this spring. This extensive investigation of Joseph's Coat Springs (JC3) represents a significant contribution to our understanding of the linkages between the geochemistry and microbiology in one of the most interesting and unique geothermal springs in Yellowstone National Park.

REFERENCES

- Ackerman, G.G. 2006. Biogeochemical Gradients and Energetics in Geothermal Systems of Yellowstone National Park. Masters Thesis. Montana State University. Bozeman, MT.
- Aguiar, P., T.J. Beveridge, and A.-L. Reysenbach. 2004. *Sulfurihydrogenibium azorense*, sp. nov.: a novel thermophilic hydrogen-oxidizing microaerophile from terrestrial hot springs in the Azores. *International Journal of Systematic and Environmental Microbiology*. 54: 33-9.
- Ahmad, S., Md.M. Haque, S.M. Ashraf, S. Ahmad. 2004. Urethane modified boron filled polyesteramide: a novel anti-microbial polymer from a sustainable resource. *European Polymer Journal* 40: 2097-2104
- Allewalt, J.P., M.M. Bateson, N.P. Revsbech, K. Slack, D.M. Ward. 2006. Effect of Temperature and Light on Growth of and Photosynthesis by *Synechococcus* Isolates Typical of Those Predominating in the Octopus Spring Microbial Mat Community of Yellowstone National Park. *Applied and Environmental Microbiology* 72: 544-550.
- Allison, J. D., D. S. Brown, and K.J. Novo-Gradac. 1991. MINTEQA2/PRODEFA2, a geochemical assessment model for environmental systems: Version 3.0 User's Manual. Athens, Georgia, Environmental Research Laboratory, Office of Research and Development, USEPA.
- Altschul, S. F., T. L. Madden, A.A. Schäffer, J. Zhang, Z. Zhang, W. Miller, and D.J. Lipman. 1997. Gapped BLAST and PSI-BLAST: a new generation of protein database search programs. *Nucleic Acid Res* 25: 3389.
- Amend, J. P. and E. L. Shock 2001. Energetics of overall metabolic reactions of thermophilic and hyperthermophilic Archaea and Bacteria. *FEMS Microbiology Reviews* 25: 175.
- Amend, J. P., K. L. Rogers, E. L. Shock, S. Gurrieri, and S. Inguaggiato. 2003. Energetics of chemolithotrophy in the hydrothermal system of Volcano Island, southern Italy. *Geobiology* 1: 37-58.
- American Public Health, A., L. S. Clesceri, A.W. Greenberg and A.D. Eaton. 1998. Part 4500-NH 3 H. Standard methods for the examination of water and wastewater. Washington DC, APHA. 20th ed.: 4-111.

- American Public Health, A., L. S. Clesceri, A.W. Greenberg and A.D. Eaton. 1998. Part 4500 - S 2-D. Standard methods for the examination of water and wastewater. Washington DC, APHA: 4-165.
- An, C., K. Tang, Q. Yang, and Y. Qian. 2003. Formation of Crystalline Stibnite Bundles of Rods by Thermolysis of an Antimony(III) Diethyldithiocarbamate Complex in Ethylene Glycol. *Inorganic Chemistry* 42: 8081-8086
- Aoshima, M., Y., Nishibe, M. Hasegawa, A. Yamagishi, T. Oshima. 1996. Cloning and sequencing of a gene encoding 16S ribosomal RNA from a novel hyperthermophilic archaeobacterium NC12. *Gene* 180: 183-187.
- Arab, H., H. Volker, M. Thomm. 2000. *Thermococcus aegaeicus* sp. nov. and *Staphylothermus hellenicus* sp. nov., two novel hyperthermophilic archaea isolated from geothermally heated vents off Palaeochori Bay, Milos, Greece. *International Journal of Systematic and Evolutionary Microbiology* 50: 2101.
- Bada, J.L. 2004. How life began on Earth: a status report. *Earth and Planetary Science Letters* 226: 1-15.
- Baker, B.J., J.F. Banfield. 2003. Microbial communities in acid mine drainage. *FEMS Microbiology Ecology* 44: 139-152.
- Ball, J. W., R. B. McCleskey, D.K. Nordstrom, J.M. Holloway, P.L. Verplanck. 2002. Water-chemistry data for selected springs, geysers, and streams in Yellowstone National Park, Wyoming 1999-2000. Boulder, CO, USGS.
- Barns, S.M. and S.A. Nierzwicki-Bauer. 1997. Microbial diversity in ocean, surface, and subsurface environments. *in Geomicrobiology: Interactions Between Microbes and Minerals*. ed P.H. Ribbe. Mineralogical Society of America: 35
- Belkin, S., C.O. Wirsen, and H.W. Jannasch. 1985. Biological and Abiological Sulfur Reduction at High Temperatures. *Applied and Environmental Microbiology* 49: 1057-1061.
- Blumentals, I.I., M. Itoh, G.J. Olson, and R.M. Kelly. 1990. Role of Polysulfides in Reduction of Elemental Sulfur by the Hyperthermophilic Archaeobacterium *Pyrococcus furiosus*. *Applied and Environmental Microbiology* 56: 1255-1262.
- Catling, D.C., K.J. Zahnle, C.P. McKay. 2001. Biogenic Methane, Hydrogen Escape, and the Irreversible Oxidation of Early Earth. *Science* 293: 839-843.

- Caylo, J.L., B. Ollivier, B.K.C. Patel, G. Ravot, M. Magot, E. Ageron, P.A.D. Grimont, and J.L. Garcia. 1995. Description of *Thermoanaerobacter brockii* subsp. *lactiethylicus* subsp. nov., Isolated from a Deep Subsurface French Oil Well, a Proposal To Reclassify *Theroanaerobacter finnij* as *Thermoanaerobacter brockii* subsp. *finnii* comb. nov., and an Emended Description of *Thermoanaerobacter brockii*. *International Journal of Systematic Bacteriology* 45: 783-789
- Cox, A.D., and E.L. Shock. 2003. Limits of microbial photosynthesis in hot spring ecosystems. Abstract B41D-0927. *EOS Trans AGU* 84: F309-310.
- Croal, L.R., J.A. Gralnich, D. Malasarn, and D.K. Newman. 2004. The Genetics of Geochemistry. *Annual Reviews of Genetics* 38:175-202.
- Donohoe-Christiansen, J., S. D'Imperio, C.R. Jackson, W. P. Inskip, and T.R. McDermott. 2004. Isolation and Characterization of an arsenite-oxidizing *Hydrogenobaculum* from an acid-sulfate-chloride thermal spring in Yellowstone National Park. *Environmental Microbiology* 70: 1865-8.
- Druschel, G.K., M.A.A Schoonen, D.K. Nordstrom, J.W. Ball, Y. Xu, and C.A. Cohn. 2003. Sulfur geochemistry of hydrothermal waters in Yellowstone National Park, Wyoming, USA. III. An anion-exchange resin technique for sampling and preservation of sulfoxyanions in natural waters. *The Royal Society of Chemistry and the Division of Geochemistry of the American Chemical Society* 4: 12-19.
- Edwards, J.L, M.A. Lane, E.S. Nielsen. 2000. Interoperability of Biodiversity Databases: Biodiversity Information on Every Desktop. *Science* 289: 2312-2314
- Filella, M., N.Belzile, Y.-W.Chen. 2002. Antimony in the environment: A review focused on natural waters I. *Earth-Science Reviews*. 57:125–176.
- Filella, M., P.M. May. 2003. Computer simulation of the low-molecular-weight inorganic species distribution of antimony(III) and antimony(V) in natural waters. *Geochimica et Cosmochimica Acta* 67: 4013-4031.
- Foght, J., J. Aislabie, S. Turner, C.E. Brown, J. Ryburn, D.J. Saul, W. Lawson. 2004. Culturable Bacteria in Subglacial Sediments and Ice from Two Southern Hemisphere Glaciers. *Microbial Ecology* 47: 329-340.
- Fouke, B., Bonheyo, G., Sanzenbacher, B., and Frias-Lopez, J. 2003. Partitioning of bacterial communities between travertine depositional facies at Mammoth Hot Springs, Yellowstone National Park, USA. *Can J Earth Sci* 40:1531–1548.

- Fournier, R.O. 2005. Geochemistry and Dynamics of the Yellowstone National Park Hydrothermal System. *in* Geothermal Biology and Geochemistry in Yellowstone National Park. *eds* W.P Inskeep and T.R. McDermott.
- Gihring, T.M., G.K. Druschel, R.B. McCleskey, R.J. Hammers, and J.F. Banfield. 2001. Rapid Arsenite Oxidation by *Thermus aquaticus* and *Thermus thermophilus*: Field and Laboratory Investigations. *Environmental Science and Technology* 35: 3857-3862.
- Hague, A. 1880. Notes on the Deposit of Scorodite from Arsenical Waters in the Yellowstone National Park. *American Journal of Science* 34: 171-175.
- Hazen, T., and T.J. Phelps. 2004. Reducing Boron Toxicity by Microbial Sequestration. U.S. Department of Energy Journal of Undergraduate Research. <http://www.scied.science.doe.gov>.
- Hoaki, T., M. Nishijima, H. Miyashita, T. Maruyama. 1995. Dense Community of Hyperthermophilic Sulfur-Dependent Heterotrophs in a Geothermally Heated Shallow Submarine Biotope near Kodakara-Jima Island, Kagoshima, Japan. *Applied and Environmental Microbiology* 61: 1931-1937.
- Hoffmann, M.R., B.C. Faust, F.A. Panda, H.H. Koo, and H.M. Tsuchiya. 1981. Kinetics of the removal of Iron Pyrite from Coal by Microbial Catalysis. *Applied and Environmental Microbiology* 42: 259-271.
- Hugenholtz, P., Pitulle, C., K. L. Hershberger, N.R. Pace. 1998. Novel division-level bacterial diversity in a Yellowstone hot spring. *Journal of Bacteriology* 180: 366-376.
- Hunter-Cevera, J.C. 1998. The value of microbial diversity. *Current Opinion in Microbiology* 1: 278-285.
- Inskeep, W.P., G.G. Ackerman, W.P. Taylor, M.A. Kozubal, S. Korf, R.E. Macur. 2005. On the energetics of chemolithotrophy: case studies of geothermal springs in Yellowstone National Park. *Geobiology*. 3: 297.
- Inskeep, W.P. and T.R. McDermott. 2005. Geomicrobiology of acid-sulfate-chloride springs in Yellowstone National Park. *In* Geothermal Biology and Geochemistry in Yellowstone National Park. *eds* W.P Inskeep and T.R. McDermott, Montana State University, Bozeman MT.

- Inskeep, W. P., R. E. Macur, G. Harrison, B.C. Bostick, and S.Fendorf. 2004. Microbial mineralization of As(V)-hydrous ferric oxyhydroxide mats in an acid-sulfate chloride geothermal spring of Norris Geyser Basin, Yellowstone National Park. *Geochimica et Cosmochimica Acta*. 68: 3141-55.
- Inskeep, W.P., R.E. Macur, N. Hamamura, T.P. Warelow, S.A. Ward, and J.M. Santini. 2007. Detection, diversity and expression of aerobic bacterial arsenite oxidase genes. *Environmental Microbiology* 9: 934-943.
- Inskeep, W. P., T. R. McDermott, and S. Fendorf. 2002. *Arsenic (V)/(III) Cycling in Soils and Natural Waters: Chemical and Microbiological Processes*. New York City, Marcel Dekker.
- Itoh, T., K. Suzuki, and T. Nakase. 2002. *Vulcanisaeta distribuate* gen. nov., sp. nov., and *Vulcanisaeta souniana* sp. nov., novel hyperthermophilic, rod-shaped crenarchaeotes isolated from hot springs in Japan. *International Journal of Systematic and Evolutionary Microbiology* 52: 1097-1104
- Itoh, T., 2003. Taxonomy of nonmethanogenic hyperthermophilic and related thermophilic archaea. *Journal of Bioscience and Bioengineering* 96: 201-212.
- Itoh, T., K. Suzuki, P.C. Sanchez, and T. Nakase. 1999. *Caldivirga maquilingensis* gen. nov., sp. nov., a new genus of rod-shaped crenarchaeote isolated from a hot spring in the Philippines. *International Journal of Systematic Bacteriology* 49: 1157-1163.
- Itoh, T., K. Suzuki, P.C Sanchez, and T. Nakase. 2003. *Caldisphaera lagunensis* gen. nov., sp. nov., a novel thermoacidophilic crenarchaeote isolated from a hot spring at Mt Maquiling, Philippines. *International Journal of Systematic and Evolutionary Microbiology* 53: 1149-1154.
- Itoh, T., K. Suzuki, and T. Nakase. 1998. *Thermocladium modestius* gen. nov., sp. nov., a new genus of rod-shaped, extremely thermophilic crenarchaeote. *International Journal of Systematic Bacteriology* 48: 879-887.
- Jackson, C. R., H. W. Langner, et al. J. Donahoe-Christiansen, W.P. Inskeep, and T.R. McDermott. 2001. Molecular analysis of microbial community structure in an arsenite-oxidizing acidic thermal spring. *Environmental Microbiology* 3(8): 532.
- Jackson, B.E. and M.J. McInernery. 2002. Anaerobic microbial metabolism can proceed close to thermodynamic limits. *Nature* 415: 454-456.

- Jannasch, H.W., C.O. Wirsen, S.J. Molyneaux, and T.A. Langworthy. 1998. Extremely Thermophilic Fermentative Archaeobacteria of the Genus *Desulfurococcus* from Deep-Sea Hydrothermal Vents. *Applied and Environmental Microbiology* 54: 1203-1209.
- Jannasch, H.W., and M.J., Mottl. 1985. Geomicrobiology of Deep-sea Hydrothermal Vents. *Science* 229: 717-725.
- Jorgensen, B.B., 1990. A Thiosulfate Shunt in the Sulfur Cycle of Marine Sediments. *Science* 249: 152-154.
- Jorgensens, B.B., and F. Bak. 1991. Pathways and Microbiology of Thiosulfate Transformations and Sulfate Reduction in a Marine Sediment (Kattegat, Denmark). *Applied and Environmental Microbiology* 57: 847-856.
- Kappler, A., D. Emerson, K. Edwards, J.P. Amend, J.A. Gralnick, P. Grathwohl, T. Hoehler, and K.L. Straub. 2005. Microbial activity in biogeochemical gradients - new aspects of research. *Geobiology* 3: 229-233.
- Kashefi, K., D.E. Holmes, A-L Reysenbach, and D.R. Lovley. 2002. The use of Fe(III) as an electron acceptor to recover preciously uncultured hyperthermophiles: isolation and characterization of *Geothermobacterium ferrireducens* gen nov., sp. nov. *Applied and Environmental Microbiology*. 68: 1735-42.
- Katayama, Y., Y. Uchino, A.P. Wood, and D.P. Kelly. 2006. Confirmation of *Thiomonas delicata* (formerly *Thiobacillus delicatus*) as a distinct species of the genus *Thiomonas* Moreira and Amils 1997 with comments on some species currently assigned to the genus. *International Journal of Systematic and Evolutionary Microbiology* 56: 2553-2557.
- King, S.A., S. Behnke, K. Slack, D.P. Krabbenhoft, D.K. Nordstrom, M.D. Burr, R.G. Striegl. 2006. Mercury in water and biomass of microbial communities in hot springs of Yellowstone National Park, USA. *Applied Geochemistry* 21: 1869-1879.
- Kozubal, M., R.E. Macur, W.P. Taylor, G. Ackerman, S. Korf, A. Nagy, and W.P. Inskeep. 2007. Isolation, Characterization and Distribution of a Novel Iron-Oxidizing Thermophilic Acidophilic Archaeon from Acid-Sulfate-Chloride Geothermal Springs of Yellowstone National Park. *Applied and Environmental Microbiology* (submitted for review).
- Langner, H. W., C. R. Jackson, T.R. McDermott, and W.P. Inskeep. 2001. Rapid oxidation of arsenite in a hot spring ecosystem, Yellowstone National Park. *Environmental Science & Technology* 35: 3302.

- Ley, R.E., J.K. Harris, J. Wilcox, J.R. Spear, S.R. Miller, B.M. Bebout, J.A. Maresca, D.A. Bryant, M.L. Sogin, N.R. Pace. 2006. Unexpected Diversity and Complexity of the Guerrero Negro Hypersaline Microbial Mat. *Applied and Environmental Microbiology* 72: 3685-3695.
- Madigan, M. T., J.M. Martinko, and J. Parker. 2003 *Brock Biology of Microorganisms*, 10th ed. Prentice Hall, Upper Saddle River, NJ.
- Macur, R.E., H.W. Langner, B.D. Kocar, and W.P. Inskeep. 2004a. Linking geochemical processes with microbial community analysis: Successional dynamics in an arsenic-rich, acid-sulfate-chloride geothermal spring. *Geobiology* 2: 163-177.
- Macur, R.E., C.R. Jackson, L.M. Botero, T.R. McDermott, and W.P. Inskeep. 2004b. Bacterial populations associated with the oxidation and reduction of arsenic in an unsaturated soil. *Environmental Science and Technology* 38: 104-111.
- McCleskey, R.B., J.W. Ball, D.K. Nordstrom, J.M. Holloway, and H.E. Taylor. 2005. Water-Chemistry Data for Selected Hot Springs, Geysers, and Streams in Yellowstone National Park, Wyoming, 2001-2001. Boulder, CO, USGS.
- Meyer-Dombard, D.R., E.L. Shock, and J.P. Amend. 2005. Archaeal and bacterial communities in geochemically diverse hot springs of Yellowstone National Park, USA. *Geobiology* 3: 211-227.
- Miroshnichenko, M.L., F.A. Rainery, H. Hippe, N.A. Chernyh, N.A. Kostrikina, and E.A. Bonch-Osmolovskaya. 1998. *Desulfurella kamchatkensis* sp. nov. and *Desulfurella propionica* sp. nov., new sulfur respiring thermophilic bacteria from Kamchatka thermal environments. *International Journal of Systematic Bacteriology* 48: 475-479.
- Morgan, L.A., and W.C. Pat Shanks. 2005. Influences of Rhyolitic Lava Flows on Hydrothermal Processes in Yellowstone Lake and on the Yellowstone Plateau. *in* *Geothermal Biology and Geochemistry in Yellowstone National Park*. eds W.P. Inskeep and T.R. McDermott.
- Muyzer, G., E. C. de Waal, A.G. Uitterlinden. 1993. Profiling of complex microbial populations by denaturing gradient gel electrophoresis analysis of polymerase chain reaction-amplified genes encoding for 16S rRNA. *Applied and Environmental Microbiology* 59: 695.

- Nakagawa, S., Z. Shtaih, A. Banta, T.J. Beveridge, T. Sako, and A.L. Reysenbach. 2005. *Sulfurihydrogenibium yellowstonense* sp. nov., an extremely thermophilic, facultatively heterotrophic, sulfur-oxidizing bacterium from Yellowstone National Park, and emended descriptions of the genus *Sulfurihydrogenibium*, *Sulfurihydrogenibium subterraneum* and *Sulfurihydrogenibium azorense*. *International Journal of Systematic and Evolutionary Microbiology* 55: 2263-2268.
- Nannipieri, P., J. Ascher, M.T. Ceccherini, L. Landi, G. Pietramellara, G. Renella. 2003. Microbial diversity and soil functions. *European Journal of Soil Science* 54: 655-670.
- Newman, D.K. and J.F. Banfield. 2002. Geomicrobiology: How molecular scale interactions underpin biogeochemical systems. *Science*. 296: 1017.
- Nisbet, E.G., and N.H. Sleep. 2001. The habitat and nature of early life. *Nature*. 409:1083-1091
- Nordstrom, D.K. and G. Southam. 1997 "Geomicrobiology of sulfide mineral oxidation. *in* Geomicrobiology: Interactions Between Microbes and Minerals. ed P.H. Ribbe. Mineralogical Society of America: 35
- Nordstrom, D.K., J.W. Ball, R. B. McClesky. 2005. Ground water to surface water: chemistry of thermal outflows in Yellowstone National Park. *in* Geothermal Biology and Geochemistry in Yellowstone National Park. eds W.P Inskeep and T.R. McDermott.
- Perevalova, A.A., V.A. Svetlichny, I.V. Kublanov, N.A. Chernyh, N.A. Kostrikina, T.P. Tourova, B.B Kuznetsov, E.A. Bonch-Osmolovskaya. 2005. *Desulfurococcus fermentans* sp. nov., a novel hyperthermophilic archaeon from a Kamchatka hot spring, and emende description of the genus *Desulfurococcus*. *International Journal of Systematic and Evolutionary Microbiology* 55: 995-999.
- Pfenning, N., K.D. Lippert. 1966. Über das Vitamin B₁₂-Bedürfnis phototropher Schwefelbakterien. *Archives of Microbiology* 55: 245-256.
- Phoenix, V.R., R.W. Renaut, B. Jones, F. G. Ferris. 2005. Bactreial S-layer preservation and rare arsenic-antimony-sulphide bioimmobilization in siliceous sediments from Champagen Pool hot spring, Waiotapu, New Zealand. *Journal of the Geological Society*. 162:323.

- Ravot, G., B. Ollivier, B.K.C. Patel, M. Magot, and J.L. Garcia. 1996. Emended Description of *Thermosipho africanus* as a Carbohydrate-Fermenting species Using Thiosulfate as an Electron Acceptor. *International Journal of Systematic Bacteriology* 46: 321-323.
- Reysenbach, A.L., M. Ehringer, K. Hershberger. 2000. Microbial diversity at 83 °C in Calcite Springs, Yellowstone National Park: another environment where the *Aquificales* and "Korarchaeota" coexist. *Extremophiles* 4: 61-67.
- Reysenbach, A.-L., and S. Cady. 2001. Microbiology of ancient and modern hydrothermal systems. *Trends in Microbiology*. 9: 79-86.
- Reysenbach, A.L., and E.L. Shock. 2002. Merging genomes with geochemistry at hydrothermal ecosystems. *Science*. 296:1077.
- Reysenbach, A.L., A. Bantan, S. Civallo, J. Daly, K. Mitchel, S. Lalonde, K. Konhauser, A. Rodman, K. Rusterholtz, C. Takacs-Vesbach. 2005. Aquificales in Yellowstone National Park. *in* *Geothermal Biology and Geochemistry in Yellowstone National Park*. eds W.P Inskeep and T.R. McDermott.
- Roberstson, C.E., J.K. Harris, J.R. Spear, N.R. Pace. 2005. Phylogenetic diversity and ecology of environmental Archaea. *Current Opinion in Microbiology* 8: 638-642.
- Rogers, K.L., J.P. Amend. 2005. Archaeal diversity and geochemical energy yields in a geothermal well on Vulcano Island, Italy. *Geobiology*. 3: 319-332.
- Rogers, K.L., J.P. Amend. 2006. Energetics of potential heterotrophic metabolisms in the marine hydrothermal system of Vulcano Island, Italy. *Geochimica et Cosmochimica Acta* 70: 6180-6200.
- Rothschild, L.J., R.L. Mancinelli. 2001. Life in extreme environments. *Nature*. 49: 1092-1101.
- Silver, S. 1996. Bacterial Resistances to toxic metal ions-a review. *GENE* 176: 9.
- Silver, S., and L.T. Phung. 2005. Genes and Enzymes Involved in Bacterial Oxidation and Reduction of Inorganic Arsenic. *Applied and Environmental Microbiology* 71: 599-608.
- Skirnisdottir, S., G.O. Hreggvidsson, S. Hjorleifsdottir, V.T. Marteinson, S.K. Petursdottir, O. Holst, and J.K. Kristjansson. 2000. Influence of Sulfide and Temperature on Species Composition and Community Structure of Hot Spring Microbial Mats. *Applied and Environmental Microbiology* 66: 2835-2841.

- Spear, J. R., J. J. Walker, McCollom, and N.R. Pace. 2005. Hydrogen and bioenergetics in the Yellowstone geothermal ecosystem. *Proceedings of the National Academy of Sciences*. 102: 2555-2560.
- Spear, J.R., J.J. Walker, N.R. Pace. 2006. Microbial Ecology and Energetics in Yellowstone Hot Springs. *Yellowstone Science* 14: 17-24.
- Stauffer, R.E., J.M. Thompson. 1984. Arsenic and antimony in geothermal waters in Yellowstone National Park, Wyoming, USA. *Geochimica et Cosmochimica Acta* 48: 2547-2561.
- Stetter, K.O., W. Zillig, 1989. Thermoproteales: a novel type of extremely thermoacidophilic anaerobic archaeobacteria isolated from Icelandic solfataras. *Zentralbl. Bakteriell. Parasitenkd. Infektionskr. Hyg. Abt.1 Original* 1983 C2: 205-227.
- Stumm, W., and J.J. Morgan. 1996. *Aquatic Chemistry: Chemical Equilibria and Rates in Natural Waters*. John Wiley and Sons, New York.
- Suzuki, M.T., S.J. Giovannoni. 1996. Bias Caused by Template Annealing in the Amplification of Mixtures of 16s rRNA Genes by PCR. *Applied and Environmental Microbiology* 62: 625-630.
- To, T.B., D.K. Nordstrom, K.M. Cunningham, J.W. Ball, R.B. McClesky. 1999. New method for the direct determination of dissolved Fe(III) concentration in acid mine waters. *Environmental Science and Technology*. 33: 807-813.
- Vairavamurthy, A., B. Manowitz, G.W. Luther, and Y. Jeon. 1993. Oxidation state of sulfur in thiosulfate and implications for anaerobic energy metabolism. *Geochimica et Cosmochimica Acta* 57: 1619-1623.
- Volkl, P., R. Huber, E. Drobner, R. Rachel, S. Burggraf, A. Trincone, and K.O. Stetter. 1993. *Pyrobaculum aerophilum* sp. nov., a Novel Nitrate-Reducing Hyperthermophilic Archaeum. *Applied and Environmental Microbiology* 59: 2918-2926.
- Ward, D. M. 1998. A natural species concept for prokaryotes. *Current Opinions in Microbiology* 1: 271.
- Ward, D.M., M.J. Ferris, S.C. Nold, and M.M. Bateson. 1998. A Natural View of Microbial Biodiversity within Hot Spring Cyanobacterial Mat Communities. *Microbiology and Molecular Biology Reviews* 62: 1353-1370.

- Wolin, E.A., M.J. Wolin, and R.S. Wolfe. 1963. Formation of Methane by Bacteria Extracts. *The Journal of Biological Chemistry* 238: 28-34.
- Woods, W.G., 1994. An Introduction to Boron: History, Sources, Uses and Chemistry. *Environmental Health Perspectives* 102: 5-11.
- Xu, Y., M. A. A. Schoonen, D.K. Nordstrom, K.M. Cunningham, J.W. Ball. 1998. Sulfur geochemistry of hydrothermal waters in Yellowstone National Park: I. The origin of thiosulfate in hot spring waters. *Geochimica et Cosmochimica Acta*. 62: 3729-43.
- Xu, Y., M.A.A. Schoonen, D.K. Nordstrom, K.M. Cunningham, J.W. Ball. 2000. Sulfur geochemistry of hydrothermal waters in Yellowstone National Park, Wyoming, USA. II. Formation and decomposition of thiosulfate and polythionate in Cinder Pool. *Journal of Volcanology and Geothermal Research* 00: 000.
- Zillig, W., K.O. Stetter, D. Prangishvilli, W. Schafer, S. Wunderl, D. Janekovic, I. Holz, and P. Palm. 1983. Desulfurococcaceae, the second family of the extremely thermophilic, anaerobic, sulfur-respiring Thermoproteales. *Zentralbl. Bakteriol. Parasitenkd. Infektionskr. Hyg. Abt. C3*: 304-317.

APPENDIX A

AQUEOUS CHEMISTRY DATA

Table A.1. Concentrations of Total Soluble Constituents and Measured Aqueous Chemical Species in Joseph's Coat Spring 3 (JC3).

Cations											
Sample	Distance m	pH	Temp °C	I	Na	K	Ca	NH ₄	Al	Fe	Mg
Aug-03											
JC3A	0	6.2	92	22.5	11.3	2.0	0.38	5597	1.4	< .18	38.3
JC3B	3.3	6.2	75	20.7	11.5	2.0	0.39	5600	1.3	< .18	38.7
JC3C	6.4	6.2	68	25.9	11.9	2.1	0.39	5769	1.4	< .18	40.0
Jul-04											
JC3A	0	6.1	89.1	24.5	11.7	2.0	0.38	5589	0.7	0.56	39.6
JC3B	1.7	6.3	73.9	24.6	11.6	2.0	0.39	5567	0.7	0.56	40.6
JC3C	3.3	6.5	68.9	25.6	11.5	2.1	0.40	5763	0.7	0.56	41.3
JC3D	6.4	6.5	56.8	25.7	11.7	2.1	0.41	5811	0.7	0.56	42.6
JC3E	11.2	6.4	45.5	26.2	11.8	2.1	0.41	5800	0.7	0.56	43.0
Jul-05											
JC3A	0	6.0	88.3	23.2	11.4	2.1	0.39	5979	2.1	0.71	43.1
JC3B	1.7	6.4	76.6	24.1	11.9	2.1	0.40	5995	2.0	0.65	44.8
JC3C	3.8	6.4	67.7	24.5	12.1	2.2	0.41	6093	1.9	0.71	45.5
JC3D	6.9	6.5	56.8	25.1	12.4	2.2	0.41	6148	1.8	0.76	45.8
JC3E	11.7	6.4	44.4	26.1	12.8	2.3	0.42	6324	1.9	0.73	47.4
Aug-06											
JC3A	0	6.1	90.0	ns ¹	11.2	2.1	0.38	5310	0.7	0.36	39.1
JC3B	1.7	6.5	76.0	ns	ns	ns	ns	ns	ns	ns	ns
JC3C	3.8	6.6	68.0	ns	ns	ns	ns	ns	ns	ns	ns
JC3D	6.9	6.7	58.6	ns	ns	ns	ns	ns	ns	ns	ns
JC3E	11.7	6.7	46.4	ns	12.1	2.2	0.40	5510	1.1	0.36	41.6
Mean (Source Water)		6.1	89.9	23.4	11.39	2.05	0.38	5619	1.24	0.54	40.0
Standard Deviation		0.07	1.6	1.0	0.23	0.04	0.004	275	0.64	0.17	2.12
Relative Std Dev (%)		1%	2%	4%	2%	2%	1%	4%	51%	32%	5%
µM Concentration²					11390	2005	380	5619	1.24		40.4

¹ ns = not sampled; ² concentration in µM entered into MINTEQ for calculations

Table A.1.

<i>Anions</i>						
Sample	Cl	SO ₄	F	NO ₃	P	S ₂ O ₃ ²⁻
	-----mM-----		-----μM-----			
<i>Aug-03</i>						
JC3A	9.5	4.2	328	10.8	4.8	635.3
JC3B	7.9	3.5	280	9.3	8.7	530.6
JC3C	10.0	4.4	357	12.4	4.8	653.8
<i>Jul-04</i>						
JC3A	10.6	4.2	318	12.54	2.4	819
JC3B	10.8	4.2	340	11.3	2.3	834
JC3C	11.6	4.3	324	13.0	2.2	815
JC3D	11.3	4.4	345	13.0	2.1	842
JC3E	11.4	4.6	352	12.9	2.3	788
<i>Jul-05</i>						
JC3A	9.3	4.5	381	5.5	< 1.6	719.0
JC3B	9.8	4.7	402	6.2	< 1.6	765.0
JC3C	9.9	4.7	405	6.2	< 1.6	763.0
JC3D	10.1	4.8	415	5.9	< 1.6	734.0
JC3E	10.5	5.1	429	6.5	< 1.6	712.0
<i>Aug-06</i>						
JC3A	11.82	3.95	360.8	ns	2.3	830.0
	ns ¹	ns	ns	ns	ns	ns
	ns	ns	ns	ns	ns	ns
	ns	ns	ns	ns	ns	ns
JC3E	11.84	4.04	372.4	1.3	2.3	900.0
Mean (Source Water)	10.3	4.18	347	9.6	3.2	750.8
Standard Deviation	1.2	0.21	29.3	5.7	1.5	91.8
Relative Std Dev (%)	11%	5%	8%	59%	46%	12%
μM Concentration²	10300	4180	347	9.6	3.2	840

¹ ns = not sampled; ² concentration in μM entered into MINTEQ for calculations

Table A.1

<i>Trace Elements and Other Total Soluble Constituents</i>						
Sample	Si	B	As	Zn	Ba	Mn
	-----mM-----		-----µM-----			
Aug-03						
JC3A	3.9	5.60	117.0	< .15	0.8	4.64
JC3B	4.0	5.76	125.5	< .15	0.6	4.77
JC3C	4.1	5.91	133.1	0.15	0.6	4.82
Jul-04						
JC3A	3.9	5.51	138.2	0.15	0.9	4.65
JC3B	4.0	5.58	138.2	0.19	0.7	4.74
JC3C	4.1	5.73	145.6	0.42	0.7	4.80
JC3D	4.2	5.83	142.6	0.24	0.6	4.93
JC3E	4.2	5.91	150.4	0.71	0.7	4.99
Jul-05						
JC3A	4.1	5.48	131.8	0.15	0.7	4.75
JC3B	4.2	5.70	128.9	0.29	0.8	4.90
JC3C	4.3	5.78	130.4	1.04	0.8	4.99
JC3D	4.3	5.87	130.4	0.69	0.8	4.99
JC3E	4.5	6.06	135.0	0.47	0.8	5.21
Aug-06						
JC3A	3.69	5.65	118.6	< .15	0.8	4.19
JC3B	ns ¹	ns	ns	ns	ns	ns
JC3C	ns	ns	ns	ns	ns	ns
JC3D	ns	ns	ns	ns	ns	ns
JC3E	3.90	6.02	139.4	0.15	0.7	4.37
Mean (Source Water)	3.9	5.56	126	0.15	0.79	4.6
Standard Deviation	0.2	0.08	10	0.0	0.09	0.3
Relative Std Dev (%)	4%	1%	8%	0%	12%	5%
µM Concentration²	3900	5560		0.15		

¹ ns = not sampled; ² concentration in µM entered into MINTEQ for calculations

Table A.1

<i>Dissolved Gases</i>							
Sample	CO ₂ (aq) <i>mM</i>	SI (CO ₂)	Total Sulfide	O ₂ (aq) <i>μM</i>	CH ₄ (aq)	H ₂ (aq) <i>nM</i>	DIC ⁵ <i>mM</i>
<i>Aug-03</i>							
JC3A	0.19	2.1	17.7	ns	0.934	90	
JC3B	0.04	1.9	14.3	ns	0.038	< 5	
JC3C	0.02	1.8	13.0	ns	< .01	< 5	
<i>Jul-04</i>							
JC3A	0.15	-	27.1	< 3.1	0.850	176	
JC3B	0.05	1.7	20.8	< 3.1	0.134	11	
JC3C	0.02	1.5	15.9	< 3.1	0.030	7	
JC3D	0.01	1.4	14.1	< 3.1	0.014	19	
JC3E	0.01	1.2	10.6	12.5	< .01	10	
<i>Jul-05</i>							
JC3A	0.15	1.9	14.5	< 3.1	0.721	115	
JC3B	0.05	1.5	8.6	< 3.1	0.165	33	
JC3C	0.02	1.4	5.6	< 3.1	0.050	20	
JC3D	0.02	1.0	3.8	< 3.1	< .01	19	
JC3E	0.01	0.8	2.1	< 3.1 ⁴	< .01	15	
<i>Aug-06</i>							
JC3A	0.11	2.0	28.0	< 3.1	1.020	50	0.35
JC3B	0.04	nc ²	28.0	< 3.1	0.780	52	0.22
JC3C	0.03	nc	20.9	< 3.1	bd ³	42	0.16
JC3D	0.04	nc	19.7	< 3.1	bd	59	0.13
JC3E	0.03	nc	16.8	< 3.1	bd	77	0.07
Mean (Source Water)							
	0.15	2.0	21.8	bdl	0.88	107.7	
Standard Deviation							
	0.03	0.2	6.7	na	0.13	52.8	
Relative Std Dev (%)							
	22%	10%	31%	na	14%	49%	
μM Concentration³			21.8				350

¹ ns = not sampled; ² nc = not calculated; ³ bd = below detection; ³ concentration in μM entered into MINTEQ for calculations

⁴ 35.9 μM O₂(aq) was detected in July 2005 at a point 2m further in the transect. ⁵ DIC was calculated using CO₂(aq) conc. and MINTEQ for years 03' - 05'; 06' data represent actual DIC conc.

Table A.1

<i>Iron, Arsenic and Antimony Species</i>									
Sample	Fe _{TS}	Fe ^{II}	Fe ^{III}	As _{TS}	As ^{III}	As ^V	Sb _{TS}	Sb ^{III}	Sb ^V
----- <i>μM</i> -----									
Aug-03									
JC3A	< .18	< .17	< .17	117	93.4	23.6	ns	ns	ns
JC3B				126	97.5	28.0	ns	ns	ns
JC3C				133	86.9	46.1	ns	ns	ns
Jul-04									
JC3A	0.6	0.51	< .17	138	119	19.4	1.24	ns	ns
JC3B	0.6	0.33	0.24	138	112	25.9	ns	ns	ns
JC3C	0.6	0.30	0.27	146	103	42.7	ns	ns	ns
JC3D	0.6	0.56	< .17	143	84.6	57.9	ns	ns	ns
JC3E	0.6	0.34	0.23	150	75.2	75.2	ns	ns	ns
Jul-05									
JC3A	0.7	0.33	0.37	132	113	18.9	1.13	0.95	0.18
JC3B	0.6	0.33	0.31	129	107	21.6	1.19	0.92	0.27
JC3C	0.7	0.39	0.31	130	105	25.4	1.39	1.08	0.31
JC3D	0.8	0.31	0.46	130	71.1	59.3	1.55	1.04	0.52
JC3E	0.7	0.31	0.43	135	23.4	111.6	2.00	1.20	0.81
Aug-06									
JC3A	0.6	0.70	< 0.0	128	101	26.5	0.50	0.19	0.31
JC3B	ns ¹	ns	ns	139	106	32.7	0.51	0.11	0.40
JC3C	ns	ns	ns	145	93.8	51.4	0.54	0.14	0.40
JC3D	ns	ns	ns	151	80.9	70.1	0.51	0.05	0.46
JC3E	ns	ns	ns	158	69.2	88.8	0.57	0.00	0.57
Mean (Source Water)	0.6	0.5	< .2	129	107	22.1	0.96	0.57	0.25
Standard Deviation	0.1	0.2	na	8.9	11.4	3.6	0.4	0.5	0.1
Relative Std Dev (%)	12%	35%	na	7%	11%	16%	42%	94%	36%
μM Concentration²		0.5	0.1		107	22.1		0.19	0.31

¹ ns = not sampled; ² concentration in μM entered into MINTEQ for calculations